41èmes Journées des Actinides

8th School on the Physics and Chemistry of the Actinides

7.-12. April 2011, Stará Lesná, Slovakia

Programme and Proceedings

Editors: Mária Zentková, Marián Mihalik, Marián Reiffers

41èmes Journées des Actinides: Programme and Proceedings

Editors: Mária Zentková, Marián Mihalik, Marián Reiffers
Publisher: Slovenská fyzikálna spoločnosť, Dúbravská cesta 9, 845 27 Bratislava, Slovenská republika
Cover design: EQUILIBRIA, s.r.o.
Printed by: EQUILIBRIA, s.r.o.

ISBN 978-80-970625-1-4
EAN: 9788097062514

Preface

Since 1971, the "*Journées des Actinides"* (JdA) meeting is an annual conference dedicated to the scientific programs on 5*f* elements, including physics, chemistry and materials researches. This conference is a traditional informal actinide forum bringing together experts from fields involved, taking place in a very informal way, emphasizing exchanges and discussions on current issues in actinide science.

The role of JdA is very specific because of its informal organization (in opposition to larger events like ACTINIDES conferences, organized every 4 years as a world congress), and because of its timing early in the year (typically March or April) allowing ideas/issues to be discussed before their formal presentation at large summer conferences. The whole organization of this event is adapted to its character. Apart from standard oral and poster sessions there are also informal interactions extended practically around the clock. All this is enabled by the fact that these events are organized as a rule in a hotel, in which all participants stay. This is particularly useful at such multi-disciplinary event, to favour personal contacts, cross-fertilization and mutual understanding. Publications in the form of extended (2 pages) abstracts collected in the booklet are made available at the time of conference.

The multi-disciplinary approach of the actinides science field results in a large variety of topics including strongly correlated behaviour, superconductivity, quantum criticality; materials science; theory, electronic structure; nuclear fuel cycle; environment, inorganic and organometallic chemistry.

The decrease of interest of younger generation in science and more particularly in nuclear related matters, the specific constraint in the latter field on safety and security regulations, which lead to the concentration of research activities into specialized institutes, can have a potentially hazardous impact on maintaining information achievements among the young generation of researchers. These facts also strengthen the necessity to have a forum bringing together researchers from such specialized institutions with people (professors and students) from academia, with both sides profiting from such information exchange. Such interaction leads frequently to joint collaborations, exchanges of students, and for many young scientists, JdA is the first international meeting at which they can present and discuss their (preliminary) results in an International Conference environment but in a less formal atmosphere.

The "8th *School on Physics and Chemistry of the Actinides*" (SPCA) is organised as a tutorial session to JdA. The previous SPCA was held in 2008 in Wroclaw prior to the 38^{ièmes} Journées des Actinides.

We wish you a pleasant stay in Stará Lesná and a scientifically successful meeting

Organising committee

Technical information

Oral Presentation

All oral presentations will have 20 minutes (presentation/discussion 15/5 minutes). Authors and session chair persons are asked to strictly follow these time limits. Presentations must be made in Electronic Form (PowerPoint, PDF). Computerized projection facilities will be offered for oral presentations, including an LCD projector, a computer and a screen. Presentations from Personal Laptops will not be allowed. All speakers are required to submit an electronic version of their presentation by 8:00 pm of the day prior to their presentation. Presentations must be submitted in Microsoft Power Point format (but may be saved as a PDF). It is strongly recommended that speakers save their Power Point presentations with True Type fonts attached. Acceptable transfer media include: CD and USB flashdrive (memory sticks). All presentations will be scanned for viruses and subsequently loaded on the main projector computer for the following day presentations. Authors are strongly encouraged to bring an additional electronic copy for added security against unanticipated software/hardware anomalies. Presentations prepared on platforms other than Windows (Mac, etc.) should be checked by the Author for compatibility with the Windows Platform prior to the Presentation.

Posters

All posters are required to conform to Portrait Orientation. Poster Board dimensions are 1m wide x 1 m high. The organization will provide boards and materials to fix your poster. Please note that the poster room will be opened from Sunday to Tuesday. Hence, posters should be installed just after your arrival and must be removed by the end of the poster session.

Conference Secretary

A secretary board will be available during the whole conference in the reception room.

	Thursday ***7th April***	***Friday*** ***8th April***	***Saturday*** ***9th April***	
8:30 | 10:10		Thomas Gouder	James G. Tobin	**8:30 | 10:10**
		break	**break**	
10:20 | 12:00	***Registration***	Alexander Shick	Halevy Itzhak	**10:20 | 12:00**
12:00 | 13:00	***Lunch***	***Lunch***	***Lunch***	**13:00 | 13:00**
13:00 | 14:40	Tomasz Klimczuk	Mark Read	Halevy Itzhak	**13:00 | 14:40**
	break	**break**	**break**	
14:50 | 16:30	Antonio Pereira Gonçalves	Mark Read	Ladislav Havela	**14:50 | 16:30**
	break	**break**		
16:40 | 18:20				**16:40 | 18:20**
19:00 | 22:00	***Party***	***Dinner***		**19:00 | 22:00**

Tomasz Klimczuk (JRC-ITU, Germany): ▪ "Synthesis of actinide compounds"
Antonio Pereira Gonçalves (ITN, Portugal) ▪ "Phase diagrams for actinide intermetallics"
Thomas Gouder (JRC-ITU, Germany): ▪ "Surface science in actinides"
Mark Read (AWE, United Kingdom): ▪ "Computational Chemistry: Application in Actinide Simulation" Part I.
Mark Read (AWE, United Kingdom): ▪ "Computational Chemistry: Application in Actinide Simulation" Part II.
Alexander Shick (Institute of Physics, Czech Republic) ▪ "Electronic structure theories of actinides"
James G. Tobin (Lawrence Livermore National Laboratory, USA): ▪ "Soft x-ray and Vacuum Ultraviolet based Spectroscopy of the Actinides"
Halevy Itzhak (NRCN, Israel) ▪ "Mossbauer spectroscopy, traditional and with synchrotron radiation"
Halevy Itzhak (NRCN, Israel) ▪ "High pressure research, technique , tools and new results"
Ladislav Havela (Charles University, Czech Republic) ▪ "Magnetic properties of actinides"

Saturday, 9th April 2011

17^{30}-19^{00}	**Registration**
19^{00}-22^{00}	**Welcome Party**

Sunday, 10th April 2011

9^{00} - 9^{10}	**Welcome address**
9^{10} - 10^{50} **Sunday**	**Session I** STRONGLY CORRELATED BEHAVIOUR, SUPERCONDUCTIVITY, QUANTUM CRITICALITY
9^{10} - 9^{30}	**1O1** Investigation of the Unoccupied Electronic Structure of UO_2 with BIS and XAS *J.G. Tobin, S.-W. Yu, J. C. Crowhurst, S. Sharma, J. K. Dewhurst, P. Olalde-Velasco, W. L. Yang, W. J. Siekhaus*
9^{30} - 9^{50}	**1O5** Magnetic Properties of Epitaxial UO_2 Thin Films *R. Springell, Z. Bao, R. Caciuffo, T. Gouder, H. Walker, G.H. Lander*
9^{50} - 10^{10}	**1O10** Localization vs Delocalization: Model Calculations for Electron Spectroscopies in 5f Systems *Gertrud Zwicknagl*
10^{10} - 10^{30}	**1O8** $Pu_{19}Os$ Simulating β-Pu as the Most Strongly Correlated Plutonium Phase *Ladislav Havela, Silvie Mašková, Rachel Eloirdi, Jean-Christophe Griveau, Eric Colineau, Alexander Shick*
10^{30} - 10^{50}	**1O9** Basic properties of the First Actinide Based Oxypnictide Compound: NpFeAsO *Tomasz Klimczuk, R. Springell, H. C. Walker, E. Colineau, J.-C. Griveau, D. Bouexière, R. Eloirdi, P. Gaczyński, R. J. Cava and R. Caciuffo*

10^{50} - 11^{20}	**Coffee break**

11^{20} - 13^{00} Sunday	**Session II** STRONGLY CORRELATED BEHAVIOUR, SUPERCONDUCTIVITY, QUANTUM CRITICALITY
11^{20} - 11^{40}	**1O2** Magnetic, Electrical and Thermodynamic Properties of $UCuT_xAl_{11-x}$ Alloys where T = Mn, Fe and x = 4 and 5 *Adam Pikul, Wojciech Suski, Konrad Wochowski, Andrzej Gilewski, Tadeusz Mydlarz and Dariusz Badurski*
11^{40} - 12^{00}	**1O3** Dual Character of 5f Electrons, the Case of Antiferromagnetic UN. Comparison with Other Uranium Compounds *R. Troć, M. Samsel-Czekała*
12^{00} - 12^{20}	**1O6** Sample Preparation and Low Temperature Properties of Some U Germanide Intermetallics *M.S. Henriques, J.-C. Griveau, A. Lignie, L.C.J. Pereira, E.B. Lopes, S. Surblé, L. Havela, E. Santava, S. Heathman, O. Tougait, A.P. Gonçalves*
12^{20} - 12^{40}	**1O4** 5*f* magnetism of UTGe Compounds Affected by Hydrogenation *A. M. Adamska, L. Havela, Nhu-T.H. Kim-Ngan*
12^{40}-13^{00}	**1O7** Magnetic and Lattice Anisotropies in U_2Ni_2Sn *S. Mašková, L. Havela, A. V. Andreev, S. Daniš, Y. Skourski, J. Wosnitza K. Kothapalli, H. Nakotte*

13^{00} - 15^{00}	**Lunch**

15^{00} – 16^{40} Sunday	**Session III** THEORY, ELECTRONIC STRUCTURE
15^{00} – 15^{20}	**2O1** Electronic Structure of Plutonium Hydrides: DFT + *U* Calculations in the FPLAPW Basis *Bingyun Ao, Juanjuan Ai, Tao Gao, Xiaolin Wang*
15^{20} – 15^{40}	**2O2** Electronic structure of $(U;Ce)Ru_2Al_{10}$ by first-principles calculations and X-ray photoemission *M. Samsel-Czekała, E. Talik, M. Pasturel, R. Troć*
15^{40} – 16^{00}	**2O3** Prediction of Giant Spin Hall Effect Due to Uranium Impurities in Gold *A. B. Shick and L. Havela*
16^{00} – 16^{20}	**2O4** *Ab initio* Investigation of Electronic Structure of Actinide 218 Materials *Jan Rusz, Saad Elgazzar, P. M. Oppeneer, E. Colineau, J.-C. Griveau, N. Magnani, J. Rebizant and R. Caciuffo*

$16^{20} – 16^{40}$	**2O5** Atomistic Simulation of Pure and Defected Uranium Dioxide Bulk and Surfaces *Mark S D Read*

$16^{40} – 17^{00}$	**Coffee break**

$17^{00} – 18^{20}$ **Sunday**	**Session IV** MATERIALS SCIENCE
$17^{00} – 17^{20}$	**3O2** Is There an Ordered Magnetic Structure in U_2Fe_3X (X = Si, Ge)? *El'ad N. Caspi, Itzhak Halevy, Oleg Rivin, Hanania Ettedgui, Shay Salhov*
$17^{20} – 17^{40}$	**3O5** U-Mo alloys prepared by splat cooling *Nhu-T.H. Kim-Ngan, L. Havela, A.M. Adamska, J. Kastil, J. Prchal, I. Tkach*
$17^{40} – 18^{00}$	**3O9** Structural inSights into the Nucleation and Early Stages of Hydride Formation on Uranium. *T. B. Scott, J. Petherbridge, C.P. Jones and J. Glascott*
$18^{00} – 18^{20}$	**3O4** Thermodynamic Investigations of the Actinide Oxides *Octavian S.Vălu, Ondrej Beneš, Rudy J. M. Konings*

$19^{00} – 20^{30}$	**Dinner**

Monday, 11th April 2011

$9^{00} – 10^{40}$ **Monday**	**Session V** MATERIALS SCIENCE
$9^{00} – 9^{20}$	**3O1** Atomistic Model of Helium in Plutonium *P.H.Chen, B.Y.Ao, X.C.Lai, X.L.Wang*
$9^{20} – 9^{40}$	**3O3** Development of Ce-La Alloys as Pu-Ga Surrogate Alloys *Michael Ling*
$9^{40} – 10^{00}$	**3O7** Surprising Reduction of Surface PuO_2 by an Adsorbed Ice Layer *T. Gouder and A. Seibert*
$10^{00} – 10^{20}$	**3O8** Magnetic Properties, Crystallographic Structure and Electronic Properties of Np_2Co_{17} and Np_2Ni_{17} *A. Hen , I. Halevy, E. Collino, R. Eloirdi, J-C. Griveau, P. Gaczynski, E.N. Caspi, G. Kimmel, I. Yaar, W. Potzel, R.G.M. Caciuffo and J. Gal*

$10^{20} – 10^{40}$	**3O6** X-ray and ^{237}Np Mössbauer Effect Study of NpPtSn *P. Gaczyński, T. Klimczuk, E. Colineau, K. Gofryk, J.-C. Griveau, R. Eloirdi, R. Jardin, F. Wastin, J. Rebizant and R. Caciuffo*

$10^{40} – 11^{00}$	**Coffee break**

$11^{00} – 12^{20}$ **Monday**	**Session VI** NUCLEAR FUEL CYCLE, ENVIRONMENT
$11^{00} – 11^{20}$	**4O1** Two-Step Excitation of Chemiluminescence in Detection of Trace Amounts of Lanthanides and Actinides in Solutions *I.N. Izosimov, N.G. Gorshkov, V.A. Mikhalev, S.N. Nekhoroshkov, Yu. I. Trifonov, N.G. Firsin*
$11^{20} – 11^{40}$	**4O2** Ecological Aspects of Nuclear Facility Decommissioning *Alojz Slaninka, Ondrej Slávik, Vladimír Míchal*
$11^{40} – 12^{00}$	**4O3** Uranium(IV)-silica Colloids at Near-neutral pH *Harald Zänker, Stephan Weiss, Christoph Hennig, Isabell Dreissig, Gert Bernhard*
$12^{00} – 12^{20}$	**4O4** Resonance Ionization Mass Spectrometry (RIMS) for Ultratrace Determination of Neptunium-237 *N. Stöbener, S. Raeder, T. Gottwald, G. Passler, T. Reich, N. Trautmann, K. Wendt*

13^{00} - 15^{00}	**Lunch**

$14^{00} – 15^{00}$	**International Advisory Committee meeting**

15^{00} - 19^{00}	**Trips in High Tatra**

$19^{00} – 23^{00}$	**Conference Dinner**

Tuesday, 12th April 2011

$9^{00} – 10^{40}$ Tuesday	**Session VII** NUCLEAR FUEL CYCLE, ENVIRONMENT INORGANIC AND ORGANOMETALLIC CHEMISTRY
$9^{00} – 9^{20}$	**4O5** Uptake of Np(V) by Natural Clay – A Micro-scale Spectroscopic Study *Daniel R. Fröhlich, Samer Amayri, Jakob Drebert, Joachim Krause, Tobias Reich*
$9^{20} – 9^{40}$	**4O6** Water Chemisorption on a Sputterdeposited Uranium Dioxide Film – Effect of Defects *S. Cohen, N. Shamir, S. Zalkind, A. Seibert, T. Gouder and M. H. Mintz*
$9^{40} – 10^{00}$	**4O8** Extraction Properties of Thiacalixarene Dendrimer Molecules *Špendlíková Irena, John Jan, Lhoták Pavel*
$10^{00} – 10^{20}$	**4O9** Separation of Curium from Americium *Kamila Šťastná*
$10^{20} – 10^{40}$	**5O1** Uranyl Interaction with Short Chain Carboxylic Acids in Aqueous Solutions Studied by Time-resolved Laser-induced Fluorescence Spectroscopy (TRLFS) *Vladimir Sladkov, Nicole Barre*

$10^{40} – 11^{00}$	**Coffee break**

$11^{00} – 12^{00}$ Tuesday	**Poster Session**

$12^{00} – 12^{50}$ Tuesday	**Session VII** CONFERENCE SUMMARY
$12^{00} – 12^{20}$	Chemistry
$12^{20} – 12^{40}$	Physics
$12^{40} – 12^{50}$	Announcements on the 42JdA and 43JdA

$13^{00} – 15^{00}$	**Lunch**

Posters
1P1 Evidence of Superconductivity for a UFeGe Sample *A.P. Gonçalves, M.S. Henriques, M. Almeida, L. Havela, A. Adamska, O. Tougait, J.S. Brooks, A. Kiswandhi, E. Steven*
1P2 High-Pressure Resistivity of UPd_3 *Jiří Prchal, Ladislav Havela, Alexander V. Andreev*
3P1 Observations and Characterisation of Helium Bubbles in Aged Plutonium Subjected to Extended Heat Treatments *D.W. Wheeler, P.D. Bayer, M.B. Matthews, M. Brierley*
3P2 Phase Equilibrium, Crystal Structure and Physical Properties of Compounds in the U-Mo-B System *Leonid Salamakha, Ernst Bauer, Herwig Michor, Gerfried Hilscher, Corrado Rizzoli, Oksana Sologub, Antonio Gonçalves , Stepan Mudryi*
3P3 Self-irradiation effects on the static strength of Pu and Pu-Ga alloys *Brandon W. Chung, David S. Hiromoto*
3P4 Crystal Structures of Binary U-Ru Compounds *M. Pasturel, A. P. Gonçalves, O. Tougait, H. Noël*
3P5 A New Experimental Perspective on the $U-O_2-H_2O$ Reaction System *N. Harker, T. B. Scott, J. Petherbridge, and J. Glascott*
3P6 Mapping of Magnetization Densities in UNi_2 by Polarized Neutron Diffraction *Arsen Gukasov, Marián Mihalik, Mária Zentková, Slavomír Maťaš, Karel Prokeš*
4P1 Extraction and Immobilization of Strontium in the Silicoantimonates *Yu. Kuryleva, A. Shumikhina, D. Zakharyevich*
4P2 Uranium(V) Species in Alkali Chloride Based Melts *Dmitry S. Maltsev, Vladimir A. Volkovich, Denis E. Aleksandrov, Boris D. Vasin*
4P3 Sorption of Neptunium(V) on Mackinawite (FeS) *M. Lübke, J. Drebert, T. Reich*
5P1 Thorium and Uranium Carbide Cluster Cations in the Gas Phase *António P. Gonçalves, Ana F. Lucena, Cláudia C. L. Pereira, Joaquim Marçalo, John K. Gibson, Lester Andrews*

Investigation of the Unoccupied Electronic Structure of UO_2 with BIS and XAS

J.G. Tobin[1], S.-W. Yu[1], J. C. Crowhurst[1], S. Sharma[2], J. K. Dewhurst[2], P. Olalde-Velasco[3,4], W. L. Yang[3], W. J. Siekhaus[1]

[1] *Lawrence Livermore National Laboratory, Livermore, CA, USA, 94550, e-mail: Tobin1@LLNL.Gov*
[2] *Max-Planck Institute for Microstructure Physics Weinberg 2, Halle, Germany*
[3] *Advanced Light Source, Lawrence Berkeley National Laboratory, Berkeley, CA, USA*
[4] *Instituto de Ciencias Nucleares, UNAM, Mexico, Distrito Federal 04510,*

As part of an effort to probe the electronic structure of 4f [1] and 5f [2] oxides, Bremstrahlung Isochromat Spectroscopy (BIS or high energy Inverse Photoelectron Spectroscopy) [1] and X-ray Absorption Spectroscopy (XAS) have been carried out upon uranium dioxide. These measurements will be set within the context of our recent X-ray Emission (XES) and Resonant Inverse Photoelectron Spectroscopy (RIPES) investigations of Uranium and Cerium Oxides [1 - 4]. In XAS measurements at the Advanced Light Source (ALS), the O1s, U4d, U4f, and U5d spectral structures were observed. The O1s, $U4d_{5/2}$ and $U4f_{7/2}$ X-ray absorption spectra have been used to sort the energetic positions of the O2p, U5f and U6d states within the unoccupied bands, i.e the conduction bands of UO_2. Calculations performed within the Uncorrected generalized gradient approximation of the optical response of UO_2 permit direct comparison with the absorption spectra and confirm the experimental results. These results support the contention that UO_2 is an f-f Mott-Hubbard insulator, where the electronic repulsion between 5f electrons is responsible for the insulating state.

References

[1] J.G. Tobin, S.W. Yu, B.W. Chung, G.D. Waddill, L. Duda and J. Nordgren, "Observation of Strong Resonant Behavior in the Inverse Photoelectron Spectroscopy of Ce Oxide," Phys. Rev. B, in press (2011).
[2] S.-W. Yu and J.G. Tobin, "Confirmation of Sample Quality: X-ray and Ultraviolet Photoelectron Spectroscopy of Uranium Dioxide," J. Vac. Sci. Tech. A, in press (2011).
[3] J.G. Tobin, S.W. Yu, B.W. Chung, G.D. Waddill, and J. D. Denlinger, "Direct Comparison of the X-ray Emission and Absorption of Cerium Oxide," J. Vac. Sci. Tech. A, under submission (2011).
[4] J.G. Tobin, S.-W. Yu, B.W. Chung, G.D. Waddill and AL Kutepov, "Narrowing the Range of Possible Solutions to the Pu Electronic Structure Problem: Developing a new Bremstrahlung Isochromat Spectroscopy Capability," IOP Conf. Series: Materials Science and Engineering **9** (2010); 012054 doi:10.1088/1757-899X/9/1/012054.

Acknowledgements

Lawrence Livermore National Laboratory is operated by Lawrence Livermore National Security, LLC, for the U.S. Department of Energy, National Nuclear Security Administration under Contract DE-AC52-07NA27344. Some of the work, performed by JGT and SWY, was supported by the DOE Office of Science, Office of Basic Energy Science, Division of Materials Science and Engineering. Partial funding was also provided by Laboratory Directed Research and Development (LDRD) Program (10-SI-016) of Lawrence Livermore National Laboratory. The Advanced Light Source (ALS) is supported by the Director, Office of Science, Office of Basic Energy Sciences, of the U.S. Department of Energy under Contract No. DE-AC02-05CH11231.

Magnetic, Electrical and Thermodynamic Properties of $UCuT_xAl_{11-x}$ Alloys where T = Mn, Fe and x = 4 and 5

Adam Pikul[1], Wojciech Suski[1,2], Konrad Wochowski[1], Andrzej Gilewski[2], Tadeusz Mydlarz[2] and Dariusz Badurski[1]

[1]Polish Academy of Sciences, W.Trzebiatowski Institute of Low Temperature and Structure Research, P.O.Box 1410, 50-950 Wrocław 2, Poland, e-mail: w.suski@int.pan.wroc.pl
[2]International Laboratory of High Magnetic Fields and Low Temperatures, P.O.Box 4714, 50-985 Wrocław 47, Poland

The magnetic, electrical and thermodynamic properties of $UCuT_xAl_{11-x}$ alloys, where T = Mn or Fe and x = 4 or 5 are presented. The behavior of the Fe alloys is ferromagnetic-like with the Curie points amounting to 180 and 230 K, and the saturation magnetic moments under magnetic field of 5 T equal to 4.75 and 6.02 μ_B/f.u., respectively, whereas under magnetic field of about 34 T the magnetic moments amount to 6.9 and 9.0 μ_B/f.u. for the alloys with x = 4 and 5, respectively (Fig.1). The Curie points are reflected in the temperature dependence of the specific heat in which the anomalies are found at 180 - 200 and 230 K for alloys with x = 4 and 5, respectively (Fig.2a,b,c,d), however it has not reflection in the temprature dependence of the electrical resistivity (Fig.3). The field dependence of magnetization at T = 1.9 K for both compounds exhibits considerable hysteresis. There is pronounced difference between ZFC and FC magnetization in its temperature dependence below the Curie point for materials with x = 4 and 5. The Mn alloys exhibit ferrimagnetic-like character for which, supposedly, an interplay of the uranium and manganize sublattices are responsible. Magnetic transitions are determined at T_N = 300 (x = 4) and 380 K (x = 5). However, those anomalies do not find a confirmation in the temperature dependence of the specific heat and the electrical resistivity. Magnetic moments determined at T = 1.9 K and in magnetic field of 5T are very low and in both cases amount to about 0.35 μ_B/f.u. and these values are slightly higher in the magnetic field of 34 T reaching value of about 1.5 μ_B/f.u. Also for the Mn alloys the clear difference between ZFC and FC magnetization in its temperature dependence below the Curie point is observed. The temperature dependence of the reciprocal magnetic susceptibility χ^{-1} of the Fe alloys obtained in magnetic field of 100 Oe. The approximately linear temperature dependence of χ^{-1} is observed above T = 250 K and 210 K for x = 5 and 4, respectively. The linear part can be described by modified Curie-Weiss law. The temperature independent part of magnetic susceptibility is small, whereas the effective magnetic moments and the Weiss constant are higher for the alloy with x = 5.

The electrical resistivity versus temperature of all investigated materials is weakly temperature dependent with low RRR. We do not know if this feature is innate for these materials or only results from imperfections of the samples.

The termodynamic properties of the $UCuT_xAl_{11-x}$ alloys are presented in Fig.2a-d The specific heat versus temperature in each case presents in principle smooth curves and for the Fe alloys weak anomalies corresponding to the Curie points (arrows in Figs.) are seen. The insets present the $C/Tvs.T^2$ dependences at low temperature which allows to determine the cofficient of eletronic specific heat, γ and the Debye temperature, Θ_D. For the Fe alloys γ is moderately enhanced, possible due the magnetic ordering, however, for the Mn compounds this enhacement is substantial. Unfortunatelly, we cannot present any firm conclusion about its reason. Moreover these data are not very precize because we have no results for nonmagnetic references.

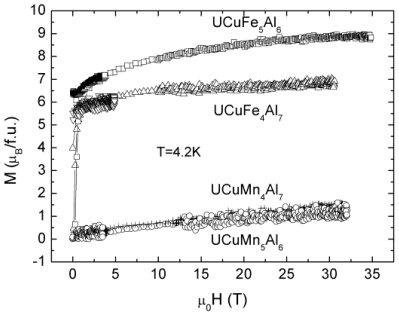

Fig. 1. Magnetization vs. temperature at 4.2 K.

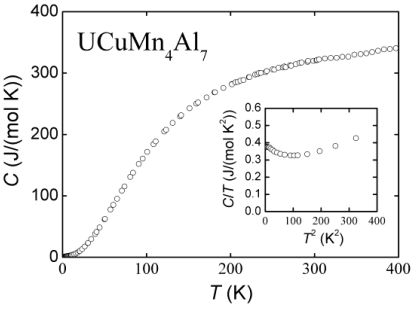

Fig. 2 c. Specific heat vs. temperature.

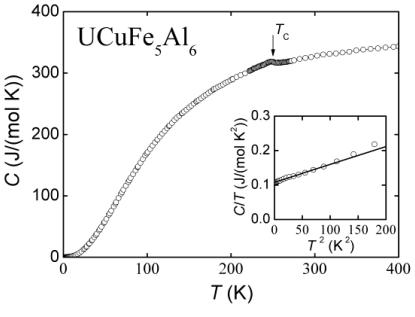

Fig. 2 a. Specific heat vs. temperature.

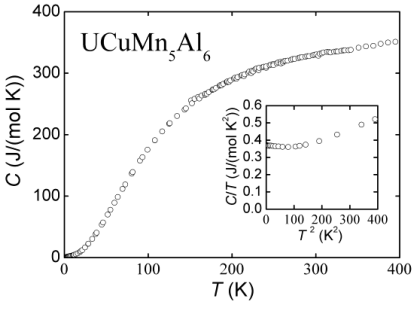

Fig. 2 d. Specific heat vs. temperature.

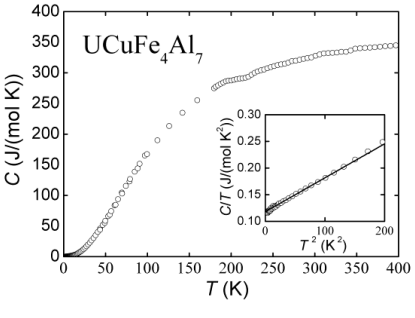

Fig. 2 b. Specific heat vs. temperature.

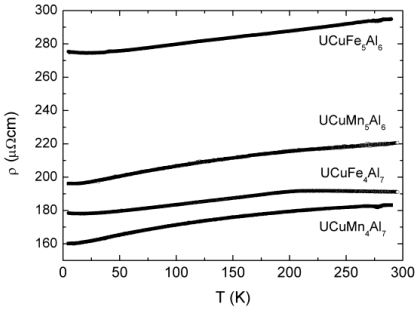

Fig. 3. Electrical resistivity vs. temperature.

Dual Character of 5f Electrons, the Case of Antiferromagnetic UN. Comparison with Other Uranium Compounds

R. Troć, M. Samsel-Czekała

Institute of Low Temperature and Structure Research, Polish Academy of Sciences, Okólna 2, 50-422 Wrocław, Poland, e-mail: r.troc@int.pan.wroc.pl

The question arising from recent theoretical and experimental reports on so-called dual phenomenon of 5f electrons seems to be the key question in understanding a large diversity and complexity in the physical properties observed for numerous uranium binary and ternary compounds. The electronic properties of these materials are a result of some competition between the tendency towards delocalization of these electrons due to hybridization with conduction electrons and a simultaneous formation of local moments capable to become magnetically ordered at lower temperatures. Such a competition finally leads to the co-existence of two different states, i.e localized and itinerant band-like ones. This feature becomes possible due to a sufficient number of initial 5f electrons in a uranium atom, N=3, i.e. $5f^3$ configuration. From this total number roughly two electrons can be treated as localized while the remaining 5f electron becomes band-like. It seems that such a differentiated division among the 5f electrons of uranium takes place below some determined temperature. As an example of such a puzzling phenomenon of the 5f electrons we present here the behavior of the mononitride UN, crystallizing in a simple crystal structure of NaCl type. Very early studies of this compound established an antiferromagnetic (AFM) order of the type I with T_N = 53 K. Numerous authors who studied this nitride even at present time regard that all 5f electrons in UN have an itinerant nature, which leads also to an itinerant character of antiferromagnetism occurring in this compound. In our recent ample paper on UN [1], we have found also good agreement between band structure and our photoelectron spectroscopy (XPS) study like other authors applying even more modern spectroscopy measurements. However, one should take into account also the other aspect of properties of UN being closed to atomic-like ones. In our work [1], we showed that, except for following almost strictly a Curie-Weiss behavior and high value of the effective moment (μ_{eff} = 2.7 μ_B), the resistivity curve above T_N is reminiscent of the ones observed in numerous rare-earth compounds, explained in terms of scattering conduction electrons by localized 5f electrons, perturbed by the crystal electrical field. To the same conclusions one can come considering other transport and thermal behaviors of UN [1]. The problem starts when one considers the AFM state. On the one hand, this AFM state of UN is stable in applied magnetic fields up to 35 T [2] like that in URu_2Si_2, where the presence of $5f^2$ localized state has been undoubtedly proved, but on the other hand in this nitride just below T_N, the resistivity curves $\rho(T)$ show along all three main crystallographic directions a weak rise and passing through a small maximum (hump) suggesting a decrease of the number of conduction electrons (see Fig. 1). This feature probably arises from a partial gapping of the Fermi surface (FS) and is reminiscent of that observed in metallic Cr. In the literature, such small humps on $\rho(T)$ have been reported in the cases of several uranium compounds, like UCu_5, UGe_2, URu_2Si_2, $UNiGa_5$, and others. A similarity of the hump, shown in Fig. 1, to that observed for metallic Cr leads to speculations about developing of spin density wave (SDW) state in UN and in the compounds mentioned above by the hybridized part of 5f electrons except for a normal AFM order of localized part of these electrons. The additional presence of the SDW order implies a substantial change in transport and thermal behaviors and leads to an evolution of some sort of small moment of the

order of 10^{-2} μ_B (too small to be seen by neutrons), which coexists with a well established AFM order with much larger moment probably induced by a molecular field of two interacting singlets, as is e.g. the case of URu_2Si_2. The analysis of specific heat results [3] obtained for UN, where we have not observed any change upon applying the magnetic fields as high as 9 T, confirms in similar way as the high field magnetization study mentioned above that the magnetic order in UN has not an itinerant nature. This can be only negligibly modulated by the presence of the SDW effect, however, invisible by neutron diffraction scattering. On the other hand, this effect may be deduced from analyzing nesting properties of the Fermi surface, presented here for the first time.

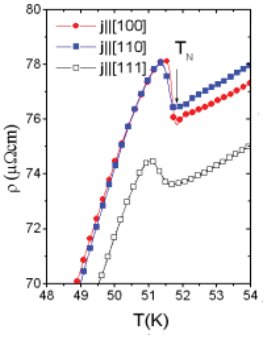

Fig. 1. Peaks of electrical resistivity in UN, occurring just below T_N, measured for current **j** along three main crystallographic directions (inset to Fig. 7 in Ref. [1]).

Our non-spin-polarized FS in UN was calculated using the fully relativistic local-orbital (FPLO) code [4] in the local density approximation (LDA) approach, based on band structure results presented in [1]. The FS is formed by two sheets originated from two conduction bands. The small FS sheet, coming from the upper band, consists of only small electron cigars. The large FS sheet, originating from the lower band (visualized in Fig. 2) contains hollike structure, open along the ΓX lines (i.e. along the three equivalent crystal axes [100]=[010]=[001] in the fcc unit cell). This FS sheet along the ΓX direction and equivalent exhibits nesting properties with nesting vectors (marked in Fig. 2) having their length equal to 0.5|ΓX|. This nesting vectors can be responsible for arising AFM SDW as in Cr, possible along the three main crystallographic axes. Therefore, in this presentation we will concentrate on the comparison of the electronic structure with this canonic example of the SDW behavior as is the Cr metal.

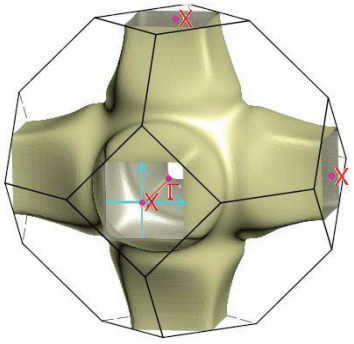

Fig. 2. The lower-band FS sheet of UN, calculated in the LDA approach, drawn in the BZ boundaries. It contains holes inside and two equivalent nesting vectors are marked by blue arrows.

References

[1] M. Samsel-Czekała et al., *Phys. Rev. B* **76**, 144426 (2007).
[2] C.J. Shinkel, R Troć, *J. Magn. Magn. Mater.* **9**, 339 (1978).
[3] R. Troć, A. Pikul, in: Abstract booklet of 38 Journées des Actinides (Wrocław 2008), p. 147 (S-25).
[4] K. Koepernik, H. Eschrig, *Phys. Rev. B* **59**, 1743 (1999); FPLO code (http://www.FPLO.de; version 5.00-18)

5*f* magnetism of UTGe Compounds Affected by Hydrogenation

A. M. Adamska[1,2], **L. Havela**[1], **Nhu-T.H. Kim-Ngan**[3]

[1] *Department of Condensed Matter Physics, Charles University, Prague, The Czech Republic, e-mail: anna@mag.mff.cuni.cz*
[2] *Faculty of Physics and Applied Computer Science, AGH University of Science and Technology, Kraków, Poland*
[3] *Institute of Physics, Pedagogical University, Kraków, Poland*

Intermetallic compounds of 5*f* elements, including uranium, are particularly sensitive to hydrogen absorption. In the case of purely band systems the most important parameter determining the magnetic properties is the interatomic distances between e.g. uranium atoms. However, most of uranium intermetallics are characterized by a 5*f*-ligand hybridisation, then the strength of hybridisation becomes a crucial parameter. Hydrogen intrusion can easily modify the hybridised band by withdrawing electronic states due to bonding with the atoms which contribute to the band. Hydrogenation of UTSi compounds, where T = Co, Pd, Ni [1,2] and UTGe compounds, where T = Fe, Co, Rh [3] led to a notable lattice expansion and an increase of respective magnetic ordering temperatures. Our results on the hydrides of the compounds with UTGe stoichiometry (T – chosen 3 *d*, 4 *d*, 5 *d* transition metal) complete the study. Fig. 1 shows the types of crystal structure adopted by hydrogenated UTGe compounds depending on the hydrogen content. In Fig. 2, one can observe the variations of magnetic ordering temperatures of the UTGe hydrides and their parent compounds (T_C/T_N for pure UTGe are shown by black, white triangles connected by dashed line as a guide to eye).

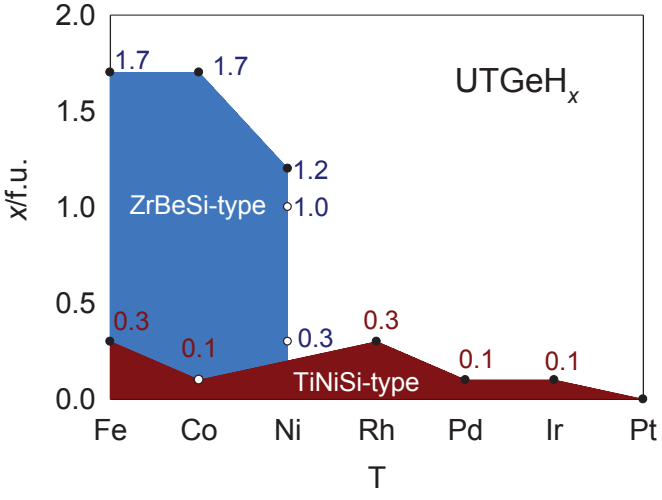

Fig. 1. Two types of UTGe hydrides and their H concentration.

In the case of UFeGe and UCoGe, two types of hydrides can be formed. Low H_2 pressure (2 bar) transformed the monoclinic type of structure of UFeGe into the standard TiNiSi-type, expanded by about 0.5 %. The highest applied H_2 pressure of ≈ 160 bar resulted in the β-hydride, which crystallizes in the hexagonal ZrBeSi-type of structure, reaching 5.5 % volume expansion and 1.7 H/f.u. As in parent compound none of the hydrides reveals any real magnetic order. Hydrogenating UCoGe under p_{H2} = 0.5 bar one can obtain an α-hydride with

small volume expansion of 0.1 % and H content of 0.1 H/f.u. The hydride is non-magnetic and non-supercoducting in contrast to pure UCoGe (a ferromagnet with $T_C \approx 3$ K and superconductor with $T_{sc} \approx 0.4$ K) [4]. The hydrogenation under the H_2 pressure of 2 bar allowed to obtain the stable β-hydride ($UCoGeH_{1.7}$), crystallizing in ZrBeSi-type of stucture. The volume expands by 10.7 % and T_C increases up to ≈ 50 K.

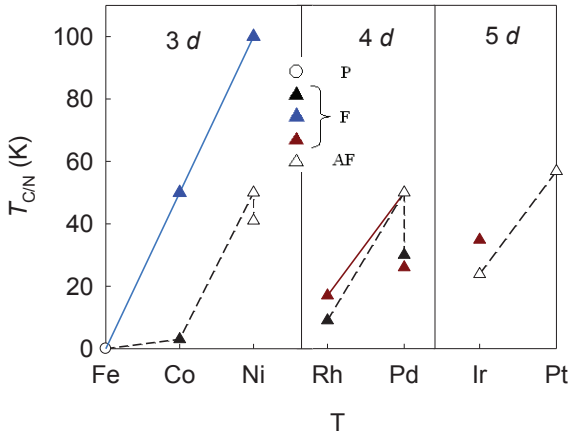

Fig. 2. An illustration of the change of the critical temperatures for UTGe hydrides (blue and brown triangles) in respect to parent compounds (black and white triangles).

The hydrogenation of UNiGe at high pressures yields $UNiGeH_{1.2}$ with the ZrBeSi type of structure; the volume expands by 7.6 %. Pure UNiGe exhibits two antiferromagnetic phase transitions, one below below $T_N \approx 42$-44 K [5] and the second one just below 50 K [6], whereas $UNiGeH_{1.2}$ is a ferromagnet with T_C around 100 K. Other intermediate hydrides of UNiGe ($UNiGeH_{1.0}$ and $UNiGeH_{0.3}$), obtained at hydrogen pressure of 2 bar and less exhibit two phase transitions, the antiferromagnetic one with T_N below 35-38 K and most probably an uncompensated antiferromagnetic phase below 7-10 K. No formation of α-hydride was observed. In the case of new α-hydride of URhGe (TiNiSi type of structure) with hydroden concentracion of 0.3 H/f.u. and the volume expansion of 1.3 %, T_C was shifted from 9 K for URhGe [5] up to 17 K for the hydride. Hydrogenation of UPdGe and UIrGe did not change the TiNiSi type of sturcture, it leads only to the volume expansion of 0.5 % and 0.7 %, respectively. For UPdGe, two phase transitions were reported, the ferromagnetic one at $T_C \approx$ 30 K and the antiferromagnetic one at $T_N \approx 50$ K [5]. Hydrogen absorption in UPdGe does not change T_N, but it leads to a decrease of T_C to 26 K. In the case of UIrGe, the antiferromagnetic ground state ($T_N \approx 16$ K) [5] was transformed into ferromagnetic one for $UIrGeH_{0.1}$. Such a transition was revealed by a well-pronounced but broad peak of *ac* susceptibility with maximum around 30 K. The onset of ferromagnetism can be assumed around 40 K, but the system looks magnetically inhomogeneous. No hydrogen absorption is reported for UPtGe.

References

[1] K. Miliyanchuk et al., *J. Alloys Comp.* **383,** 103-107 (2004).
[2] A.V. Kolomiets et al., *Phys. Rev. B* **66,** 144423 (2002).
[3] A.M. Adamska et al., *IOP Conf. Ser.: Mater. Sci. Eng.* **9** 012051 (2010).
[4] N.T. Huy et al., *Phys. Rev. Lett.* **99**, 067006 (2007).
[5] R. Troc et al., *J. Magn. Magn. Mater.* **73**, 389-397 (1988).
[6] A. Purwanto et al., *Phys. Rev. B* **53**, 759-765 (1996).

Magnetic Properties of Epitaxial UO_2 Thin Films

R. Springell[1], Z. Bao[2], R. Caciuffo[2], T. Gouder[2], H. Walker[3], G.H.Lander[4]

[1] *Department of Physics and Astronomy, University College London, LondonWC1E 6BT, UK*
[2] *European Commission, Joint Research Center, Institute for Transuranium Elements, Postfach 2340, D-76125 Karlsruhe, Germany, e-mail: Zhaohui.Bao@eu.europa.ec*
[3] *European Synchrotron Radiation Facility, Boite Postale 220X, F-38043 Grenoble, France*
[4] *Institut Laue-Langevin (ILL) 6 rue Jules Horowitz BP 156, 38042 Grenoble Cedex 9, France*

As one of the most investigated actinide compounds, UO_2 exhibits many interesting properties resulting from the behaviors of 5f electrons. Magnetic ordering of the bulk UO_2 has been reported over last decades by variety techniques, the transition to an antiferromagnetic (AF) state occurs at T_N = 30.8K [1]. However, analyzing the magnetic properties of thin films allow us to have a better understanding of the order-disorder phase transition related to the surface effect.

In this work, thin films are prepared by reactive sputtering from 99.9% depleted uranium metal under an appropriate oxygen pressure at 600°C substrate temperature [2]. By using the substrate $LaAlO_3$, heteroepitaxial films are obtained with thickness from 10 to 50nm. Films were covered by a protective capping layer (Mg). *In situ* XPS measurements confirm the right stoichiometry of the films.

We found an antiferromagnetic ordering on a sample of 17.8nm from resonant x-ray magnetic scattering (RXMS). The temperature dependence of the magnetic reflection at the Bragg peak (210) shows a continuous change in intensity; it is a clear second order transition, where as the bulk is a first order one. Our result is consistent with the investigation near the surface of bulk UO_2 by Watson et al [3]. Fig.1 shows the normalized integrated intensity of magnetic scattering at Bragg peak (210). The scattering intensities near T_N are well described by a power law. As shown in Fig.1 the red solid fitting line corresponding to $I = I_0(1-T/T_N)^{\beta}$. The Néel temperature we observed is at 30.1K, with the exponent $\beta = 0.55$.

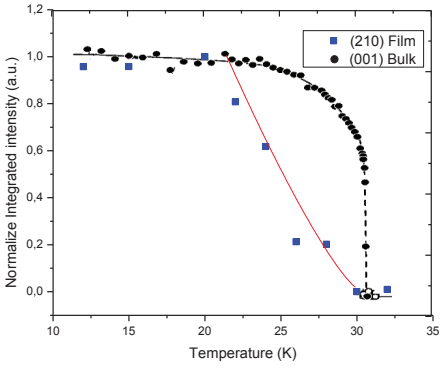

Fig. 1. Normalized temperature dependence of the magnetic scattering at the (210) Bragg peak (solid square), the solid line corresponds an exponent β = 0.55. The results taken from Watson et al [3] at (001) refection peak (solid circle) of a bulk sample.

Key words: *UO2, Epitaxial thin film, Sputtering, XPS, RXMS, Antiferromagnetic ordering, Néel Temperature, Surface effect*

References

[1] B.C Frazer et al. Phys. Rev. 17, 188 (1965).
[2] T.Gouder et al. Phys. Rev.B. 70, 235108 (2004)
[3] G.M Watson et al., Phys. Rev.B, 61, 8966 (2000).

Sample Preparation and Low Temperature Properties of Some U Germanide Intermetallics

M.S. Henriques[1], J.-C. Griveau[2], A. Lignie[3], L.C.J. Pereira[1], E.B. Lopes[1], S. Surblé[2], L. Havela[4], E. Santava[5], S. Heathman[2], O. Tougait[3], A.P. Gonçalves[1]

[1] Instituto Tecnológico e Nuclear/CFMC-UL, Estrada Nacional 10, 2686-953 Sacavém, Portugal
e-mail: mish@itn.pt
2 European Commission, Joint Research Center, Institute for Transuranium Elements, Postfach2340, 76125 Karlsruhe, Germany
3 Sciences Chimiques de Rennes, Chimie du Solide et Matériaux, Université Rennes 1, UMR CNRS 6226, 263 Avenue du Général Leclerc, 35042 Rennes, France
4 Dept. Condensed Matter Physics, Fac. Mathematics and Physics, Charles Univ., 12116 Prague, Czech Republic
5 Institute of Physics, Academy of Sciences of the Czech Republic, Prague 8, Czech Republic

Studies on binary and ternary intermetallic compounds containing U and Ge exhibit a wide variety of properties. One of the intriguing phenomena is the coexistence of superconductivity and ferromagnetism, reported first for UGe_2 (under pressure) [1] and URhGe [2], and later for UCoGe [3,4]. For these compounds the richness of the low temperature types of behaviour seems to arise due to an important combination of conditions: they should be close to the onset of magnetism (strongly paramagnetic or weakly ferromagnetic) and the specimens must have sufficiently high quality [1].
The interplay between competing interactions can be driven by external factors (as pressure, magnetic field or chemical doping), but also impurities have an important role in the delicate balance. The sample quality is thus of major concern for these compounds and a great emphasis has to be put on detailed analysis, considering phase transitions and phase diagrams. This can be done by X-ray diffraction, electron microscopy, and electrical transport measures. In particular, the resistivity curves can provide very clear information about the clean-limit condition through the Residual Resistivity Ratio (RRR), which is the ratio between sample resistivity at room temperature and the actual residual resistivity.
A short review will be presented about the relation of sample quality and low temperature phase diagrams for such exotic compounds UGe_2, URhGe and UCoGe. The unconventional superconductivity seems to be rather controlled by the annealing than by the sample preparation method. In addition, experimental results on attempts to tune the ferromagnetism of U_2Fe_3Ge by pressure and doping will also be discussed. According to X-ray diffraction measurements performed up to 25 GPa, there is no evidence of any structure phase transition (Fig. 1). When the sample is analyzed by resistivity under pressure, the T_C and RRR decrease as the pressure is increased up to 2.5 GPa. Above this pressure, the ferromagnetic transition cannot be followed any more, which can be attributed to the enhanced role of fluctuations near the transition and/or to increasing non-hydrostaticity. Doping of this compound with Si showed that T_C does not change significantly for Si contents up to 5%, but it changes by further substitution as shown in Fig. 2. Nevertheless, SEM-EDS analysis showed that secondary phases appear in the matrix in this case.

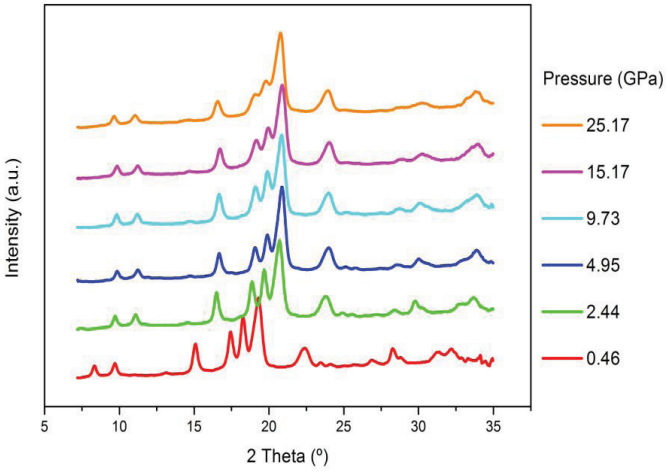

Fig.1. Evolution of the X-ray diffraction patterns for the U_2Fe_3Ge sample with increasing hydrostatic pressure.

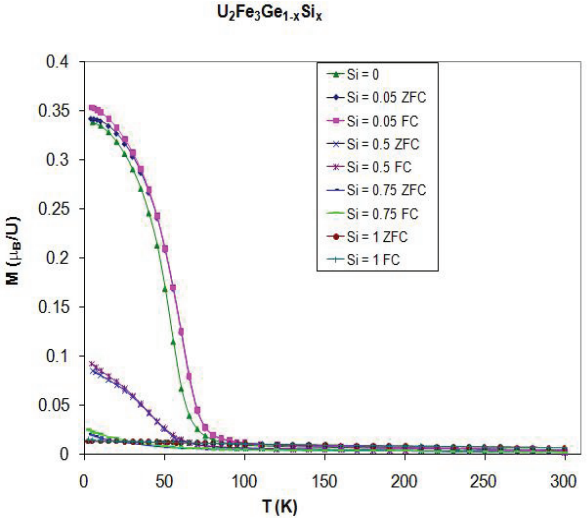

Fig.2. Magnetization as a function of temperature for $U_2Fe_3Ge_{(1-x)}Si_x$ samples.

References

[1] SS Saxena, P Agarwal et al., *Nature* **406** (2000) 587.
[2] D Aoki et al., *Nature* **413** (2001) 613.
[3] NT Huy et al., *Phys. Rev. Lett*. **99** (2007) 667006.
[4] E Hassinger et al., *J. Phys. Soc. Japan* **77** (2008) 073703.

Magnetic and Lattice Anisotropies in U_2Ni_2Sn

S. Mašková[1], L. Havela[1], A. V. Andreev[2], S. Daniš[1], Y. Skourski[3], J. Wosnitza[3], K. Kothapalli[4], H. Nakotte[4]

[1]*Department of Condensed Matter Physics, Charles University, Ke Karlovu 5, 12116 Prague 2, Czech Republic, e-mail: maskova@mag.mff.cuni.cz*
[2]*Institute of Physics, Academy of Sciences, Na Slovance 2, 18221 Prague, Czech Republic*
[3]*Hochfeld-Magnetlabor, FZ Dresden-Rossendorf, D-01314 Dresden, Germany*
[4]*Department of Physics, New Mexico State University, 88003-8001 Las Cruces, NM*

U_2Ni_2Sn represents an important case for considerations the origin of magnetic anisotropy in U intermetallics. Majority of U_2T_2X compounds, crystallizing in the tetragonal structure (Mo_2FeB_2 type), have the closest U-U spacing along the *c*-axis. Magnetic moments are, as a rule, in the basal plane. In U_2Ni_2Sn, the U-U spacing in the basal plane is slightly smaller. What is the anisotropy in this case? Existing reports are contradictory…

A powder neutron diffraction experiment revealed that the known antiferromagnetic order (T_N = 26 K) has a propagation vector $\boldsymbol{q}$ = (0,0,1/2) and AF coupling also within the basal plane [1]. But the interpretation in terms of a collinear structure with basal-plane orientation of the U-moments (μ_U = 1.05 μ_B) was somewhat preferred in this powder experiment, only later and never published neutron diffraction data on allegedly single crystalline sample probably pointed to *c*-axis orientation [2].

We have successfully prepared a single-crystal of U_2Ni_2Sn by Czochralski method (checked for a good quality by Laue method). The temperature dependence of the crystal structure parameters was studied by means of X-ray diffraction using Siemens D500 diffractometer (Co Kα radiation). The crystal structure refinement has been performed by FullProf software. The results of the refinement show that the *a*-parameter increases with increasing temperature (Fig. 1). On the contrary, the *c*-parameter of U_2Ni_2Sn is surprisingly decreasing within the whole *T*-range. Comparing to other previously studied 2:2:1 U-compounds, the *a*-parameter shows the opposite tendency than found for e.g. U_2Pd_2Sn [3], where it is the *a*-parameter, which increases with decreasing *T*. A relation to different magnetic coupling is unclear.

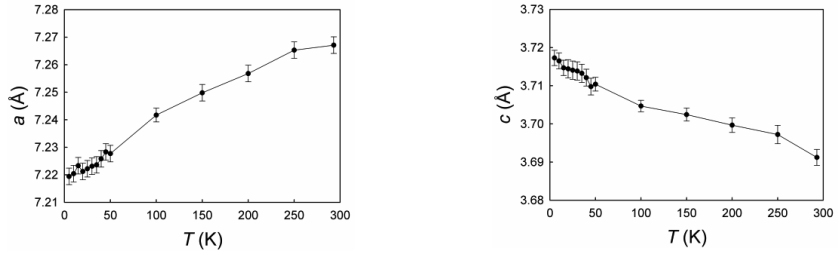

Fig. 1. Temperature dependence of lattice parameters *a* (left panel) and *c* (right panel) obtained from XRD.

So as to establish the magnetic anisotropy, the *T* dependence of magnetic susceptibility was measured along the *c*-axis and in the basal plane using a SQUID magnetometer (Fig. 2). It reveals that the *c*-axis is an easy axis of magnetization, supporting the rule with magnetic moments perpendicular to the shortest U-U direction. The magnetic susceptibility can be approximated by a Curie-Weiss law with an effective moment μ_{eff} = 3.8 μ_B/mol f.u. and

paramagnetic Curie temperature θ_p = -75 K for the susceptibility measured along the [001] direction and θ_p = -248 K in the basal plane. The measured paramagnetic moment μ_{eff} = 2.68 μ_B/U atom is far below the expected value for the localized $5f^3$ (U^{3+} – 3.62 μ_B) or $5f^2$ (U^{4+} – 3.58 μ_B) state.

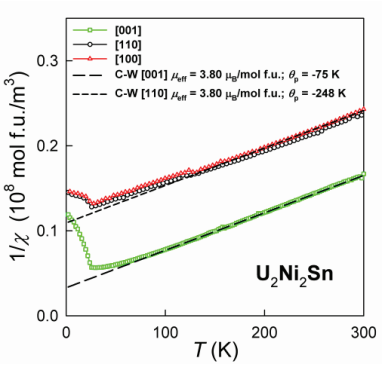

Fig. 2. Temperature dependence of inverse magnetic susceptibility in fields 3 T and 6 T applied along the main axes of the U_2Ni_2Sn single crystal. The dashed lines are C-W fits with parameters shown in the legend.

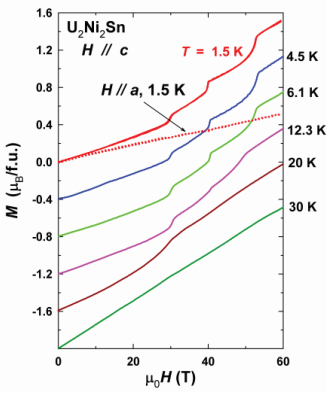

Fig. 3. High-field magnetization curves with magnetic field along the main crystallographic directions of the U_2Ni_2Sn single crystal at various temperatures.

The field dependence of magnetization shows 3 metamagnetic transitions at approx. 30, 39 and 50 T (Fig. 3). The magnetization does not show any tendency to saturation in the highest possible fields.

The specific heat (Fig. 4) shows a sharp magnetic phase transition at T_N = 26 K corroborating the results from magnetic measurements. The linear extrapolation of C_P/T vs. T^2 dependence to T = 0 K let us estimate the Sommerfeld coefficient γ = 200 mJ/mol f.u. K^2 (higher than reported earlier for a polycrystal [4]).

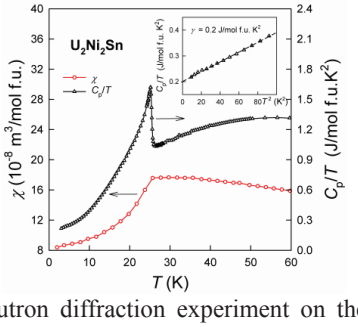

Fig. 4. Comparison of temperature dependence of the magnetic susceptibility along the main axes in magnetic field μ_0H = 3 T and the specific heat in form C_P/T (in zero field). The inset shows the linear extrapolation of C_P/T vs. T^2 dependence to T = 0 K.

A neutron diffraction experiment on the singe crystal is in progress so as to confirm the orientation of magnetic moments without magnetic field.

References

[1] F. Bourée, B. Chevalier, L. Fournès, F. Mirambet, T. Roisnel, V. H. Tran, and Z. Zolnierek, *J. Magn. Magn. Mater.* **138**, 307 (1994).

[2] D. Laffargue, B. Chevalier, S. F. Matar, and F. Bourée, *Proc. 26iémes Journées des Actinides* (1996), Sklarska Poreba, Poland, p. 53.

[3] A. Purwanto et al., *Phys. Rew.* B **50**, 6792 (1994).

[4] K. Kindo et al., *J. Mag. Mag. Mater.* **140-144**, 1369 (1995).

$Pu_{19}Os$ Simulating β-Pu as the Most Strongly Correlated Plutonium Phase

Ladislav Havela[1], Silvie Mašková[1], Rachel Eloirdi[2], Jean-Christophe Griveau[2], Eric Colineau[2], Alexander Shick[3]

[1] *Department of Condensed Matter Physics, Charles University, Ke Karlovu 5, CZ-12116 Prague 2, The Czech Republic Republic , e-mail: havela@mag.mff.cuni.cz*
[2] *European Commission, Joint Research Centre, Institute for Transuranium Elements, 76125 Karlsruhe, Germany*
[3] *Institute of Physics, Academy of Sciences of the Czech Republic, Prague 8, The Czech Republic*

Plutonium is a very complicated element, mainly due to a close proximity to the threshold of delocalization of the 5*f* electronic states. At present both new theoretical approaches and new reliable experimental data are badly needed to reveal the hierarchy of interactions, affecting physics, materials science, and metallurgy of Pu systems. From the six known allotropic phases of Pu, two have a prominent position. α-Pu is a low-volume (high-density) phase, with a complicated monoclinic structure. The *fcc* phase δ-Pu has the largest volume, and although it exists only at elevated temperatures, it can be stabilized by doping and its low-temperature characteristics are known. Both phases are (despite their large volume difference) weakly paramagnetic, with enhanced Sommerfeld coefficient of electronic specific heat γ (more enhanced for the δ than for the α phase). It was traditionally supposed that all the differences are due to the volume changes, affecting the 5*f* localization. How about the other phases?

We intended to establish basic characteristics of β-Pu by simulating it by a Pu-rich intermetallic compound, $Pu_{19}Os$, which has its crystal-structure details closely related to β-Pu. This is particularly true for one of the two varieties, ζ-$Pu_{19}Os$, which is a high temperature phase [1]. The reported room-temperature density 18.02 g/cm^3 is only slightly lower than that of β-Pu, if the latter is corrected for the thermal expansion (18.20 g/cm^3), and is very different from those of α-Pu (19.82 g/cm^3) or δ-Pu (15.92 g/cm^3). This phase was found thermodynamically stable between 468 and 707 K. Below that range, the structure transforms into the other variety, η-$Pu_{19}Os$, with structure of slightly higher density (18.12 g/cm^3) [2]. We succeeded to synthesize both phases.

The magnetic susceptibility is weakly increasing with decreasing T for both phases, from $8*10^{-9}$ m^3/mol Pu at 300 K to $9*10^{-9}$ m^3/mol Pu in the low-T limit. It is therefore higher than for α- and δ-Pu, both being $6\text{-}7*10^{-9}$ m^3/mol [3]. Temperature dependence of specific heat exhibits quite a non-Debye type of behaviour, similar to δ-Pu alloys [4,5]. The lowest temperature achieved (below 4 K) were nevertheless sufficient to perform a reliable extrapolation to $T \rightarrow 0$. The obtained γ-values, (55±2) mJ/mol Pu K^2 for ζ-$Pu_{19}Os$ and (74±2) mJ/mol Pu K^2 for η-$Pu_{19}Os$, are higher than the high-temperature estimates, which indicated a γ enhancement similar to δ-Pu at low T [4]. The errors reflect both the accuracy coming from the fit and the possible errors in the mass determination. The slopes of the C_p/T vs. T^2 plot, which determine the Debye temperatures, are even higher than for δ-Pu. It reveals Θ_D even lower than for δ-Pu, but the values Θ_D = 96 K for η-$Pu_{19}Os$ and 101 K for ζ–$Pu_{19}Os$ in fact fall within the spread of δ-Pu stabilized by 6.1 % Ce (103 K) [6] and by 8% Am (95 K) [5].

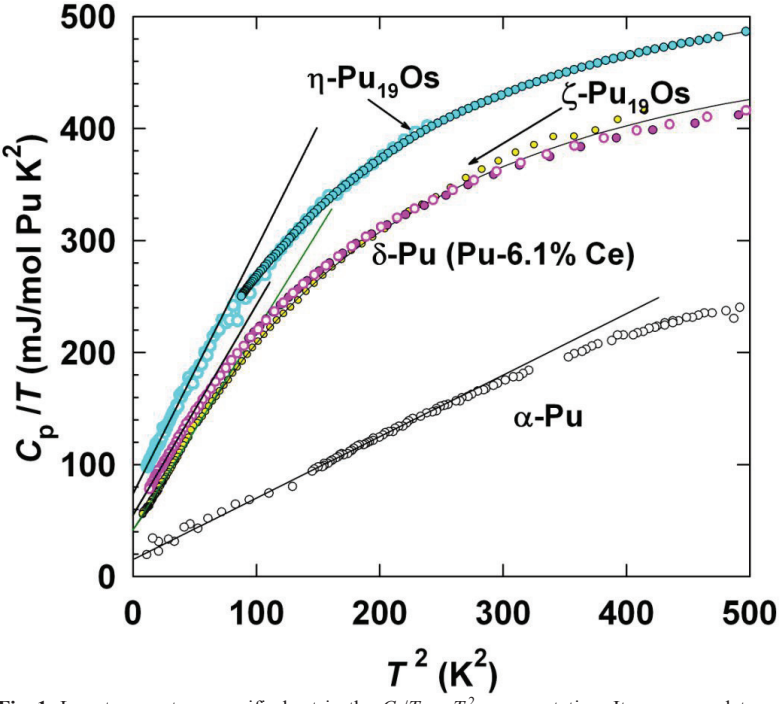

Fig. 1. Low-temperature specific heat in the C_p/T vs T^2 representation. It compares data on large (full circles) and small (empty circles) samples of η-$Pu_{19}Os$ (cyan) and ζ-$Pu_{19}Os$ (magenta) with similar data on δ-Pu (stabilized by 6.1 at.% Ce - from ref. 6) and α-Pu (from ref. 4) – both grey circles, δ-Pu yellow filled.. The full line was obtained from inelastic neutron scattering data of δ-Pu stabilized by 5% Al [4] and shows that it well reproduces the lattice part also for 6.1 at.% Ce The straight lines are fits to the low-temperature linear part, which were used to estimate the respective γ and Θ_D values mentioned in the text.

The results indicate that β-Pu is probably the most strongly correlated Pu phase, what was hinted already by electrical resistivity, exhibiting a pronounced maximum around 40 K [7]. The volume and related Pu-Pu spacing is clearly not the primary tuning parameter for Pu metal, as the β-Pu density stays close to the ground-state α-phase and is much higher than that of δ-Pu.

Acknowledgements: We thank to D. Bouexiere and G. Pagliosa for technical support. This work was supported by the Acad. Sci. of the Czech Republic (AV0Z10100520), and by the Grant Agency of the Czech Republic (P204/10/0330). Participation in the European Commission JRC-ITU Actinide User Laboratory program through the support of the European Community-Transnational Access to Research Infrastructures Action of the "Structuring the European Research Area" specific program, contract RITA-CT-2006-026176, is acknowledged.

References

[1] D.T. Cromer, *Acta Cryst. B* **35**, 1945 (1979).
[2] D.T. Cromer, *Acta Cryst. B* **34**, 913 (1978).
[3] S. Meot-Reymond and J.M. Fournier, *J. Alloys Comp.***232**, 119 (1996).
[4] J.C. Lashley, J. Singleton, A. Migliori, J.B. Betts, R.A. Fisher, J.L. Smith and R.J. McQueeney, *Phys. Rev. Lett.* **91**, 205901 (2003).
[5] P. Javorský, L. Havela, F. Wastin, E. Colineau and D. Bouëxière, *Phys. Rev. Lett*. **96**, 156404 (2006).
[6] L. Havela, P Javorsky, A. B. Shick, J. Kolorenc, E. Colineau, J. Rebizant, F. Wastin, J.C. Griveau, L. Jolly, G. Texier, F. Delaunay and N. Baclet, *Phys. Rev. B* **82**, 155140 (2010).
[7] E. King and J.A. Lee, *Cryogenics* **3**, 177 (1963).

Basic Properties of the First Actinide Based Oxypnictide Compound: NpFeAsO

Tomasz Klimczuk,[1,2] R. Springell[3], H. C. Walker[4], E. Colineau[1], J.-C. Griveau[1], D. Bouexière[1], R. Eloirdi[1], P. Gaczyński[1], R. J. Cava[5] and R. Caciuffo[1]

[1] *European Commission, JRC, Institute for Transuranium Elements, Postfach 2340, 76125 Karlsruhe, Germany, e-mail: Tomasz.Klimczuk@ec.europa.eu*
[2] *Faculty of Applied Physics and Mathematics, Gdansk University of Technology, Narutowicza 11/12, 80-952 Gdansk, Poland,*
[3] *London Centre for Nanotechnology and Department of Physics and Astronomy, University College London, London WC1E 6BT, United Kingdom*
[4] *European Synchrotron Radiation Facility, BP220, F-38043 Grenoble Cedex, France*
[5] *Department of Chemistry, Princeton University, Princeton NJ 08544, USA*

We report on the synthesis of NpFeAsO, the first actinide based oxypnictide. This new compound is isostructural to the *R*FeAsO system (*R*=Rare Earth), possessing lattice parameters, Fe-As interatomic distances, and Fe-As-Fe bond angles falling within the empirical 'optimum' for the observation of the highest superconducting transition temperatures. A series of bulk measurements performed on the parent compound, including susceptibility, heat capacity and resistivity, show no evidence for the expected spin density wave (SDW) formation, nor antiferromagnetic (AFM) ordering of the iron sublattice. Instead, a distinct antiferromagnetic ordering occurs at T_N = 57 K, which is four times higher in temperature than the highest T_N observed in the *R*FeAsO (*R*=Pr) family.

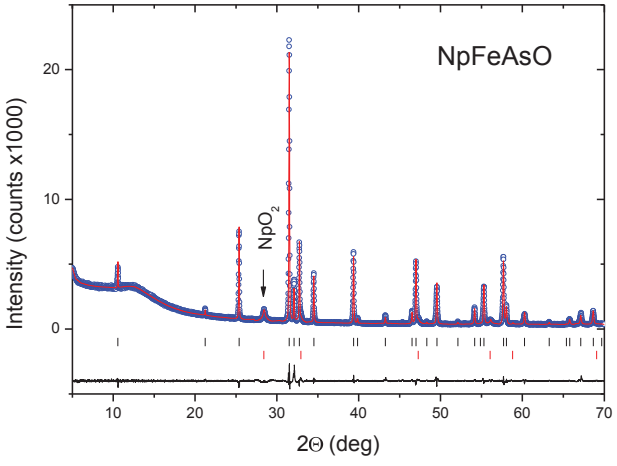

Fig. 1. Rietveld refinement of room temperature x-ray powder diffraction data for NpFeAsO. Upper part: blue circles - observed data, red solid line – calculated intensities. The lower part shows the differences between the observed and calculated pattern. The tick marks correspond to the Bragg peaks from the NpFeAsO (P4/nmm, ZrCuSiAs structure, space group *P*4/nmm): a = 3.86604(5) Å, c = 8.36218(13) Å.

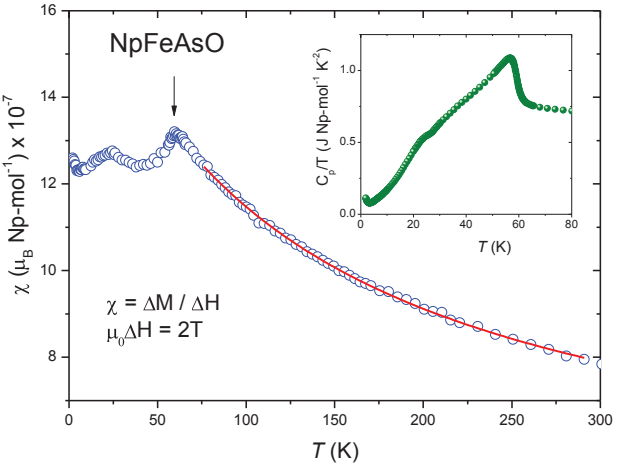

Fig. 2. The susceptibility of the parent NpFeAsO compound, corrected for trace amounts of ferromagnetic Fe. The red solid line shows a Curie-Weiss (C-W) fit to the susceptibility, which yields an effective magnetic moment of $\mu_{eff} = 2.8\ \mu_B\ mol^{-1}$ and $\Theta_{CW} = -128$ K. The inset shows C/T versus temperature.

We attempted doping the iron and the oxygen sites by cobalt and fluorine, respectively. The changes of the lattice parameters and the unit cell volume, are consistent with those published for $R Fe_{1-x}Co_xAsO$ and $R FeAsO_{1-x}F_x$, and indicate that the doping was successful. The subtle changes of the interatomic distances, due to chemical doping, will be discussed.

There is no hint of superconductivity transition observable in the susceptibility and specific heat data for the F-doped or Co-doped NpFeAsO samples down to 2 K. This observation, together with the lack of both SDW and AFM ordering of the iron ions in the parent material, are in agreement with the scenario that the same magnetic interactions are responsible for both antiferromagnetism and superconductivity in 1111 systems.

Localization vs Delocalization: Model Calculations for Electron Spectroscopies in 5f Systems

Gertrud Zwicknagl

Institut f. Mathematische Physik, Techn. Universitaet Braunschweig,Braunschweig, Germany
e-mail: g.zwicknagl@tu-bs.de

Intermetallic compounds containing actinide ions exhibit broad spectrum of different physical phenomena at low temperatures. The latter include heavy quasiparticles, unconventional superconductivity and various forms of magnetic ordering. The sometimes enigmatic properties of these compounds derive from the strong correlations among the 5f electrons. Previous model calculations suggested that the intra-atomic Hund's rule-type correlations may lead to partial localization which is reflected e. g. in the co-existence of itinerant 5f-derived heavy quasiparticles and local magnetic excitations. The ground state properties and the low-energy excitations, however, do not provide microscopic evidence on the itinerancy or localization of the 5f states.
Here we present model calculations for electron spectroscopies emphasizing the consequences of strong intra-atomic correlations of the 5f electrons. Starting from the Anderson model in the mixed-valence regime we discuss results for a single impurity embedded in a metal and compare the results to the case of small clusters.

Evidence of Superconductivity for a UFeGe Sample

A.P. Gonçalves,[1] M.S. Henriques[1], M. Almeida[1], L. Havela[2], A. Adamska[2], O. Tougait[3], J.S. Brooks[4], A. Kiswandhi[4], E. Steven[4]

[1] *Instituto Tecnológico e Nuclear/CFMC-UL, Estrada Nacional 10, P-2686-953 Sacavém, Portugal, e-mail: apg@itn.pt*
[2] *Dept. Condensed Matter Physics, Fac. Mathematics and Physics, Charles Univ., 12116 Prague, Czech Republic*
[3] *Lab. Chimie du Solide et Inorganique Moléculaire, UMR CNRS 6511, Univ. Rennes 1, France*
[4] *Florida State Univ., Natl. High Magnet Field Lab., Tallahassee, FL 32306 USA*

In the standard BCS theory for superconductivity, ferromagnetic order impedes the pairing of electrons in singlet states [1]. Therefore, the discovery of coexistence between superconductivity and ferromagnetism in UGe_2 [2], UIr [3], URhGe [4] and UCoGe [5] raised the question about the dominant mechanism responsible for the pairing in such unconventional class of materials. It is interesting to notice that URhGe and UCoGe belong to the uranium family of compounds with TiNiSi-type structure. As superconductivity appears frequently in compounds having the same structure type, we decided to study the UFeGe high-temperature phase (stable at T > 500K), which also crystallizes with the TiNiSi-type structure [6].

UFeGe samples were prepared by arc-melting the stoichiometric amounts of the elements. Sample (A) and Sample (B) were subjected to the annealing at 250ºC for two hours, followed by a rapid quenching into ice water. The samples were characterized by powder X-ray diffraction, SEM/EDS, and specific heat and electrical transport measurements.

X-ray diffraction indicates that sample (A) represents the UFeGe low-temperature phase, whereas sample (B) has ~20% of the low-temperature phase and ~80% of the TiNiSi phase. However, SEM/EDS observations show the presence of ~5% at. Zr in the UFeGe phase(s) in the sample (B), pointing to a considerable contamination of the initial U (indeed, later analysis of starting U indicate a Zr concentration of ~ 4 % at.).

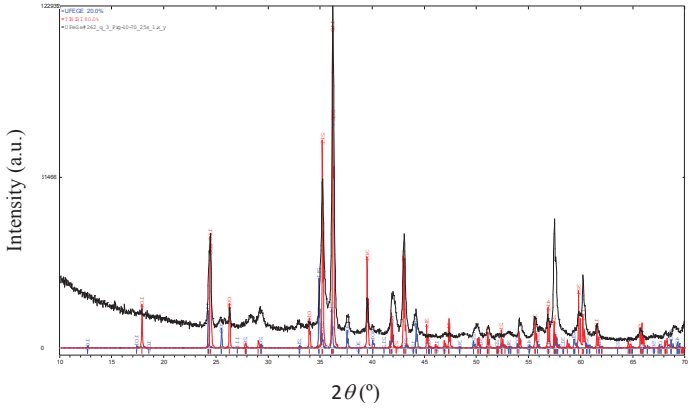

Fig.1. Powder X-ray diffraction pattern of the sample (B).

The field dependence of the electrical resistance of the sample (B) at various temperatures is shown in Fig. 2. Superconductivity was observed in this sample, with a critical temperature T_c

~1 K. Specific heat measurements made on sample (A) have shown no sign of transitions down to 0.4 K, pointing to a normal ground state of the UFeGe low-temperature phase and to a superconducting UFeGe phase with TiNiSi-type structure.

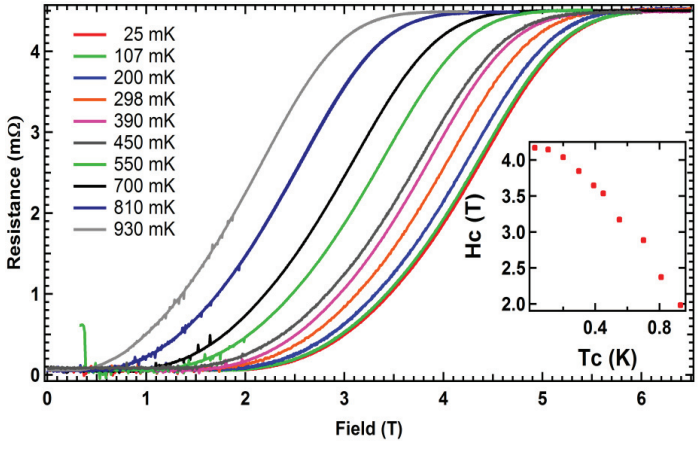

Fig.2. Field dependence of resistance for sample (B) at various temperatures (inset: phase diagram of UFeGe extracted with the criterion of half-height of the resistance vs. temperature curves above).

Nevertheless, the presence of Zr impurities does not discard other possible origins for the superconductivity. In particular, the transition temperature (~1 K) is similar to what is observed for Zr-Fe alloys [7] However, the critical field, $B_C > 4$ T, (see inset in Fig. 2) seems to exceed the Pauli limit (B_P ~1.8 T) and it is much higher than those reported for Zr-Fe alloys.

In conclusion, superconductivity was observed in a sample mainly constituted by the high-temperature UFeGe (TiNiSi-type structure) phase. However, the presence of Zr minority phases needs to be clarified and further studies are still required to elucidate the source of this behavior.

References

[1] N.F. Berk, J.R. Schrieffer, *Phys. Rev. Lett*. **17** 433 (1966).
[2] S.S. Saxena et al., *Nature* **406** 587 (2000).
[3] T. Akazawa et al., *J. Phys. Condens. Matter* **16** L29 (2004).
[4] D. Aoki et al., *Nature* **413** 613 (2001).
[5] N.T. Huy et al., *Phys. Rev. Lett*. **99** 067006 (2007).
[6] F. Canepa et al., *J. Alloys Compd*. **234** 225 (1996).
[7] B. T. Matthias, et. al., *Phys. Rev*. **100** 626 (1955).

High-Pressure Resistivity of UPd_3

Jiří Prchal,[1] Ladislav Havela[1], Alexander V. Andreev[2]

[1] *Charles University in Prague, Department of Condensed Matter Physics Faculty of Mathematics and Physics, Ke Karlovu 5, 12116 Prague 2, Czech Republic, e-mail: prchal@karlov.mff.cuni.cz*
[2] *Institute of Physics, Academy of Sciences, Na Slovance 2, 18221 Prague 8, Czech Republic*

UPd_3 is known as a $5f^2$ localized system with a quadrupolar ordering, unique at least among U binaries. It has the $TiNi_3$ structure (space group $P63/mmc$, lattice parameters a = 5.73 Å, c = 9.66 Å), i.e. double hexagonal close-packed. The uranium ions are stacked in layers with the sequence ABACABAC, such that there are two inequivalent uranium sites, with locally hexagonal and quasi-cubic site symmetry, respectively. The inter-uranium distance is 4.11 Å, which is larger than the Hill limit. Theoretical calculations (SIC-LSD) predicted delocalization of one 5*f* electron in pressures about 25 GPa [1]. Although neither structural phase transition nor a volume collapse have been identified in our earlier high-pressure XRD study [2], some part of theoretical community believes that such pressures should dramatically affect the resistivity even if there is no phase transition, as there can be a gradual crossover only. In any case, pressure should eventually lead to the delocalization, only its magnitude is questionable.

The high-pressure resistivity was measured by using the Bridgman-type pressure cells in pressures up to 10.5 GPa with the diameter of the pressure space of 1 mm. We used solid pressure transmitting medium (steatite) and superconducting transition of Pb for determination of the pressure inside the pressure space. The clamped cell was placed at a CCR, which allowed to reach approx. 4 K as the lowest temperature.

We measured the temperature dependence of electrical resistivity in gradually increasing pressures using a small single crystal sample. The sample was prepared by the Czochralski method using a tri-arc furnace. The expected delocalization should lead to dramatic variations. The entire character of resistivity, when the 5*f* states are brought to the Fermi level, should be modified. As one can see (Fig.1), pressures up to 10 GPa (volume compression about 5%) do not bring any sign of incipient delocalization.

The resistivity agrees approximately with the polycrystal data obtained at ambient pressure [3], with a broad dip around 40 K and steeper decrease below 10 K. In our case the decrease starts at somewhat higher temperature, 12 K. Our data do not distinguish directly fine details indicating individual quadrupolar ordering transitions in the range below 7 K, which are observable only for annealed crystal [4].

The high pressure (up to 10 GPa) does not have surprisingly any visible influence on the low temperature anomaly, which implies that the physics of crystal electric fields acting on localized 5*f* states remains very little affected. This insensitivity to pressure, observed also in resonant inelastic X-ray scattering at the U-L_3 edge [5], remains quite a mystery.

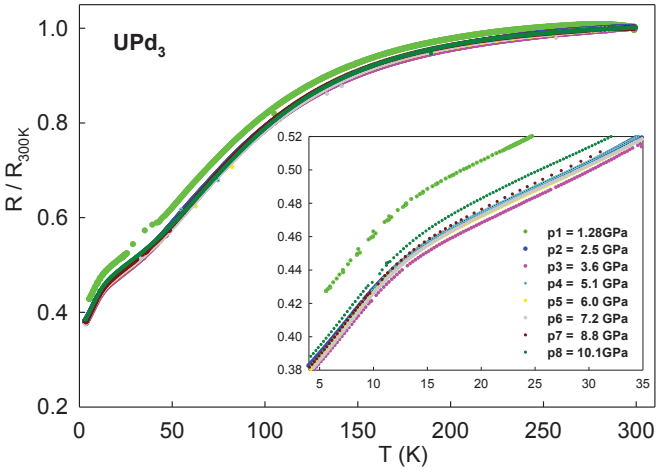

Fig.1. Resistivity of the UPd_3 at pressures up to 10 GPa. The anomaly due to the quadrupolar ordering is slightly shifted to lower temperatures with increasing *p*. The slightly higher data values for the lowest pressures are likely due to a small shift of contacts.

References

[1] L. Petit, A. Svane, W.M. Temmerman, Z. Szotek, Phys.Rev.Lett. 88 (2002) 216403.
[2] S. Heathman, M. Idiri, J. Rebizant, P. Boulet, O.S. Normile, L. Havela, V. Sechovsky, T. Le Bihan, Phys.Rev.B 66 (2003) 180101(R).
[3] P. Zaplinski et al., in: Proceedings of the International Conference on CEF and Structure Effects in f-Electron Systems, J.E. Crow, R.P. Guertin, and T.W. Mihalisin, Plenum, New York 1980, pp. 295-300.
[4] W. Ubachs, A.P.J. van Deursen, A.R. Vroomen, A.J. Arko, Solid Sate Commun. 60 (1986) 7.
[5] J.-P. Rueff, S. Raymond, A. Yaresko, D. Braithwaite, Ph. Leininger, G. Vanko, A. Huxley, J. Rebizant, N. Sato, Phys.Rev.B 76 (2007) 085113.

Electronic Structure of Plutonium Hydrides: DFT + *U* Calculations in the FPLAPW Basis

Bingyun Ao,[1] Juanjuan Ai[2], Tao Gao[2], Xiaolin Wang[1]

[1] *China Academy of Engineering Physics, P. O. Box 919-71, Mianyang 621900, Sichuan, China*
e-mail: aobingyun24@yahoo.com.cn
[2] *Institute of Atomic and Molecular Physics, Sichuan University, Chengdu 610065, Sichuan,China*

Understanding the 5f states of actinide elements has always been the physical center of this engaging and challenging field. Among this series, plutonium (Pu) lies just at the critical point where 5f electrons delocalization to localization transition in the actinides occurs, which results in the occurrence of numerous bizarre properties in the fundamental science of physics, material and chemistry. Beyond all doubt, Pu has been recognized as the most complex metallic element and attracted extraordinary scientific and engineering interests since its discovery. Increasing experimental and theoretical efforts have been taken into the deep understanding of the 5f electrons of Pu, its alloys and compounds, which has been comprehensively reviewed by Moore *et al*. in their two up-to-date articles [1,2]. However, as pointed out by the authors, there are still many unanswered questions, and arguments persist on the topics of electronic structure, magnetism, and the character of bonding. Furthermore, as referred to the mysterious aging of Pu and lack of enough experimental observations due to its toxicity, radioactivity, chemical activity and high cost, its complex properties become even more puzzled. Therefore, more and more first-principles techniques from traditional density functional theory (DFT) to semiempirical and exact strongly-correlated electronic structure calculation methods such as DFT + *U* and dynamical mean field theory (DMFT) have been developed and performed to explore the electronic structure of metallic Pu, its alloys and compounds during the last three decades. Unfortunately, to our knowledge, almost no literature is available on the electronic structure calculations of Pu hydrides which can be viewed as comparably important as widely studied Pu oxides in the fields of surface corrosion chemistry and nuclear fuel cycle.

Pu can be loaded with hydrogen forming complicate continuous solid solution and compounds and causing remarkable electronic-structure changes. We report on the first-principles calculations of the electronic structure of stoichiometric cubic PuH_2 and hexagonal PuH_3 combining the full potential linearized augmented plane wave basis (FPLAPW) with the density functional theory plus a Hubbard parameter *U* (DFT + *U*) for considering the strong Coulomb correlation between localized Pu 5f electrons. The comparison with standard DFT calculations shows a good agreement of the crystal structural parameters, elastic constants and electric properties with experimental findings. Most importantly, the findings provide the evidence for the first that the spectacular metal-insulator transition (MIT) happens on the phase transformation from PuH_2 to PuH_3 and the increase of the ionicity in the transformation can partially explain the catalysis of Pu hydriding.

References

[1] K.T. Moore et al., *Rev.Mod. Phys.* **81**, 235 (2009).
[2] K.T. Moore., *Micron* **41**, 336 (2010).

Electronic structure of (U;Ce)Ru_2Al_{10} by first-principles calculations and X-ray photoemission

M. Samsel-Czekała,[1] E. Talik[2], M. Pasturel[3], R. Troć[1]

[1] *Institute of Low Temperature and Structure Research, Polish Academy of Sciences, Okólna 2, 50-422 Wrocław, Poland, e-mail: m.samsel@int.pan.wroc.pl*
[2] *Institut of Physics, University of Silesia, Uniwersytecka 4, 40-007 Katowice, Poland*
[3] *Sciences Chimiques de Rennes, Université Rennes 1, UMR CNRS 6226, Campus de Beaulieu, 263 av. Général Leclerc, 35042 Rennes Cedex, France*

We present results of band structure calculations, employing the fully relativistic version of the FPLO code [1] within the local density approximation (LDA), and of X-ray photoelectron spectroscopy (XPS) experiments (using Al Kα radiation) for uranium ternary compound, URu_2Al_{10}, and its analogue with cerium, $CeRu_2Al_{10}$. Their band energies, Fermi surfaces (FS) and densities of states (DOS) have been computed. For comparison with the experimental XPS spectra, the corresponding theoretical valence band XPS spectra were calculated.
Recent investigations [2] have shown that both systems adopt the orthorhombic structure of the $YbFe_2Al_{10}$-type (*Cmcm*) [3], where U or Ce atoms are located in a cage of Ru-Al polyhedra, forming a clathrate-like structure. Based on the magnetic, transport, and heat capacity measurements [2], URu_2Al_{10} is a non-magnetically ordered (at least down to 2 K) metal, for which a mixed-valence state of uranium was postulated, such as in U_2Ru_2Sn and U_2RuGa_8. In turn, it appears that $CeRu_2Al_{10}$ exhibits some unusual complex metal-to-insulator and antiferromagnetic phase transitions below 27 K [4].
Our calculated DOS, displayed in Fig. 1(a), and FS in URu_2Al_{10} are metallic-like in agreement with the transport measurements [2]. Three conduction bands are dominated, around the Fermi level (E_F), by the U 5f electrons, being strongly hybridized with the U 6d, Ru 4d and the Al 3spd electrons. Hence, the metallic bond is formed by all atoms. The U 5f states contribution to DOS is very broad and complex, containing a unique triple-peak structure located around E_F – see hatched area in Fig. 1(a). The lowest-energy peak cuts E_F while the two others, located above E_F, are formed due to the spin-orbit (SO) splitting. The idea of a mixed-valence state in URu_2Al_{10}, as proposed in [2], is somehow supported owing to a possibility of excitations from the U 5f peak in the vicinity of E_F to the one just above E_F. As to the Ru 4d electrons, they form also a pronounced broad multi-peak well below E_F - see Fig. 1(b). There is some psedogap visible in the total DOS at -0.73 eV. It makes that some deficit of electrons in real crystal may shift the Fermi-level to the pseudogap region, leading to a typically semimetallic behavior.
The calculated DOS, displayed in Fig. 1(b), and FS in $CeRu_2Al_{10}$ exhibit more semimetallic behavior (DOS at E_F is about two times lower and FS has more reduced sheets than in the uranium compound). The Ce 4f peak, split by SO of 1 eV into two sub-peaks, is almost completely localized above E_F and only the bottom of its lower-energy edge is crossing E_F. These electrons are hybridized with the Ce 5d, Ru 4d, and Al 3spd electrons. The very vicinity of the Ce 4f peak to E_F can explain the observed metal-to-insulator transitions in $CeRu_2Al_{10}$ [4]. Finally, the Ru 4d contribution to DOS occurs in comparable region to that in URu_2Al_{10}.
The computed and experimental valence-band XPS spectra of both compounds are displayed in Fig. 2. As seen, the theoretical spectrum of URu_2Al_{10} contains two main peaks - see Fig. 2(a). The largest and narrow peak, crossing E_F, mainly originates from the contribution of the U 5f states. The other peak, occurring in the energy range between 1 and 10 eV below E_F and

split into three subpeaks, is dominated by the Ru 4d electrons. However, the U 5f peak is somewhat shifted above E_F in the experiment, performed at room temperature (RT). Hence, the experimental 5f-peak is more localized at RT.

Both theoretical and experimental valence-band XPS spectra of $CeRu_2Al_{10}$, displayed in Fig. 2(b), contain the distinct Ru 4d-electron peak, similar to than in URu_2Al_{10}. Note that the Ce 4f contributions are quite well localized above E_F and almost completely invisible in the spectra presented in Fig. 2(b).

The XPS spectrum of the U 4f-core lines in URu_2Al_{10} have been decomposed into two asymmetric $4f_{5/2}$ and $4f_{7/2}$ main sublines. The U $4f_{7/2}$ subline is accompanied by two small-intensity symmetric, so-called 3-eV and 7-eV, satellites. The presence of the 3-eV-satellite is always controversial. It points to some contamination of the sample by uranium oxides as well as gives an evidence for an additional final state of $5f^3$ (at the same position as that in UO_2), although the $5f^3$ state is expected also for the mixed-valence behaviour. It should be noticed that there is no sign of so-called 1-eV satellite, existing in the 4f-core spectra of spin-fluctuating URu(Al;Ga) systems [5]. Finally, the 7-eV satellite is usually ascribed to some additional localization effects of U 5f electrons that are possible in our XPS measured at RT.

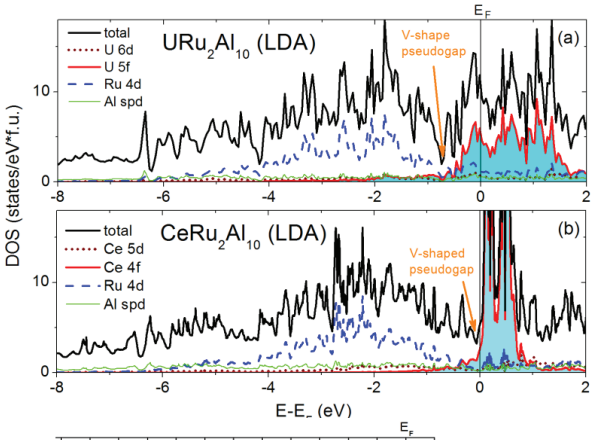

Fig. 1. Calculated DOS in URu_2Al_{10} (a) and $CeRu_2Al_{10}$ (b).

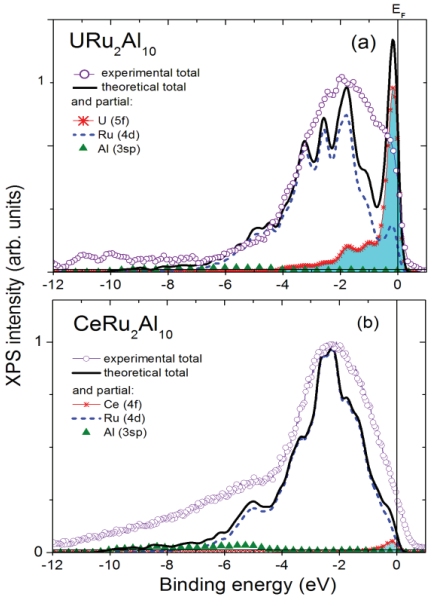

Fig. 2. Valence-band XPS spectra in URu_2Al_{10} (a) and CRu_2Al_{10} (b). Note that the Ce 4f contribution is almost invisible.

References

[1] K. Koepernik and H. Eschrig, *Phys. Rev. B* **59**, 1743 (1999); FPLO5.00-18 version (http://www.FPLO.de).

[2] R. Troć et al., *Intermetallics*, in print.

[3] S. Niemann and W. Jeitschko, *Z. Kristallogr.* **210**, 338 (1995).

[4] A.M. Strydom, *Physica B* **404**, 2981 (2009).

[5] M. Samsel-Czekała et al., *Phys. Rev. B* **77**, 155113 (2008); **78**, 245120 (2008).

Prediction of Giant Spin Hall Effect Due to Uranium Impurities in Gold

A. B. Shick[1] and L. Havela[2]

[1] *Institute of Physics, Academy of Sciences of the Czech Republic, Na Slovance 2, CZ-18221 Prague 8, Czech Republic,e-mail: shick@fzu.cz*
[2] *Department of Condensed Matter Physics, Charles University, Ke Karlovu 5, CZ-12116 Prague 2, Czech Republic*

When a charge current is flowing through a solid, the transversal spin current is induced due to the spin-Hall effect (SHE). It has been observed in semiconductors [1] and metals [2]. From practical point of view, SHE provides a new functionality of materials for spin-electronics, allowing for generation of spin currents in non-magnetic materials without spin-injection from a ferromagnet.

The SHE is caused by the spin-orbit coupling (SOC) and can occur even in non-magnetic solids. Its mechanism is believed to be similar to that of anomalous Hall effect in ferromagnetic materials. The most distinguished point of the SHE is that it does not require ferromagnetic order. The spin-orbit scattering of the conduction electrons through skew and side-jump scattering leads to separation of different spins in different directions [4]. This effect is controlled by spin Hall angle γ_s, which usually varies in a range of 0.001-0.01.

In what follows we describe the electronic structure and estimate the skew scattering on U impurities in Au. As a computational model, we use UAu_{15} supercell, shown in inset of Fig. 1, with the lattice parameter of elemental Au. The conventional relativistic LDA calculations show the formation of narrow (~1 eV) f-manifold split by spin-orbit coupling (SOC) and located over the top of Au-host wide (~7 eV) d-band. The f-states are hybridized mainly with s- and p-bands of Au.

Method	n_{5f}	$n_{5/2}$	$n_{7/2}$	$\lvert\gamma_s\rvert$
LDA	2.71	2.17	0.54	0.21
LDMA(HIA)	2.70	2.33	0.38	0.25
LDA+Exact Diagonalization	2.70	2.47	0.23	0.28

Table I.: The f-shell occupations (total and partial j=5/2,7/2) and the magnitude of the spin Hall angle γ_s for U impurity in Au resulting from LDA, LDMA(HIA) and LDA+ED calculations.

Next, we employ the charge self-consistent LDMA-Hubbard I (HIA) method [4] with the Coulomb-U =3 eV. In Table I. the total and partial j=5/2,7/2 occupations of the 5f-manifold are shown. It is seen that the total n_{5f} occupation stays practically unchanged when the Coulomb-U =3 eV is added, while the partial occupations are modified due to the effective enhancement of the spin-orbit splitting. In Fig. 1 we show LDA+HIA calculated DOS for U-f-states. The DOS character does not agree with the experimental valence-band photoemission (PES) [5] for diluted U_xAu_{1-x} alloys. It means that multiplet transitions alone cannot explain the experimental PES and the hybridization with the host band has to be accounted explicitly.

To proceed further, we solve a single impurity Anderson model whose parameters were extracted from LDA calculations using the finite-temperature exact diagonalization (ED) method for the complete 7-orbital f-shell hybridized with discretized bath of the host-band states. The corresponding DOS is shown in Fig. 1. It is in fair agreement with PES data [5]: the sharp quasiparticle α–peak is located at the Fermi level, and β–shoulder is developing.

Finally, we estimate the magnitude of SHE angle from the calculated electronic structure. The absolute values of γ_s are shown in Table I. It is seen that SHE angle can reach giant value of ~0.3. Recently, an experimental observation of γ_s~0.1 was reported [6] in multi-terminal device with Au Hall cross and FePt spin-injector. We predict that diluting the U impurities in Au would further increase the SHE angle.

Acknowledgements: This work was supported by the Academy of Sciences of the Czech Republic (AV0Z10100520), and by the Grant Agency of the Czech Republic (P204/10/0330).

References

[1] Y. K. Kato, R. S. Myers, A. C. Gossard, and D. D. Awschalom, Science **306**, 1910 (2004).
[2] S. O. Valenzuela and M. Tinkham, Nature **442**, 176 (2006).
[3] H.-A. Engel, B. I. Halperin, and E. I. Rashba, Phys. Rev. Lett. **95**, 166605 (2005).
[4] A. B. Shick, J. Kolorenc, A. I. Lichtenstein, and L. Havela, Phys. Rev. **B 80**, 085106 (2009).
[5] R. Eloirdi, T. Gouder, F. Wastin, J. Rebizant, F. Huber, Physica **B 359-361**, 1000 (2005).
[6] T. Seki, Y. Hasegawa, S. Mitani *et al*., Nature Mater. **7**, 125 (2008).

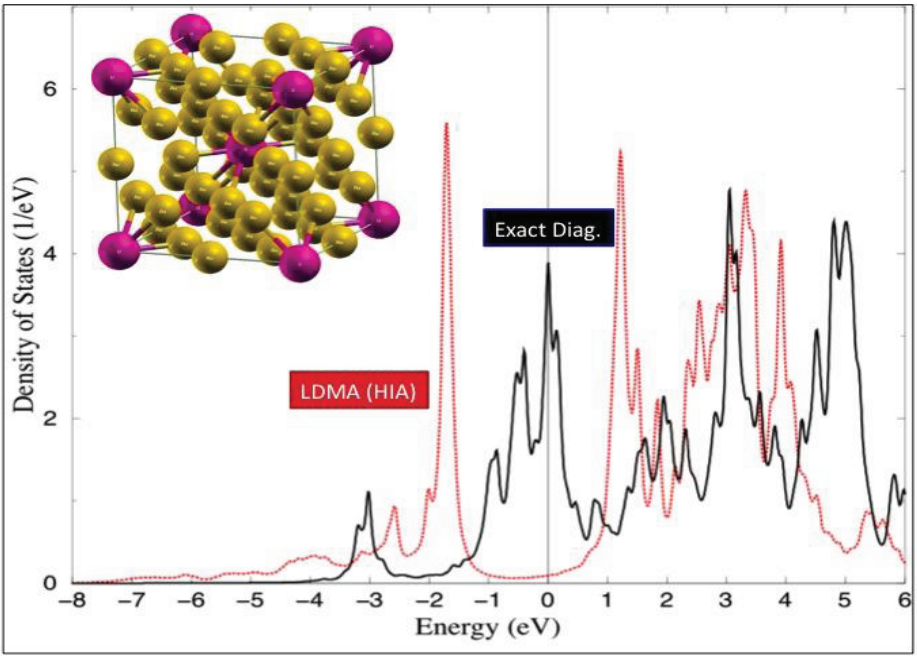

Fig. 1. Spectral DOS resulting from charge density self-consistent LDMA(HIA) as well as model-ED calculations with the Coulomb-U =3 eV. The inset shows the UAu_{15} supercell model used in the calculations.

Ab initio Investigation of Electronic Structure of Actinide 218 Materials

Jan Rusz[1], Saad Elgazzar[1], P. M. Oppeneer[1], E. Colineau[2], J.-C. Griveau N. Magnani[2], J. Rebizant[2] and R. Caciuffo[2]

[1]*Department of Physics and Astronomy, Uppsala University, Box 516, S-751 20 Uppsala, Sweden, jan.rusz@fysik.uu.se*

[2]*European Commission, JRC, Institute for Transuranium Elements, Postfach 2340, D-76125 Karlsruhe, Germany*

We report a comprehensive investigation of the electronic structure and magnetic properties of actinide 218 compounds, which crystallize in the tetragonal Ho_2CoGa_8 crystal structure [1]. Specifically, we study experimentally the group of plutonium-based compounds Pu_2MGa_8 (with M = Rh, Co, and Fe), which are structurally related to the unconventional superconductors $PuCoGa_5$ and $PuRhGa_5$ and are measured to be non-magnetic and non-superconducting down to 2 K, yet displaying relatively high linear specific-heat coefficients of 61 to 133 mJ/mol.K^2. We perform density-functional theory based calculations, in which we apply three different approaches to access the tendency of 5*f* electron localization, the local spindensity approximation (LSDA), LSDA+*U*, and the 5*f* open-core approach. For comparison to the abovementioned compounds we also investigate computationally the plutonium compounds with M = Ir and Pd, the uranium-based compounds U_2MGa_8 (with M = Co, Fe, Rh, and Ru), as well as Np_2CoGa_8, and Am_2CoGa_8. On the basis of *ab initio* LSDA calculations we optimize the equilibrium lattice parameters and the internal fractional coordinates within the Ho_2CoGa_8 crystal structure. The obtained lattice parameters, Table I, are in relatively good agreement with experimental values, when we assume delocalized 5*f* states for all compounds except Am_2CoGa_8. We discuss the computed electronic structures and the theoretical Fermi surfaces. For the Pu-218 compounds we find that LSDA calculations, in which the 5*f*'s are treated as delocalized, predict a magnetically ordered groundstate, whereas LSDA+*U* calculations predict a non-magnetic groundstate in accordance with experiment. The LSDA+U potential has quite dramatic effects on the Pu 5*f* bands. Firstly, the on-site Coulomb correlations have enlarged the splitting of the $5f_{5/2}$ and $5f_{7/2}$ subbands to 4 eV, which corresponds to the sum of on-site Coulomb term U = 3 eV and the spin-orbit interaction strength of 1 eV (see Fig. 2). Secondly, the bands have become wider due to an enhanced on-site repulsion, exchange interaction, and some hybridization. The $5f_{5/2}$ band, which was only about 0.5 eV wide in the LSDA calculation, is now almost 1 eV wide. The unoccupied $5f_{7/2}$ band, centered about 3.5 eV above the Fermi level, is more than 1.5 eV wide. The broadening of the $5f_{5/2}$ band and its slight downwards energy shift results in a much lower predicted DOS at the Fermi level. The majority of the DOS at the Fermi level corresponds in the LSDA+U calculation to interstitial states, i.e., to highly delocalized

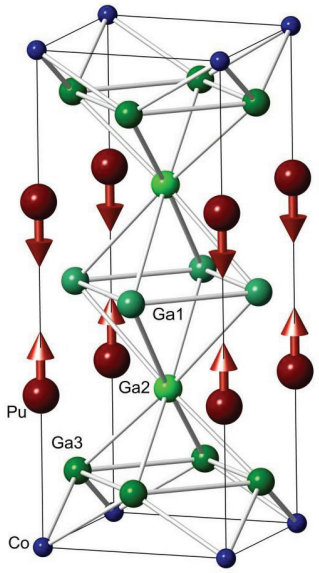

Fig.1. Crystal structure of the tetragonal Ho_2CoGa_8 structure. The magnetic moments on the actinide atoms indicate the considered antiferromagnetic arrangement.

electrons. Using the LSDA+*U* approach, we have also calculated the Fermi surface of Pu2CoGa8, shown in Fig. 3. We observe 6 bands crossing the Fermi level. The lowest one leads to a small hole surface with volume only for 0.02 states and the highest band forms a small electron sheet with similar volume. Most of the bands are very two-dimensional. On the other hand, the two lowest bands show distinct three-dimensional features. The lowest band forms a small hole sheet that has an almost spherical Γ-centered shape. I.e., its de Haas-van Alphen frequency should be largely direction-independent. The second lowest band has a much more complicated topology. For the U-218 compounds the LSDA itinerant 5*f* approach predicts a non-magnetic groundstate, in accordance with available experimental data. For Am_2CoGa_8 our calculations are consistent with the scenario of localized 5*f* electrons. We find that, on account of the elongated tetragonal structure, most of the theoretical Fermi surfaces are quasi-two-dimensional.

Compound	a_{exp}/Å	c_{exp}/Å	V_{th}/V_{exp}	z_{An}	$z_{Ga(3)}$
Pu_2CoGa_8	4.269	11.063	0.919	0.3058	0.1188
Pu_2RhGa_8	4.316	11.144	0.939	0.3070	0.1264
Pu_2IrGa_8	4.322	11.102	0.928	0.3053	0.1259
Pu_2FeGa_8	4.265	11.067	0.912	0.3055	0.1194
Pu_2PdGa_8	4.309	11.217	0.919	0.3083	0.1274
U_2FeGa_8	4.256	10.980	0.935	0.3053	0.1182
U_2RhGa_8	4.297	11.080	0.943	0.3095	0.1249
U_2RuGa_8	4.288	11.062	0.959	0.3068	0.1233
Np_2CoGa_8	4.251	11.021	0.916	0.3078	0.1194
Am_2CoGa_8	4.256	11.165	0.907	0.3075	0.1203

Table I. Experimental lattice parameters a and c [2,3,4], ratio of theoretical and experimental unit cell volumes and calculated internal structure parameters z_{An} $z_{Ga(3)}$of the studied An-218 compounds.

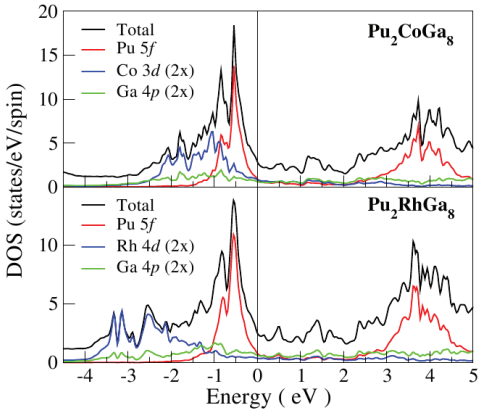

Fig. 2. Density of states of Pu_2CoGa_8 and Pu_2RhGa_8 compounds calculated using the LSDA+U with U = 3 eV and J = 0.6 eV.

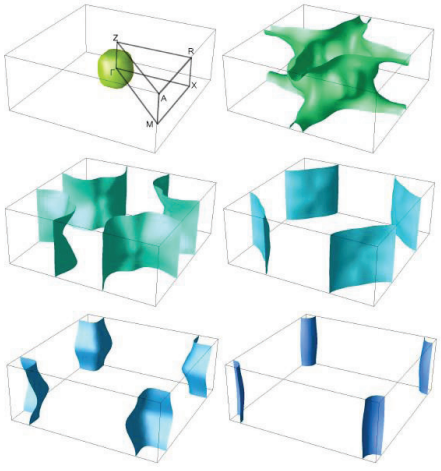

Fig. 3. Fermi surface topology of Pu_2CoGa_8 calculated with the LSDA+U.

References

[1] S. Elgazzar, J. Rusz, P. M. Oppeneer, E. Colineau, J.-C. Griveau, N. Magnani, J. Rebizant, and R. Caciuffo, Phys. Rev. B **81**, 235117 (2010).
[2] M. Schonert , S. Corsepius, E.-W. Scheidt and G. R. Stewart, J. Alloys Compounds **224**, 108 (1995)
[3] S. Ikeda, T. Okubo, Y. Inada, Y. Tokiwa, K. Kaneko, T.D. Matsuda, E. Yamamoto, Y. Haga and Y. Onuki, J. Phys.: Condens. Matter **15**, S2015 (2003)
[4] P. Boulet, D. Bouxiere, J. Rebizant, E. Colineau, and F. Wastin, *Plutonium Futures---The Science*, AIP Conference Volume **673** (2003), p. 136-138, edited by G. D. Jarvinen

Atomistic Simulation of Pure and Defected Uranium Dioxide Bulk and Surfaces

Dr Mark S D Read[1]

[1] *AWE, Aldermaston, AWE, Reading, Berkshire, RG7 4PR, UK*

An overview is provided of the important contribution made by the application of computational chemistry simulation techniques to materials science research within AWE. The range of computational methods employed in furthering the understanding of fundamental mechanisms of materials ageing and calculating parameters for higher level kinetic models is summarized.

In addition, recent results from a study employing atomistic computer simulation techniques using the GULP code are discussed. Here, interest lies in improving reported pair-potentials to describe the UO_2 bulk lattice (Figure 1) under conditions experienced during the extreme conditions of radiation damage and the subsequent creation of Frenkel pair defects.

Currently, the form of cation-anion Buckingham potentials reported in the literature effects an unphysical attraction at short range (providing a greater contribution than the repulsive Coulombic component). Novel methodology has been employed to derive potentials, through empirical fitting, which remain applicable over the entire region of interest.

Following the derivation of a robust set of inter-atomic potentials, modelling techniques are validated against comparison to crystallographic data and other physical parameters subsequent to calculating the intrinsic defect chemistry of UO_2. This study is an important precursor to further research considering nonstoichiometry, substitutional defects, anion transport and diffusion mechanisms and simulation of both bulk terminated and reconstructed surfaces.

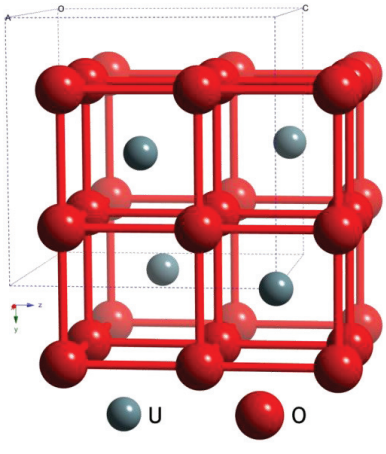

Fig. 1. Unit cell of cubic (Fm3m) UO_2 adopting the fluorite structur

Atomistic Model of Helium in Plutonium

P.H.Chen, B.Y.Ao, X.C.Lai, X.L.Wang

China Academy of Engineering Physics, Mianyang 621900, P.R. China, e-mail : chenph@live.cn

In the past decade there has been a significant interest in the radiation damage of metallic plutonium as part of efforts to understand the aging of this unusual material. To obtain physically meaningful results from atomic simulations, the key aspect is the quality of the atomic potentials between the different types of atoms. Classical molecular dynamic (MD) simulations of helium in metallic Pu require three interatomic potentials: Pu-Pu, Pu-He, and He-He. The chief obstacle in developing potentials for Pu is the very strange distorted crystal structures of Pu. Directional bonding is expected to be even stronger. Recently, progress has been achieved in the form of a modified embedded atom method (MEAM) potential for pure Pu [1]. The MEAM was created by Baskes, by modifying the EAM to include the directionality of bonding. For some of the point defect calculations, however, we observed less satisfactory agreement between DFT and the MEAM calculations when the original MEAM potential parameters were used.

In the present study, a new MEAM interatomic potential for Pu-Pu was constructed on the basis of zero-temperature electronic structure (DFT) calculations and experimental data. We followed similar procedures prescribed by Lee and Baskes [2] to fine-tune the parameters and improve the overall agreement with experiments and DFT calculations. The Pu-He potential was developed based on the Chen-Möbius lattice inversion [3] and the energy difference between B1- and B3-type Pu-He crystals. First, we constructed the extended phase space including B1 and B3 structures. The aim was to derive the proper interatomic potentials from an extended phase space including equilibrium and nonequilibrium states. This could cover more configurations and interatomic spacing of our interest than that only from one equilibrium configuration. Second, the pseudopotential total-energy calculations for two type Pu-He crystals were performed from lattice constant = 0.3-0.9 nm. Finally, the pair potential curves were directly evaluated from the total-energy difference between B1- and B3-type Pu-He crystals based on Chen-Möbius lattice inversion techniques. By means of MD, we have examined these interatomic potentials. Comparing with the experimental data, the thermodynamic and elastic properties were well reproduced by these potentials. Satisfactory agreement of vacancy and helium interstitials formation energies from DFT and MEAM calculations was also found.

References

[1] M.I.Baskes, Phys.Rev.B **62**,15532 (2000)
[2] B.J.Lee, J.H.Shim, M.I.Baskes, Phys.Rev.B **68**, 144112 (2003)
[3] S.Zhang, N.X.Chen, J.Chem.Phys **118**, 3974 (2003)

Is There an Ordered Magnetic Structure in U_2Fe_3X (X = Si, Ge)?

El'ad N. Caspi[1], Itzhak Halevy[1], Oleg Rivin[1], Hanania Ettedgui[1], Shay Salhov[1]

[1] *Nuclear Research Center Negev (NRCN), P.O. Box 9001, Beer-. Sheva 84190, Israel, e-mail: halevyi@caltech.edu*

U_2Fe_3X (X = Si, Ge) is previously reported to crystallize in the hexagonal *P63/mmc* space group [1-4]. The maximal nearest neighbor U-U distance is well below the Hill limit (≈3.5 Å) for the existence of localized magnetic moments in actinides in both compounds. Surprisingly, previously studied bulk magnetic properties of U_2Fe_3Ge [1, 2] indicate the existence of such magnetic localization. In particular, a large magnetic anomaly in the magnetization measurement as a function of temperature was observed at T = 55 K, similar to ferromagnetic ordering.1,2 Moreover, from Mössbauer measurements it was concluded that this magnetic behavior originates from local magnetic moments in the U sublattice.

To the best of our knowledge, no detailed study aimed at the determination of the magnetic structure was done for these U compounds. Therefore, additional research is needed to shed light on this unique magnetic behavior. It is especially of interest to accurately determine the U-sublattice magnetic structure. For this goal, we studied the U_2Fe_3X (X=Si,Ge) compounds using powder neutron diffraction as well as bulk magnetic measurements. For both X=Si, and Ge compounds our study shows a magnetic behavior very similar to that previously observed for the X=Ge one [1, 2]. However, no ordered magnetic structure is observed in the powder neutron diffraction patterns measured as a function of temperature down to 10K, for both compounds. This interesting behavior is reminiscent of the existence of large spin fluctuations in both compounds. Its origin will be discussed.

References

[1] S.K. Dhar, K.V. Shaha, P. Bonville, P. Manfrinetti, F. Wrubl, Solid State Comm. **147**, 217 (2008).
[2] M.S. Henriques, O. Tougait, H. Noel, L.C.J. Pereira, J.C. Waerenborgh, A.P. Gonçalves, Solid State Comm. **148**, 159 (2008).
[3] J.B. Kusma, H. Nowotny, Monat Fuer Chemie 95, 428 (1964).
[4] D. Berthebaud, O. Tougait, A.P. Gonc¸alves, H. Noël, Intermetallics **16**, 373 (2008).

Development of Ce-La Alloys as Pu-Ga Surrogate Alloys

Michael Ling

AWE, Aldermaston, Reading RG7 4PR UK, email: Michael.ling@awe.co.uk

Plutonium (Pu) is characterised by its extremely complex phase behaviour, with a crystal structure which changes with temperature, pressure, chemistry and time. When pure plutonium is heated from room temperature to melt temperature under ambient pressures, 5 phase transformations will take place in sequence. However, the high temperature δ-phase can be stabilised down to room temperature by the addition of gallium (Ga).

Upon cooling, molten Pu-Ga alloy first solidifies to form the bcc structured ε phase which is present as a single phase. It then goes through the ε+δ binary phase region until all of the ε phase transforms into a single fcc structured δ phase. On further cooling to room temperature it is possible for a partial transformation of δ to α via γ and β phases. The as-cast microstructure of the Pu-Ga alloy consists of cored grains, each with a gallium rich δ phase centre surrounded by gallium lean α phase outer region. The split between α phase and δ phase regions is determined by the initial gallium concentration. However, high temperature annealing allows redistribution of the Ga content within each grain and thereby transformation of any α phase which is present into the "stabilised" δ phase. Selection of annealing parameters (such as annealing temperature and holding time) is strongly dependent on the as-cast microstructure. The as-cast microstructure is influenced by many factors during the casting process, therefore understanding the effect of these factors is of importance in respects of both fundamental Pu material science and production practice.

One of these factors is the ε grain structure formed through solidification. The cored structure of δ phase in the as-cast microstructure is generally accepted to develop in the ε+δ region, due to the significant difference in Ga diffusion rates in the ε and δ phases. As the δ phase nucleates and grows by consuming the original ε grains, it is rational to assume that the ε grain structure will have a significant effect on the final δ phase structure. However, very little work has been done to understand this.

To study the mechanism of this effect, direct observation of ε→δ phase transformation at elevated temperature is thought to be the best approach in comparison with other research methods. However, due to its radioactive nature and the limitation of analysis facilities available, such direct observation on the Pu-Ga alloy is very difficult if not impossible at present. The use of a non-radioactive surrogate to perform a simulation study is thus an obvious option.

A Ce –La alloy containing less than 6 wt% of La was identified as a suitable surrogate for the Pu-Ga alloy. The combination of SEM imaging and EBSD analysis based on an SEM with a hot-stage was identified as the preferable technique to realise the objective of direct observation of the δ (bcc)→γ(fcc) phase transformation in a Ce-La alloy at elevated temperature, which is similar to that of the ε(bcc)→δ(fcc) phase transformation in the Pu-Ga alloy.

Ce-La alloys are not readily commercially available, are rarely reported and are not well understood even at room temperature. A feasibility study to develop preparation and analysis methods for Ce-La alloys was thus carried out. One of the main objectives of the study was to demonstrate the suitability of adopting EBSD as a means of characterising Ce-La alloy structure and phase transformations. This is due to the extreme surface reactivity and affinity of Ce for oxygen that makes it difficult

to prepare and maintain a flat and clean sample surface suitable for EBSD analysis, which is highly surface sensitive.
The suitability of Ce-La alloys as Pu-Ga surrogate alloys and the suitability of using an SEM with a hot-stage as the preferred technique to study the δ (bcc)→γ(fcc) phase transformation in a Ce-La alloy at elevated temperature will be described. The up-to-date results from the feasibility study on Ce-La alloys will be presented.

Thermodynamic Investigations of the Actinide Oxides

Octavian S.Vălu, Ondrej Beneš, Rudy J. M. Konings

European Commission, Joint Research Centre, Institute for Transuranium Elements,P.O. Box 2340, 76125 Karlsruhe, Germany, e-mail: sorin.valu@ec.europa.eu

Studies on the oxides and mixed oxides of actinide elements such as thorium, uranium and plutonium are of great interest in nuclear industry since some of the oxides are used as nuclear fuels in various types of reactors [1]. The thermodynamic properties such as enthalpy and heat capacity of these materials are needed for reactor design and safety calculations.

The first experimental studies of the pseudo-binary UO_2 – PuO_2 phase diagram were performed in the 1960s. They were based on solidus – liquidus measurements obtained by thermal arrest technique on tungsten-encapsulated samples [2-4]. In the last decade, first Carbajo [5] and more recently Guéneau et al. [6] proposed a phase diagram based on these experimental data and thermodynamic modeling and optimization. According to these assessments, the uranium and plutonium dioxides form a continuous solid solution and the solidus and liquidus temperatures show a nearly ideal behavior (Fig. 1).

Recently Kato et al. [7] published a new experimental study in which the commonly accepted phase transition temperatures were questioned and considerably higher values were proposed in the composition range from 20 to 100% PuO_2. Recent studies performed in ITU [8] in the composition range rich on plutonium (x(PuO2)>0.5) differ considerably from all these studies and suggest non-ideal behaviour of this binary system.

To investigate this in further detail, enthalpy increment measurements of $(U_{0,64},Pu_{0,36})O_2$, $(U_{0,50},Pu_{0,50})O_2$ and $(U_{0,25},Pu_{0,75})O_2$ compositions were performed using a drop calorimeter in the temperature range from 400 K to 1800 K. We also measured pure UO_2 and PuO_2 samples and compared them with literature data obtaining a good agreement, indicating that our set-up allows us to measure the enthalpy increments precisely enough to predict if the $(U,Pu)O_2$ solid solution system follows an ideal behavior. Non-ideal behaviour could be evident if from excess contributions resulting from the lattice strain due to the difference in ionic radius of Pu^{4+} (100 pm) and U^{4+} (103 pm). For every intermediate composition of the solid solution measurements were performed at given temperatures 573 K, 1273 K and 1673 K and compared with the end-members enthalpies. Further measurements on $(Th,Pu)O_2$ solid solution are being made, as the possible lattice strain effect should be more pronounced (ionic radius Th^{4+} = 108 pm).

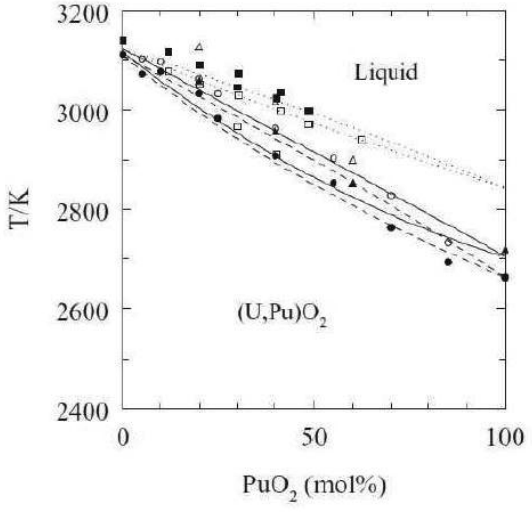

Fig. 1. Solidus and liquidus temperature in the UO_2-PuO_2 system. The circles correspond to the experimental data by Lyon and Bailey c, the triangles by Aitken et al. [3] and the squares by Kato et al. [7]; The solid lines represent the recommended liquidus and solidus by Adamson et al. [4] the broken line the ideal liquidus and solidus based on Lyon and Bailey[2] and the dotted line the liquidus and solidus suggested by Kato et al. [7].

References

[1] C. Ganguly, Development of plutonium-based advanced LMFBR fuels and thoria-based PHWR fuels in India, *IAEA-TECDOC* **352**, 107-127 (1985).
[2] W. L. Lyon and W. E. Baily, *J. Nucl. Mater*. **22**, 332 (1967).
[3] E. A. Aitken et al., A thermodynamic data program involving plutonia and urania at high temperatures, GEAP-5672, General Electric, 1968.
[4] M. G. Adamson et al.,*J. Nucl. Mater.***130**, 349 (1985).
[5] J. J. Carbajo et al., *J. Nucl. Mater.* **299**, 181 (2001).
[6] C. Guéneau et al., *J. Nucl. Mater.***378**, 257 (2008).
[7] M. Kato, K. Morimoto, H. Sugata, K. Konashi, M. Kashimura, T. Abe, *J. Nucl. Mar.* **373**, 237-245 (2008).
[8] F. De Bruycker, Thesis University of Orleans (2010).

U-Mo Aalloys Prepared by Splat Cooling

Nhu-T.H. Kim-Ngan[1,2], L. Havela[1], A. Adamska[1], J. Kastil[1], J. Prchal[1], I. Tkach[1]

[1] Faculty of Mathematics and Physics, Charles University, Ke Karlovu 5, 12116, Prague, Czech Republic, e-mail: tarnawsk@mag.mff.cuni.cz
[2]Institute of Physics, Pedagogical University, Podchorazych 2, 30-084 Krakow, Poland

Uranium metal exhibits three allotropic phases, namely α (orthohombic)-, β (tetragonal)- and γ (body-centered cubic). Electronic properties are known only for α-U stable below room temperature. Somewhat β- and γ-U may have different electronic properties, as their density is lower (18.06 g/cm^3 for γ-U comparing to 19.04 g/cm^3 for α-U). γ-U is stable only in the range 1049-1408 K, but literature data indicate that it can be preserved by quenching if U is doped by e.g. Mo on the level of 8-10wt% [1,2].

We undertook a study of (meta) stabilization of the *bcc* phase corresponding to γ-U using the ultrafast cooling (splat-cooling technique), which may yield the *bcc* phase at lower level of Mo doping and also provide a shape convenient for further studies. In the first stage, we prepared 3 samples of U with 0, 1 and 2at.% Mo by arc-melting. The as-cast samples were then transfered to a high-vacuum splat cooling system (VacuumPraha) giving the effective cooling rate of ~10^6K/s. The resulting splat-cooled discs had a diamater of ~20 mm and a thickness below 100 μm. The samples were characterized by X-ray diffraction (XRD), taken directly from the splat surface, for phase determination. The pure U splat exhibited still the usual α-phase with a small amount of UC, probably segregated at the surface. Increasing the molybdenum content to 2 at% the reflections of α-U start to disappear and those of γ-U pop up. For obtaining a pure *bcc* phase by splat cooling more Mo is clearly necessary. Higher Mo concentrations will be covered in the subsequent step. For such phases electrical resistivity, magnetic susceptibility and specific-heat data will be presented.

References

[1] I. Grenthe, J. Drozdynski, T. Fijino, E.C. Buck, T.E. Albrech-Schmitt, S.F. Wolf, in: *The Chemistry of the Actinide and Transactinide Elements*, 3rd edition, L.R. Morss, N.M. Edelstein, J. Fuger and J.J. Katz, eds, Springer 2006, Vol. 1, pp. 253-698

[2] V.P. Sinha, P.V. Hegde, G.J. Prasad, G.K. Dey, H.S. Kamath, *J. Alloys&Comp.* 506, 253 (2010).

X-ray and ^{237}Np Mössbauer Effect Study of NpPtSn

P. Gaczyński, T. Klimczuk, E. Colineau, K. Gofryk*, J.-C. Griveau, R. Eloirdi, R. Jardin, F. Wastin, J. Rebizant and R. Caciuffo

European Commission, Joint Research Centre, Institute for Transuranium Elements; Postfach 2340, 76125 Karlsruhe, Germany ,
e-mail: piotr.gaczynski@ec.europa.eu
* *present address :* Los Alamos National Laboratory, Los Alamos, New Mexico 87545, USA

During the past decades ternary actinide-based compounds containing d- and p-electron elements have attracted much attention for their large variety of physical behaviors arising mostly from the hybridization of actinide 5f electrons with s, p and /or d states on neighboring sites. An example of a system with promising physical behavior is the ATX composition where A stands for actinide atoms, T for d-element metals and X for p-electron elements.

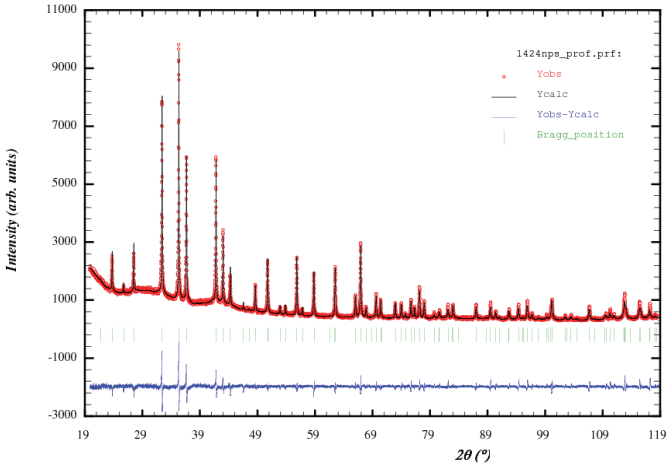

Fig. 1. X-ray diffraction pattern of NpPtSn at 295 K

The ATX compounds crystallize in various crystal structures, like the hexagonal ZrNiAl- and GaGeLi- types, the orthorhombic TiNiSi-type and the cubic MgAgAs-type.

Polycrystalline ingots of NpPtSn were obtained by arc melting stoichiometric amounts of the constituent elements under an atmosphere of high purity argon on a water-cooled copper hearth, using a Zr getter alloy. In order to ensure homogeneity, the arc melted buttons were turned over and remelted 3 times, with weight losses below 0.5%. The crystal structures of compounds were determined from X-ray powder (Siemens D500 diffractometer). The diffraction patterns were analyzed by a Rietveld-type profile refinement method using the Fullprof program [1].

NpPtSn was found to crystallize in the hexagonal ZrNiAl – type structure with the unit cell parameters a = 7.4760(4) Å and c = 4.0838(8) Å. Rietveld refinement proof occupation of the 3g (x = 0.59125) site by Np atoms, 3f (x = 0.24978) by Sn and 2c by Pt whereas the site 1b is shared by Pt and Np atoms.

^{237}Np Mössbauer spectra were recorded between 4 K and 35 K in a transmission geometry spectrometer with a ~100mCi ^{241}Am source kept at a temperature of about 4.2 K. The absorber was prepared by grinding the sample to a fine powder to ensure a constant surface density with an optimal thickness of 140mg Np/cm^2. The velocity scale was calibrated using the $NpAl_2$ standard compound. The isomer shift, IS, is given relative to $NpAl_2$. The spectra were analyzed using Lorenzian lines. The position and relative intensities of the absorption

lines of Np nuclei were calculated by solving the complete Hamiltonian for the hyperfine interaction in both the excited and ground nuclear state of ^{237}Np.
In the paramagnetic region, Mössbauer spectra exhibit two non-equivalent Np sites with relative intensities ~ 1:2. This evidence proofs Np atoms at 3g and "Pt" 2c site. The magnitude of the isomer shift indicates that neptunium atoms are in the 3+ oxidation state for both sites. At 4.2 K the complicated Zeeman pattern shows the occurrence of magnetic ordering on the Np sublattice. However, the low temperature spectra cannot be fitted assuming only two Mössbauer components.

Acknowledgements
PG acknowledges the European Commission for support in the frame of the "Training and Mobility of Researchers" programme. The high purity Np metals required for the fabrication of the compound were made available through a loan agreement between Lawrence Livermore National Laboratory and ITU, in the frame of a collaboration involving LLNL, Los Alamos National Laboratory and the US Department of Energy.

References
[1] Rodriguez-Carvajal J 1993 *Physica B* **192** 55

Surprising Reduction of Surface PuO_2 by an Adsorbed Ice Layer

T. Gouder and A. Seibert

European Commission, JRC, Institute for Transuranium Elements, Postfach 2340, 76125 Karlsruhe, Germany, e-mail: thomas.gouder@ec.europa.eu

At the backend of the nuclear fuel cycle stands the safe long-term disposal of the spent fuel. Detailed understanding of the possible degradation processes, leading eventually to the release of radionuclides into the biosphere, is of great importance. In particular, the resistance of the fuel matrix (UO_2 and U-PuO_2) towards oxidation followed by matrix dissolution, increases the long term stability. Judging this property, and in particular predicting its evolution over long time scales (up to 10^6 years), is difficult because of the complexity of the spent fuel and its surrounding in the repository. We therefore use simplified fuel model systems, to investigate the influence of individual parameters on such surface corrosion reactions. Ultimate goal is to relate the reactivity to basic physico-chemical properties of the solid, in particular its morphology and electronic structure.

As example of such study, we will discuss the surprising interaction of PuO_2 surfaces with ice adsorbed at low temperatures (80 K). Initial goal of this work was to study the formation of a hydrated surface phase under vacuum conditions, using a high surface concentration of water physisorbed as ice film. Adsorbed water molecules should possess enough mobility for reacting, when the surface is warmed up to the ice sublimation temperature. Previously, water was suspected stabilizing higher Pu oxidation states beyond +4 [1], which cannot be reached in the pure oxide [2]. In the present study, however, we did not observe further oxidation of the PuO_2 surface but instead its reduction to Pu_2O_3, after desorption of the ice layer at 160 K. We could attribute this to a photochemical process occurring at the surface. This finding may be of practical importance, since the fuel waste has α, β and γ radiation fields over long time spans. These fields are generally held responsible for the generation of radio-oxidants in the surrounding water, which lead to fuel surface oxidation and corrosion. According to the present study, the radiation could have the exactly opposite effect, favouring surface reduction, at least under the right experimental conditions.

References

[1] J.M. Haschke, T.H. Allen and L.A. Morales, Science **287** (2000), p. 285.
[2] T. Gouder, A. Seibert, L. Havela and J. Rebizant, Surface Sci. 601 (2007), L77.

3O8

Materials science

Magnetic properties, crystallographic structure and electronic properties of Np_2Co_{17} and Np_2Ni_{17}

A. Hen[1, 2], I. Halevy[3], E. Colineau[1], R. Eloirdi[1], J-C. Griveau[1], P. Gaczyński[1], E.N. Caspi[3], I. Orion[2], G. Kimmel[4], I. Yaar[3], W. Potzel[5], R. Caciuffo[1] and J. Gal[4]

[1]*European Commission, JRC, Institute for Transuranium Elements, Postfach 2340, 76125 Karlsruhe, Germany*
[2]*Nuclear Engineering Department, Ben-Gurion, P.O. Box 653, Beer- Sheva, Israel*
[3]*Nuclear Research Center-Negev (NRCN) P.O. Box 9001, Beer-Sheva, 84370, Israel*
[4]*Institute for Applied Research, Ben-Gurion Univ., P.O. Box 653, Beer- Sheva, Israel*
[5]*Physik Department E15, Technische Universität München, 85747 Garching, Germany*

The intermetallic compounds Np_2Co_{17} and Np_2Ni_{17} crystallize in the hexagonal $P6_3/mmc$ structure [1], identical to the structure of the heavy-fermion compound U_2Zn_{17} [2]. In this study, the magnetic properties, crystallographic structure and electronic properties of the Np_2Co_{17} and Np_2Ni_{17} are investigated using Mössbauer spectroscopy, X-ray diffraction measurements, SQUID magnetometry, specific heat measurements, and density functional theory calculations (DFT). The Mössbauer spectra of Np_2Co_{17} indicate that the magnetic ordering in this compound is already established above 77 K. The spectra were fitted using two close magnetic hyperfine fields, corresponding to localized-ordered magnetic moments at the two neptunium non-equivalent sites. The Mössbauer spectra of Np_2Ni_{17} and Np_2Co_{17} are shown in Fig. 1.

The Mössbauer spectra of Np_2Ni_{17} indicate a modulated antiferromagnetic structure, with T_N= 13.1 K. below T_N, a modulated magnetic moment is observed, with different modulation for each site. Np_2Co_{17} and Np_2Ni_{17} present a clear magnetic spectrum with two non-equivalent sites, as expected from the hexagonal $P6_3/mmc$ structure.
Based on the experimental results, it is suggested that both systems, carry highly localized ordered moments. However, it is questionable whether the cobalt or the nickel atoms are magnetically ordered. The electronic properties of both compounds are calculated using the DFT code WIEN97 [3], using the crystallographic parameters obtained from the X-ray powder diffraction measurements [4, 5].

The magnetic transition in the Np_2Ni_{17} is evident in the susceptibility curve obtained from SQUID measurements. The transition temperature, $T_N \approx 14$ K, coincides with that determined from a Mössbauer thermal scan, Fig 2.

The temperature dependence of the specific heat has been measured using a Quantum Design PPMS-14T platform, under static magnetic fields of intensity up to 14 tesla. The results indicate the presence of low-lying electron energy levels and the occurrence of complex magnetic ordering phenomena.

Acknowledgement: "The high purity Np metals required for the fabrication of the compound were made available through a loan agreement between Lawrence Livermore National Laboratory and ITU, in the frame of a collaboration involving LLNL, Los Alamos National Laboratory and the US Department of Energy."

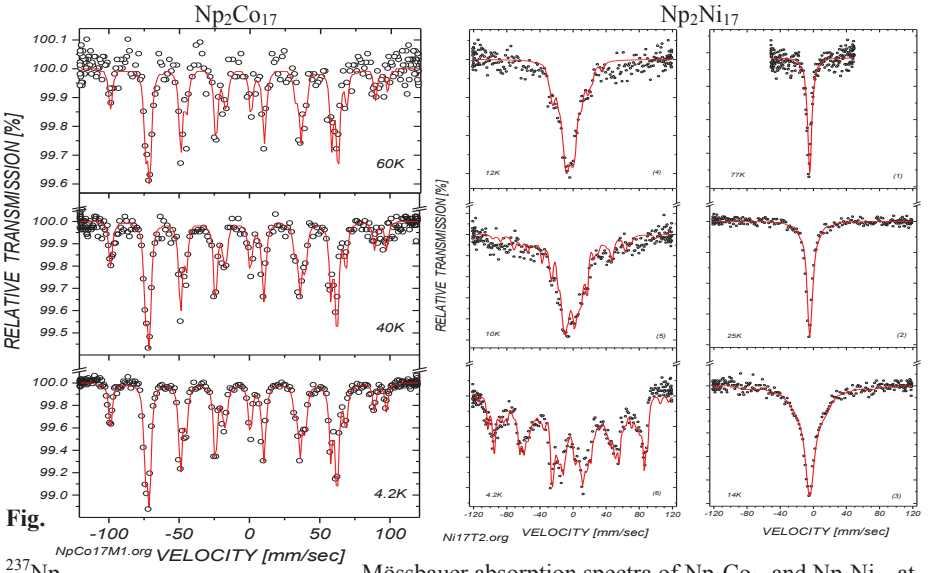

Fig. 1 ^{237}Np Mössbauer absorption spectra of Np_2Co_{17} and Np_2Ni_{17} at various temperatures. The Mössbauer source was $^{241}Am(Th)$ at 4.2K.

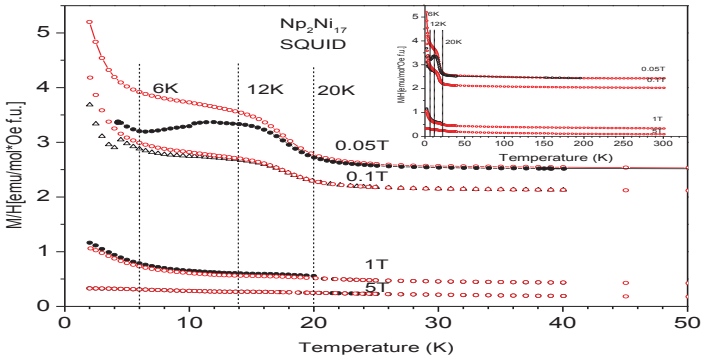

Fig. 2 Np_2Ni_{17} SQUID measurements at various external fields as a function of temperature: a magnetic transition at ~14 K is observed.

References

[1] I. Halevy, et al., 26ièmes Journées des Actinides, 1996, Szklarska Porèba, Poland.
[2] H. R. Ott et al., Phys. Rev. Lett. 52 (1984) 1551–1554.
[3] P. Blaha et al., Wien97-Code (K. Schwarz, TU Wien, ISBN 3-9501031-0-4) 1999.
[4] I. Halevy, E. N. Caspi, I. Yaar, R. Caciuffo, E. Colineau and F. Wastin Crystallographic And Magnetic Properties of the two New Actinides Compounds: Np_2Co_{17} and Np_2Ni_{17}. Actinides 2009, San Francisco, California, USA, July 12-17 2009, 8A6
[5] 1st Bilateral Workshop of the JRC-IAEC Cooperation, 2-6 May 2010 ,Ein-Gedi, Dead Sea – ISRAEL

Structural Insights into the Nucleation and Early Stages of Hydride Formation on Uranium.

T. B. Scott[1], J. Petherbridge[2], C.P. Jones[1] and J. Glascott[2]

[1]*Interface Analysis Centre, University of Bristol, England, BS2 8BS, e-mail: t.b.scott@bristol.ac.uk*
[2]*AWE,* Reading*, England,* RG7 4PR.

Observations and Characterisation of Helium Bubbles in Aged Plutonium Subjected to Extended Heat Treatments

D.W. Wheeler, P.D. Bayer, M.B. Matthews, M. Brierley

AWE, Aldermaston, Reading, Berkshire, RG7 4PR, U.K.

In previous work by the authors [1] dilatometry was used to study the evolution and growth of helium (He) bubbles in aged plutonium (Pu) alloys. The work showed that in extended isothermal heat treatments at elevated temperatures, the two ageing processes in Pu – namely, the generation of lattice damage and the evolution of He – could be measured and quantified. In the early stages of the heat treatments, annealing of the lattice damage occurred, causing the specimens to contract. This was followed by He agglomeration, leading to expansion of the material, which was attributed to growth of the helium bubbles.

The present study continues this work. Delta-Pu alloy samples, approximately 25 years of age, were given extended heat treatments in a vacuum furnace. The specimens were treated at temperatures of between 200 and 500°C for total durations of up to four weeks. Swelling was monitored by regular density measurements. At the end of the heat treatments the specimens were subjected to metallographic preparation and examined using optical and electron microscopy.

Examination of the heat treated specimens revealed that, as with the previous work [1], the heat treatments had caused He, which is present in the form of nanometre-sized bubbles as a result of Pu decay [2], to form a new network of bubbles with diameters of between 1 and 2 μm (see Figure 1). In addition, a smaller number of larger bubbles, examples of which are shown in Figure 2, were also observed. These bubbles had diameters of up to 15 μm.

The bubble sizes and distributions were measured and the results can be used to calculate the diffusion coefficient of He in Pu. This is done by equating He diffusing into a bubble to the case of diffusion into a hollow sphere from a thick wall and assuming that the He concentration is uniform throughout the wall. Using the Barrer equation [3] the diffusion coefficient can be calculated. This work has shown that the diffusion coefficient of He is dependent on the age of the Pu. He diffuses faster in young (2-4 years of age) Pu alloy than older (19-year-old) material. It is proposed that this is because the defect vacancy / He atom ratio is higher for young material than old giving a large vacancy surplus to aid diffusion.

References

1. D.W. Wheeler, P.D. Bayer, *J. Alloy. Compd.*, **444-445,** 212-216 (2007).
2. A.J. Schwartz, M.A. Wall, T.G. Zocco, W.G. Wolfer, *Phil. Mag.*, **85**, 479-488 (2005).
3. R.M. Barrer, *Diffusion in and through solids*, Cambridge University Press (1951).

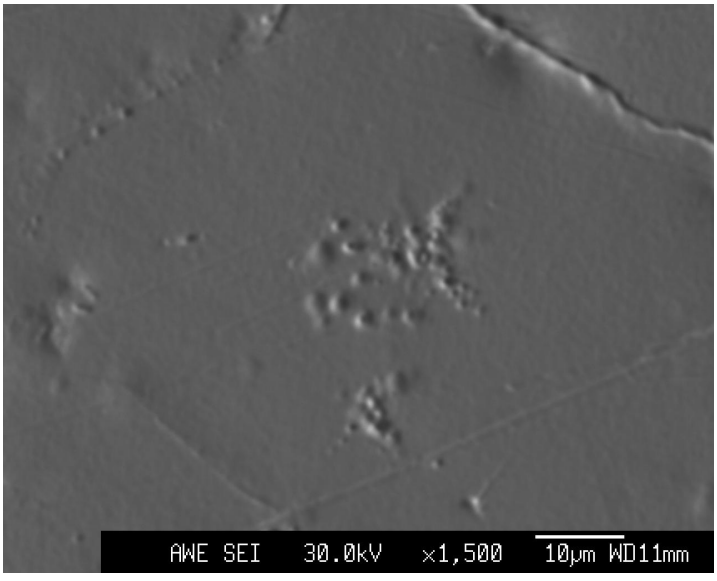

Fig. 1: Secondary electron micrograph of bubbles in a Pu alloy heat treated for 1 week at 500°C showing micron-sized bubbles in the microstructure.

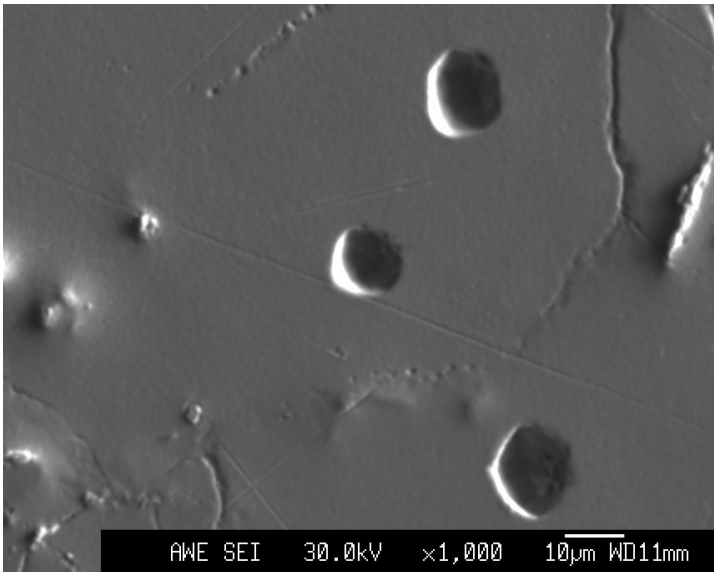

Fig. 2: Secondary electron micrograph of bubbles in a Pu alloy heat treated for 1 week at 500°C showing three bubbles approximately 10 μm in diameter in the microstructure.

3P2

Materials science

Phase Equilibrium, Crystal Structure and Physical Properties of Compounds in the U-Mo-B System

Leonid Salamakha[1,4], Ernst Bauer[1], Herwig Michor[1], Gerfried Hilscher[1], Corrado Rizzoli[2], Oksana Sologub[3], Antonio Gonçalves[3], Stepan Mudryi[4]

[1] *Institute of Solid State Physics, Vienna University of Technology, A-1040 Wien, Austria*
e-mail: salamakhaleonid1@rambler.ru
[2] *Dipartimento di Chimica GIAF, Università degli Studi di Parma, 43100 Parma, Italy*
[3] *Departameno de Química ITN, E. N. 10, P-2686-953 Sacavém, Portugal*
[4] *Department of Physics of Metals, Faculty of Physics, L'viv National University, 79005 L'viv, Ukraine*

In continuation of our research work on the U-Mo-B system, in given presentation we report the results of our studies on the phase equilibria, crystal structures and physical properties of compounds observed within the concentration range 40 – 80 at.% of boron at 900° C.
Samples were prepared by arc melting the proper amounts of the constituent elements under high purity argon on a water-cooled copper hearth. The alloys were annealed at 900° C for 14 days. The crystal structures of compounds were determined from X-ray powder (Philips X'Pert diffractometer, Cu K_α radiation, 2θ range 10-120 deg) and single crystal diffraction data (CAD 4 and Bruker AXS SMART CCD diffractometers). Phase identifications and lattice parameters refinements were performed using the Powder Cell, WinPlotr, TREOR and DICVOL programs. Bulk physical properties (electrical resistivity, specific heat, magnetism) were measured by a number of standard techniques.
Six ternary compounds were found to form in the investigated concentration region at 900° C, namely (1) ~UMo_4B_4 (unknown structure), (2) UMo_3B_7 (YMo_3B_7-type structure, *Pnma* space group, a=11.0310 Å, b=3.0995 Å, c=12.7921 Å), (3) ~UMo_2B_7 (unknown), (4) ~U_2MoB_{10} (unknown), (5) $UMoB_4$ ($ThMoB_4$-type, *Cmmm* space group, a=7.300 Å, b=9.415 Å, c=3.648 Å) and (6) U_2MoB_6 (Y_2ReB_6-type structure, *Pbam* space group, a=9.2793 Å, b=11.3742 Å, c=3.6861 Å) (Fig. 1) among them the UMo_3B_7 was observed for the first time and studied in details from the X-ray single crystal diffraction [1, 2]. The structure is related to AlB_2-type by formation of six-membered rings of boron extending infinitely in *b* direction (Fig. 2). From electrical resistivity measurements (4-contact method in the temperature range from 0.3 to 200 K and in magnetic fields up to 12 T), no evidences of magnetic ordering of any kind were observed in all temperature range. The resistivity curve of material can be described by Bloch-Gruneisen relation. Resistivity vs. magnetic field measurements for different temperatures showed positive magnetoresistance (Fig. 3). The crystal structure studies and physical properties measurements for the compounds with tentative compositions are in progress.

Acknowlegments. L.S. is thankful to ÖAD for the Ernst Mach Fellowship at the Institute of Solid State Physics of Vienna University of Technology.

References

[1] L. Salamakha et al, 38 Journées des Actinides, Wroclaw, 12-15 April, 2008, Poland
[2] L. Salamakha et al., 39 Journées des Actinides, La Grande-Motte, 28-31 March, 2009, France

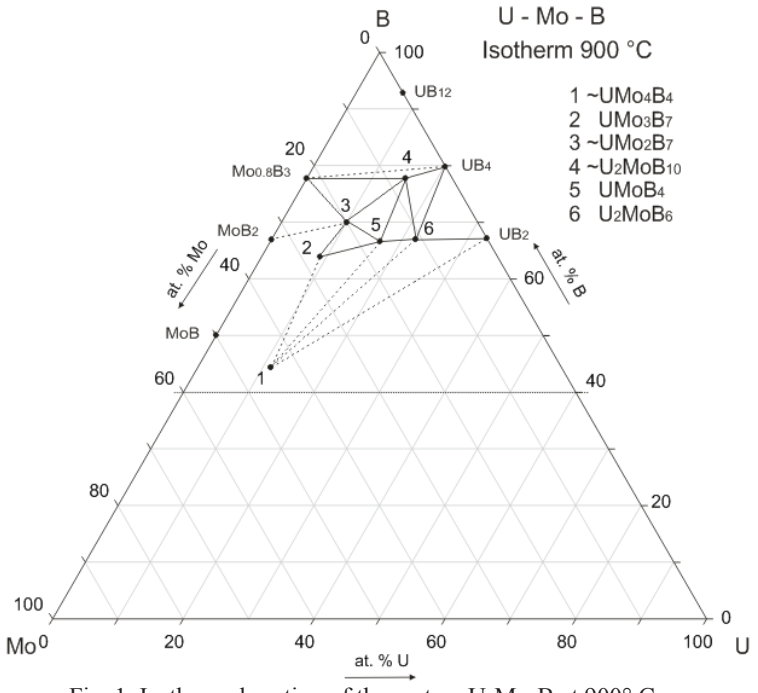

Fig. 1. Isothermal section of the system U-Mo-B at 900° C.

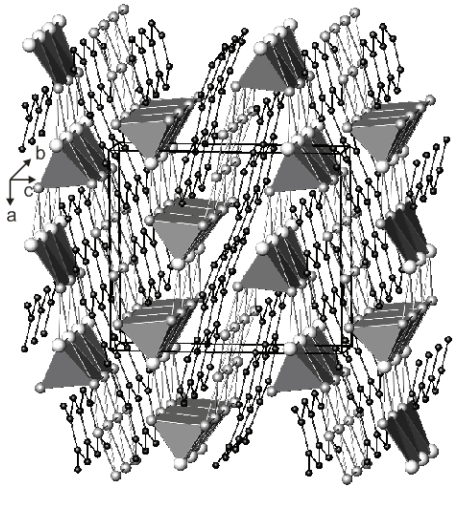

Fig. 2. Boron layers in UMo_3B_7. Empty tetrahedra and tetragonal pyramids are outlined.

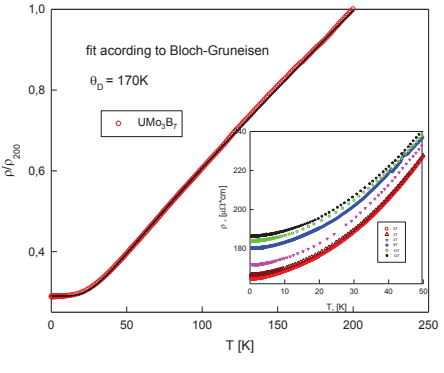

Fig. 3. Resistivity vs temperature of UMo_3B_7 at different magnetic fields.

Self-irradiation effects on the static strength of Pu and Pu-Ga alloys

Brandon W. Chung, David S. Hiromoto

[1] *Lawrence Livermore National Laboratory, P.O. Box 808, Livermore, CA 94551, e-mail: chung7@llnl.gov*

Plutonium, because of its radioactive nature, ages from the "inside out" by means of self-irradiation damage and thus produces Frenkel-type defects (vacancies and self-interstitial atoms) and defect clusters [1]. The self-irradiation damage in Pu-239 occurs mainly by alpha-particle decay, where most of the damage comes from the U-235 recoil nucleus. The defects resulting from the residual lattice damage and helium in-growth will result in changes in the static strength of plutonium with time. Because these effects would normally require decades to measure, studies are underway to assess the effects of extended aging on the mechanical properties of plutonium alloys by incorporating roughly 7.5 weight percent of highly specific activity isotope Pu-238 to accelerate the aging process by approximately 17 times [2-3]. In addition we are validating the accelerated aging approach by testing naturally aged plutonium metals [3].

Both the tensile and compressive tests are utilized to measure changes in the static strength plutonium with age. Coupling with systematic tests on Pu-238 doped accelerated aged alloys over a period of about 8 years, the evolving static strength of plutonium due to alpha decay can be projected for periods over 100 years. Our measurements on various ages of Pu-Ga alloys show increase in the yield and ultimate tensile strength with age. The initial rate of change in the strength decreases in a few years mostly due to initial increase in the concentration of Frenkel pairs that quickly attain stationary values. After the initial transient stage, the rate of change in the strength becomes reduced, reaching near steady values at 150 and 180 MPa for the engineering yield strength and ultimate tensile strength, respectively. Metallurgical evaluation of fractured surfaces of tensile parts coupled with identical engineering yield strengths between the tensile and compression tests indicate moderately ductile nature of aged Pu-Ga alloys. Our initial tests on aged alpha plutonium metals also indicate the static strength increases with the accumulation of self-irradiation damage.

We are submitting an oral presentation and preferred topic is materials science.

References

[1] W.G. Wolfer, Los Alamos Sci., **26** (2000) 274
[2] B.W. Chung et al., *J. Nucl. Mater.*, **385** (2009) 91.
[3] B.W. Chung et al., *J. Nucl. Mater.*, **355** (2006) 142.

This work performed under the auspices of the U.S. Department of Energy by Lawrence Livermore National Laboratory under Contract DE-AC52-07NA27344.

3P4

Materials science

Crystal Structures of Binary U-Ru Compounds

M. Pasturel[1], A. P. Gonçalves[2], O. Tougait[1], H. Noël[1]

[1] Sciences Chimiques de Rennes, Université de Rennes 1, UMR CNRS 6226, Campus de Beaulieu, 35042 Rennes Cedex, France, e-mail : mathieu.pasturel@univ-rennes1.fr

[2] Dep. Química, Instituto Tecnológico e Nuclear/CFMC-UL, P-2686-953 Sacavém, Portugal

In order to discover new uranium based strongly correlated electron systems presenting heavy fermion behaviour, superconductivity, giant thermopower or other interesting properties, isothermal sections of U-T-X (where T is a transition metal and X a p-block element) ternary phase diagrams have been systematically investigated by our group. During previous Journées des Actinides, results on different ternary systems such as U-Ru-Al, U-Ru-Si or U-Ru-Ge have already been presented.

The completeness of isothermal sections requires the determination of equilibria between ternary and binary phases, which are always checked both by scanning electron microscopy (SEM), complemented with energy dispersive spectroscopy (EDS), and powder X-ray diffraction (XRD). The latter requires the knowledge of crystal structures of binary and ternary compounds. In the case of U-Ru-X diagrams, only limited information is available about crystal structures of binaries on the U-Ru axis: URu_3 is well-known to adopt a cubic $AuCu_3$ structure-type, while a monoclinic cell with C2/m space-group is assumed for U_2Ru. No other data are available for URu, U_3Ru_4, U_2Ru_3 or U_3Ru_5 mentioned in literature. The hardness of these compounds makes their grinding difficult and thus almost impossible their study on a powder form. Their non-congruent melting and easy oxidization does not allow classical high temperature synthesis of single crystals. The U and Ru high reactivity with different “low temperature” melting elements prohibits many molten metal flux growth of single crystals.

We thus decided to use alternative methods to the classical arc-melting one to obtain information about the crystal structures of these binaries. Mainly, splat-cooling experiments were performed, giving thin metallic foils with extremely fine microstructure, enabling fast reaction and crystallization upon annealing. Their XRD characterization is then carried out similarly to powders. Novel features on the U-Ru binary phases and phase diagram highlighted by SEM-EDS and XRD analyses on different samples, arc-melted or splat-cooled, coupled to differential thermal analyses, will be presented.

3P5

Materials science

A New Experimental Perspective on the U-O_2-H_2O Reaction System

N. Harker[1], T. B. Scott[1], J. Petherbridge[2], and J. Glascott[2]

[1]Interface Analysis Centre, University of Bristol, England, BS2 8BS.
[2]AWE, Reading, England, RG7 4PR, e-mail: N.J.Harker@bristol.ac.uk

Mapping of Magnetization Densities in UNi_2 by Polarized Neutron Diffraction

Arsen Gukasov[3], Marián Mihalik,[1] Mária Zentková[1], Slavomír Mat'aš[2], Karel Prokeš[2]

[1] *Institute of Experimental Physics, Slovak Academy of Sciences, Watsonova 47, 040 01 Košice, Slovak Republic , e-mail: mihalik@saske.sk*
[2] *BENSC – Helmholtz-Zentrum, Glienicker Str. 100, 141 09 Berlin, Germany*
[3] *Laboratoire Léon Brillouin, CEA/Saclay, 91191, Gif-sur-Yvette, France*

UNi_2 single crystal was grown by a Czochralski method in a tri-arc furnace. The crystal was investigated by elastic neutron diffraction ($\lambda = 0.244$ nm) on the two-axis difractometer E4 in HMI Berlin and by magnetization measurements in field up to 5 T on MPMS system. Crystal structure determined from neutron diffraction data is consistent with expected $MgZn_2$ structure (space group $P6_3/mmc$). Our crystal is of good quality consisting of only one grain. The magnetic contribution to the integral intensity of reflections $I_M = I_T - I_{40K}$ is very weak, however we were able to follow the temperature dependence of this signal on top of the (1 0 2) reflection and found the magnetic phase transition at $T_c \approx 22$ K (Fig.1.). Magnetic moment of 0.077 μ_B/f.u. was obtained by normalisation of the additional integrated intensity of magnetic origin $I_M = I_{2K} - I_{30K}$ to the integrated intensity associated with the nuclear Bragg peak I_{30K}. Determined Curie temperature and magnetic moment (Fig.2.) correspond very well with values determined earlier from magnetisation data [1, 2].

We performed a polarized neutron experiment on UNi_2 single crystal using the 5cl spectrometer in CEA Saclay by collecting data at 35 K, 4K and 2 K and at magnetic fields 0T, 2 T and 5 T. The main objectives were investigation of the uranium orbital and spin moments (degree of the delocalisation), their spatial distribution and a magnetic-field influence on these components. Besides, possible moments on two different Ni sites and in the interstitial region and their field development was analyzed.

To evaluate our experimental data we proposed four different models. Three of them predict magnetic moment on U – atoms as well on Ni – atoms (hexagonal model, model with lower symmetry and model which assumes non collinear arrangement of magnetic moments on Ni(II) – atoms. The last model predicts no magnetic moment on Ni – atoms. In the frame of all

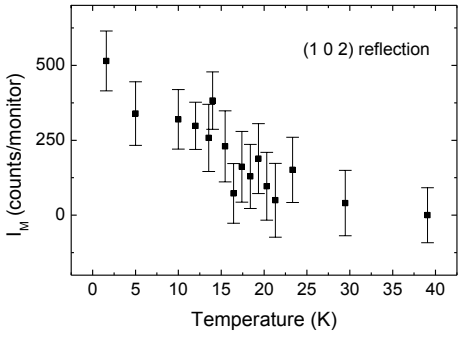

Fig.1. Temperature dependence of the magnetic contribution to the integral intensity of (1 0 2) reflection.

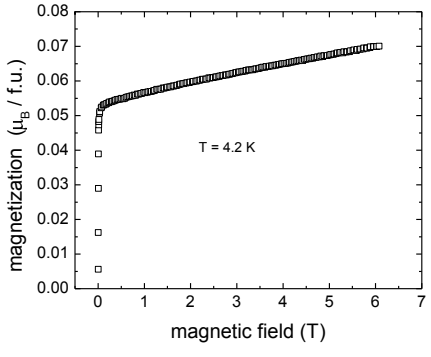

Fig.2. Field dependence of magnetization measured by SQUID magnetometer on MPMS.

models we can refine magnetic structure satisfactorilly well. The problem is: the moment on U – atoms is three – times lower as we expected and as is known from bulk magnetization measurements. The lower value of magnetic moment can be explained by small changes in crystal structure. Measurements for the nuclear structure on 4-circle spectrometer can help us to solve this problem. The dependence of magnetic moment on form factor shows a maximum at about f(Q) = 0.2. Distribution of magnetic moments is shown for projection [001] and [010] on Fig.3.

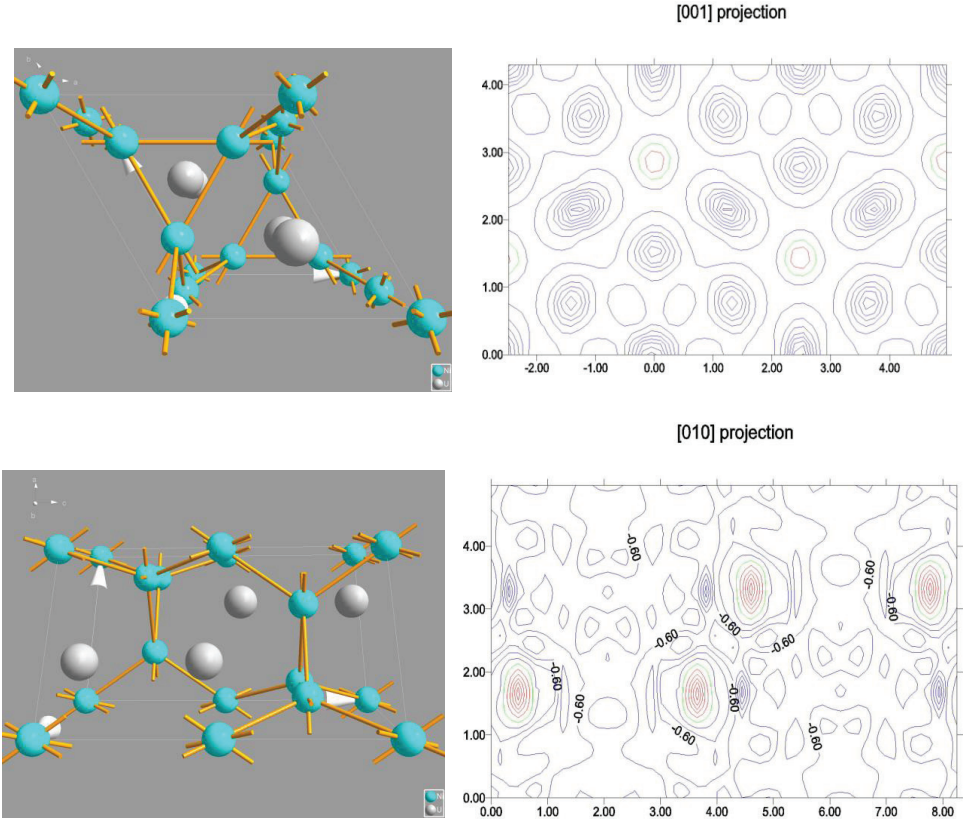

Fig.3. Crystal structure (left) and distribution of magnetic moment (right) are displayed for projections [001] and [010]. Red color represents the highest value of magnetic moment, green color lower value and the lowest value of magnetic moment is drawn by dark blue color. The moment is very well localized on the U sites and practically there is no moment on Ni sites but in the case of both projections high density of moment is seen in interstitial region.

References

[1] S. Maťaš, M. Mihalik, A.A. Menovsky, Z. Arnold, O. Mikulina, Acta Physica Slovaca 48 (1998) 811.
[2] P.H. Frings, J.J.M. Franse, A. Menovsky, S. Zemirli, B. Barbara, JMMM 54-57 (1986) 541.

Two-Step Excitation of Chemiluminescence in Detection of Trace Amounts of Lanthanides and Actinides in Solutions

I.N. Izosimov, N.G. Gorshkov, V.A. Mikhalev, S.N. Nekhoroshkov, Yu. I. Trifonov, N.G. Firsin

Khlopin Radium Institute, 2nd Murinski avn. 28, St. Petersburg 194021, Russia
e-mail: izig@mail.ru

A development of tunable lasers gives rise to appearance of new procedures for detection of trace amounts of substances in various media. The methods of laser spectroscopy used for liquids allow not only detection of traces of various substances but also determination of valence states and molecule types [1].

Pu, Np, and a number of lanthanide and actinide compounds do not produce direct luminescence in solutions and traditional procedure with time-resolution (TR) of analytical luminescence signal (TRLIF) [2] cannot be used for their detection. However, for detection of Pu, Np, and a lot of actinide and lanthanide compounds TR procedure can be used with registration of chemiluminescence of luminol (5-amino-1,2,3,4-tetrahydro-1,4-phthalazindione) arising in light-induced excitation of actinide ions. Chemiluminescence is one of the most sensitive methods of detection of actinides and lanthanides in solutions [1, 3].

In our experiments chemiluminescence arises as a result of oxidation of luminol molecule with $OH\cdot$ radical generated in optical excitation of the element to be detected and entering into composition of hydroxo complex. An excitation of hydroxo complexes in a solution up to an energy allowing electron transfer from the ligand (OH^-) to the central ion of actinide or lanthanide with subsequent splitting off of $OH\cdot$ radical is realized in successive resonance absorption two photons with actinide or lanthanide ion. For this two-step excitation of hydroxo complexes we used tunable lasers. Two-step excitation allows us to avoid direct excitation of chemiluminogen (in our experiments, luminol) and bring energy sufficient for subsequent initiation of chemiluminescence reaction [1, 3]. It is significantly that in the first step of excitation f-f transitions can be used, which abruptly increases the procedure selectivity.

An increase of the power of laser radiation in multi-step scheme of excitation should in principle result in enhancement of the sensitivity of chemiluminescence procedure. However, beginning from some value of laser radiation power, higher-order effects play a significant role.

In particular, non-resonance two-step excitation of hydroxo complexes through virtual intermediate level of the ion to be detected begins to manifest itself. In this case, the selectivity of procedure caused by the use of f-f transitions abruptly decreases.

The experiments were performed with hydroxo complexes of Sm(III). The wavelength of dye generation for the first step of excitation was chosen based on absorption spectra of solutions containing Sm(III) and luminol. Absorption spectra of samarium chloride and luminal aqueous solutions are presented in Fig. 1. Since the absorption end of luminol (sodium form) is close to the strongest line of samarium spectrum at 401 nm, the experiments on reduction of samarium with laser radiation were performed at the line of 477.5 nm (Fig. 2). In this case, the probability of excitation of luminol molecules with laser radiation is minimum.

At a power of laser radiation not exceeding 10^8 W/cm^2 per pulse (the length of laser pulse in the order of 800 ps, spectral width $\delta\lambda$ 0.04 nm) chemiluminescence arises only under addition of samarium to the solution and when the wavelength of laser generation does not fall into the

range of Sm^{3+} absorption chemiluminescence disappears. This means that absorption of two quanta with wavelength 477.5 nm is sufficient for initiation of luminol chemiluminescence. However, with further increase of the power of laser radiation above 10^8 W/cm^2 per pulse chemiluminescence begins to burn even the wavelength of laser radiation is outside the range of Sm^{3+} absorption. This means that two-quantum mechanism of excitation via virtual intermediate level of Sm^{+3} ion begins to operate. Thus, when using multi-step scheme of chemiluminescence excitation there is a need to choice the power of laser radiation to provide required sensitivity and selectivity.

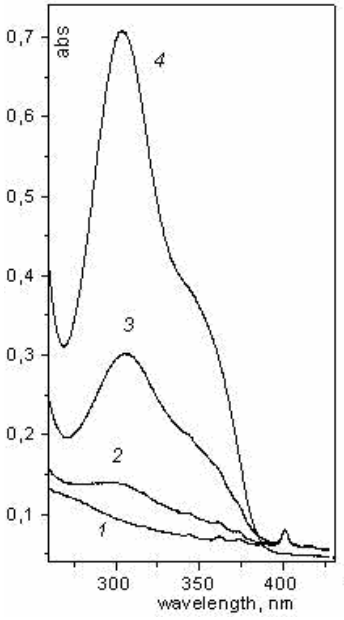

Fig. 1. Absorption spectra of aqueous solutions (1) $7.3 \cdot 10^{-3}$ M $SmCl_3$, pH 5.6, (2) $6.8 \cdot 10^{-3}$ M SmCl3 + $2.9 \cdot 10^{-5}$ M luminol, pH 5.6, (3) $6.8 \cdot 10^{-3}$ M SmCl3 + $8.79 \cdot 10^{-5}$ M luminol, pH 5.6, (4)$\cdot 10^{-4}$ luminol, pH 5.6.

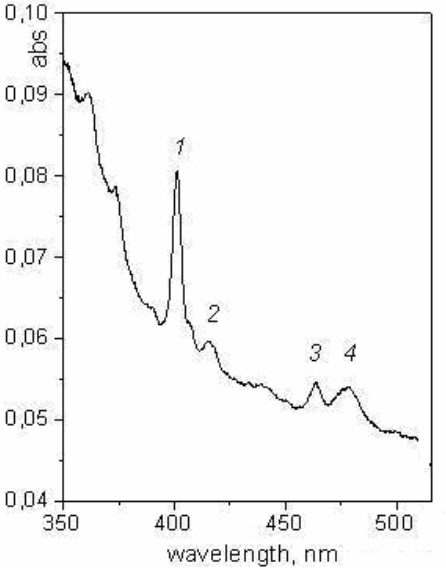

Fig.2. Absorption spectrum of aqueous solution 10^{-3} M $SmCl_3$ + $2 \cdot 10^{-5}$ M luminol: (1) 401.0, (2) 415.0, (3) 464.0, (4) 477.5 nm.

This work was financially supported by the International Science and Technology Center (ISTC Project no. 3694).

References

[1] I.N.Izosimov, Phys. Part. Nucl., **38,** 177 (2007).

Ecological Aspects of Nuclear Facility Decommissioning

Alojz Slaninka[1, 2], Ondrej Slávik[1], Vladimír Míchal[1]

[1] *VUJE, Inc., Okružná 5, SK-91864 Trnava, Slovak Republic, e-mail: slaninka@vuje.sk*
[2] *Slovak University of Technology, Department of Nuclear Physics and Technology, Ilkovičova 3, SK-81219 Bratislava, Slovak Republic*

The first part of presentation deals with description of role of nuclear energy sector in Slovakia. The short description of current status of Slovak nuclear power plants will be done. Nuclear power plants in operation produce more than 50% of electricity generation in Slovakia, what is one the highest rate in the world.

The inevitable part of nuclear energy utilization is the nuclear research & development. VUJE is recognized as the leader organization in the nuclear R&D in Slovakia. The most important previous and ongoing research & development activities will be described. It includes research with the support of the government, R&D projects within the EU Framework Programmes, the IAEA regional and national technical cooperation projects and several others. Information about VUJE's participation in European project "ALLEGRO" will be also done. This project is focused on the Gas Fast Reactor development. In Slovakia VUJE, Slovak Academy of Sciences and Slovak Technical University have agreed to cooperate together on "ALLEGRO" project.

The second aim of the work is to present some ecological aspects of NPP A1 decommissioning project. In presence the 2nd stage of NPP A-1 decommissioning is realized. Within this a large amount of contaminated materials is expected to be generated. Considering the elapsed time since the accident (about 30 years) dominant radionuclide (RN) in these materials is ^{137}Cs. It emits 662 keV gamma rays and is easily determined by well spread gammaspectrometry techniques.
Important part of NPP decommissioning is the free release (FR) of materials into the environments. FR is important due to minimizing the volume of radioactive waste (RW) generating during decommissioning. The long term storage of RW is very costly.
FR is allowed, only, when the very strict legislative requirements are fulfilled. Government Regulation No. 345/2006 contains the free release levels of massic [Bq/kg] or surface activities [Bq/cm^2] of individual RNs, as well, depending on their radiotoxicity. For example the tabulated in GR 345/2006 free release level for ^{137}Cs is 300 Bq/kg.
Demonstration of such low RN content needs well shielded measuring instruments with very low detectable activity. Moreover, according to Metrology Act No. 124/2000 they shall be metrological certified under strict conditions (typically accuracy class ± 20%). Consequently the development and operation of these monitoring systems is very costly.
One of the tasks of VUJE Inc. at NPP A1 decommissioning project is to develop approaches and radiation monitoring systems that ensure declaration of complies with the mentioned low release levels. Monitoring systems are based on the measurement of easily-detectable RNs emitting gamma radiation (e.g. ^{137}Cs at NPP A1). Hard-to-detect RNs (HDRN) like actinides ($^{239,\ 240}$Pu, ^{241}Am) or ^{90}Sr emitting only alpha or beta rays are estimated on the basis of correlation coefficients determined by radiochemical analysis (RChA) of representative samples only, because RChA is very costly.

Tab. 1. Typically correlation coefficients of actinides and ^{137}Cs in CS and CCR at NPP A-1 site.

HDRN	Massic activity ratios of ^{137}Cs to actinides	
	Contaminated soil	Contaminated concrete rubble
$^{239,240}Pu$	6.59E-02	2.50E-02
^{238}Pu	1.80E-03	5.30E-03
^{241}Am	2.11E-03	2.10E-02
^{90}Sr	3.68E-01	2.20E-01

On the NPP A-1 site there is a central monitoring post (CMP) based on trinity shielded vertically arranged semiconductor HPGe detectors cooled by liquid N_2. CMP is designated to declaration of RNs content in decommissioning material in 200 L MEVA (rotating) drums. Monitoring capacity about 10 - 15 drums per working shift has been very limited in comparison with the volume of materials (thousands m^3 of contaminated soil (CS) and contaminated concrete ruble (CCR)) to be monitored.

Recently, a pilot Soil Conveyor Monitor CM 1110 was developed by VUJE and Canberra Packard, Slovakia. Core of the system is a pair of shielded scintillation LaBr detectors above a moving belt containing an electronic scale, as well. Monitoring system is capable to sort of contaminated soil into three massic activity categories including free release of the sorted soil. Monitoring capacity of this system in free releasing mode is about 10 tons per shift. Disadvantage of this monitor is that the monitored soil shall be dried.

For next increasing the monitoring capacity at NPP A1 the Large volume Monitoring Post was recently developed by VUJE. Monitoring system includes a twin of shielded electrically cooled semiconductor HPGe detectors integrated into transportable container. System is intended basically to monitor material (CS, CCR) in rectangular standard 600 L container. If necessary it is capable after detectors counting geometry rearrangement to measure 200 L drums, as well. Metrological certification was carried out in December 2010 and the system is ready for testing operation, now. The monitor designed capacity is 10 containers or 20 drums per shift.

In order to increase soil sorting capacity and reducing the need of costly free release measurements a loader spoon sorting monitoring system was designed. Assembly includes protective casing with a pair of NaI 2" x 2" detectors, measurement table for spoon of UNC loader and signaling box for indication measurement results. The monitoring system is designed to sort CS very quickly (2-3 minutes) during its transport by UNC to respective sorted soil piles. Monitoring is expected to be with limited accuracy, but its capacity could reach sufficiently large volumes needed for planned accelerated sorting of soil.

VUJE projects, particular monitoring systems and radiochemical analysis results of actinides will be in more detail presented during presentation.

Uranium(IV)-silica Colloids at Near-neutral pH

Harald Zänker, Stephan Weiss, Christoph Hennig, Isabell Dreissig, Gert Bernhard

Institute of Radiochemistry, Helmholtz-Zentrum Dresden-Rossendorf, P.O. Box 51 01 19, D-1314 Dresden,Germany, e-mail: h.zaenker@hzdr.de

Due to their low solubility, tetravalent actinides, An(IV), are usually assumed to be immobile in natural waters. However, it is also well known that insoluble precipitation products can be mobile if they occur as colloids. For An(IV) oxyhydroxides this phenomenon has thoroughly been studied [1-3]. Here (see also [4]) we describe the formation of a new type of An(IV) colloids.

Evidence is provided by photon correlation spectroscopy (PCS), ultrafiltration and ultracentrifugation that uranium(IV) can form silicate-containing colloids. The U(IV)-silica particles are generated in near-neutral to slightly alkaline solutions containing background chemicals of geogenic nature (carbonate, silicate, sodium ions). They remain stable in aqueous suspension over years. A concentration of up to 10^{-3} M of colloid-borne U(IV) was observed which is a concentration much higher than the concentrations of truly dissolved or colloidally suspended waterborne An(IV) species hitherto reported for the near-neutral pH range. The prevailing size of the particles is below 20 nm. Apart from that, minor fractions of larger submicron particles, which tend to dominate the scattered light, are typically also present. Fig. 1 demonstrates the unmasking of the small particles in a light scattering experiment (PCS) by a relatively mild ultracentrifugation step (42,000g).

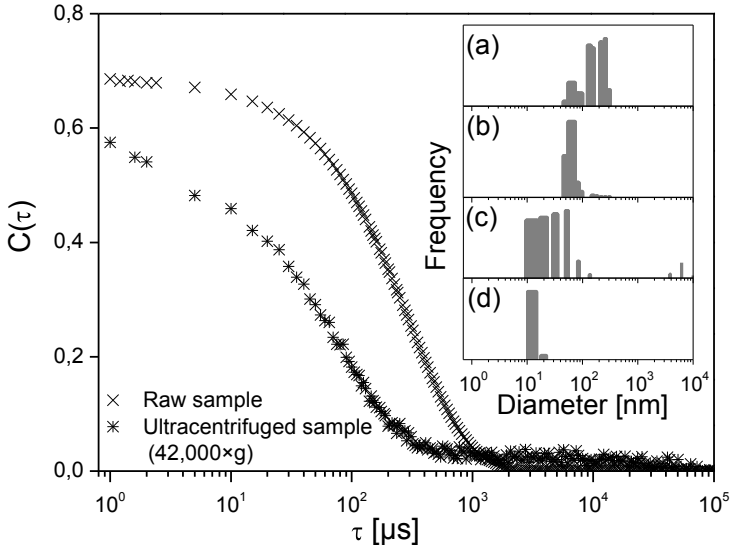

Fig. 1. Influence of ultracentrifugation on the autocorrelation function, C(τ): Initial U = 1×10^{-3} M, initial Si = 3×10^{-3} M, Initial carbonate = 5×10^{-2} M, Insert: CONTIN deconvolutions of the autocorrelation functions: Raw sample: (a) light-intensity weighted particle size distribution; (b) number weighted particle size distribution; Centrifugate: (c)

light-intensity weighted particle size distribution; (d) number weighted particle size distribution. Ultracentrifugation unmasks the small U(IV) colloids (< 20 nm).

The size of the < 20 nm particles depends on silicate concentration and pH. The higher the silicate concentration and the pH, the smaller (and obviously the more stable) are the particles that are formed (however, silicate at the concentrations tested does not form particles in the absence of uranium).
Laser Doppler velocimetry reveals that the nanoparticles are stabilized in solution by electrostatic repulsion due to a negative zeta potential caused by the silicate. The isoelectric point of the nanoparticles is shifted toward lower pH values by the silicate.
The mechanism of colloidal stabilization can be regarded as "sequestration" by silicate, a phenomenon well known from trivalent heavy metal ions of high ion potential such as iron(III) [5, 6) or curium(III) [7], but never reported for uranium(IV) so far. Extended X-ray absorption fine structure (EXAFS) spectroscopy showed that U-O-Si bonds, which increasingly replace the U-O-U bonds of the amorphous uranium(IV) oxyhydroxide with increasing silicate concentrations, make up the internal structure of the colloids. The next-neighbor coordination of U(IV) in the U(IV)-silica colloids is comparable with that of coffinite, $USiO_4$.
The assessment of uranium behavior in the aquatic environment should take the possible existence of U(IV)-silica colloids into consideration. Their occurrence might influence uranium migration in anoxic waters.

References
[1] Neck, V. et al., *Radiochim. Acta* **90**, 485 (2002).
[2] Bitea, C. et al., *Colloids Surf., A* **217**, 63 (2003).
[3] Altmaier, M. et al., *Radiochim. Acta* **92**, 537 (2004).
[4] Dreissig, I. et al., *Geochim. Cosmochim. Acta* **75**, 352 (2011).
[5] Browman, M. G. et al., *Environ. Sci. Technol.* **23**, 566 (1989).
[6] Robinson, R. B. et al., *J. Am. Water Works Assn.* **84**, 77 (1992).
[7] Panak, P. J. et al., *Radiochim. Acta* **93**, 133 (2005).

Resonance Ionization Mass Spectrometry (RIMS) for Ultratrace Determination of Neptunium-237

N. Stöbener,[1] S. Raeder[2], T. Gottwald[2], G. Passler[2], T. Reich[1], N. Trautmann[1], K. Wendt[2]

[1] *Institute of Nuclear Chemistry, Johannes Gutenberg-Universität Mainz, Fritz-Straßmann-Weg 2, 55128 Mainz, Germany, e-mail: stoebenn@uni-mainz.de*
[2]*Institute of Physics, Johannes Gutenberg-Universität Mainz, Staudingerweg 7, 55128 Mainz, Germany*

After a storage time of about 1000 years, the radiotoxicity of spent nuclear fuel is mainly determined by long-lived isotopes of Tc and the actinides. Among these isotopes, ^{237}Np is considered as a potential hazard to the environment because of its long half-life ($T_{1/2} = 2.14 \cdot 10^6$ a) and high mobility in aquatic systems. Therefore, the safety assessment of a proposed nuclear waste repository must consider the geochemical behaviour of ^{237}Np. The concentration of Np expected in case of a leakage of a repository is below 10^{-10} mol/L. Since an extrapolation of data obtained at higher Np concentrations to the ultratrace level may lead to incorrect results[1,2], experiments dealing with the geochemistry of Np require very sensitive methods for its determination. In certain cases, the short-lived isotope ^{239}Np ($T_{1/2} = 2.36$ d) can be used because smallest amounts of this isotope are detected by γ-ray spectroscopy. However, the short half-life of this isotope precludes its use in long-term studies, e.g., diffusion experiments. Resonance ionization mass spectrometry (RIMS) is a very sensitive method for the detection of actinides, which is independent on the half-life. Therefore, the development of a RIMS method for the ultratrace analysis of ^{237}Np is of interest. In RIMS, an atomic beam is evaporated from a heated filament and the atoms are ionized with radiation from several lasers. The wavelengths of the laser beams match subsequent optical transitions of the particular element. The laser ions are separated from thermally produced ions of different masses by a time-of-flight mass spectrometer (TOF-MS) and detected by ion counting. Because of the uniqueness of the optical transitions, resonant ionization schemes are element specific. Thus, mass spectra free of isobaric interferences and with a very low background can be recorded.

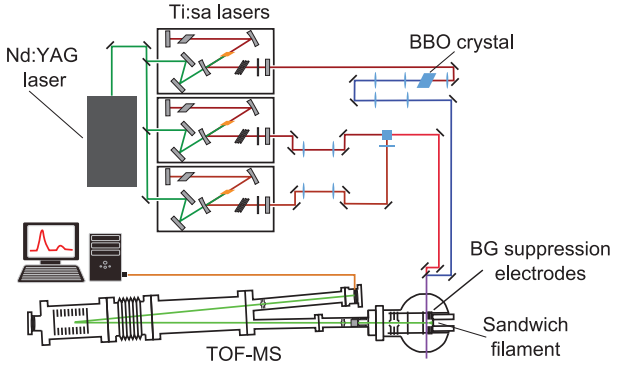

Fig. 1. Setup used for RIMS of Np. A BBO crystal is used for second harmonic generation of blue laser light. Background (BG) suppression electrodes ensure that only neutral species can interact with the laser beam.

Our experimental setup consists of three tuneable titanium-sapphire (Ti:sa) lasers pumped by a Nd:YAG laser at 532 nm and a TOF-MS equipped with multi-channel plate detectors. The filaments are prepared by electrodeposition of ^{237}Np onto a tantalum strip. In order to produce an atomic beam of Np, the strip is covered with a thin titanium layer acting as a reducing agent.

Since only few energy levels of ^{237}Np suitable for a three step excitation scheme were known, resonance ionization spectroscopy (RIS) was applied to identify such levels[3]. In RIS, a setup similar to one shown in fig. 1 was used for spectroscopy. The frequency doubled Ti:sa populated a first excited state (FES) taken from literature[4]. The second laser was scanned across possible second excited states (SES), while the third laser served for nonresonant ionization of the neptunium atoms excited into the SESs. Later, the second laser was operated at the energy of a transition into a SES and the third laser was scanned across autoionizing states (AI) above the ionization potential of Np. Numerous SES and AI states haven been identified, leading to several excitation schemes. A selection of these schemes is shown in fig. 2.

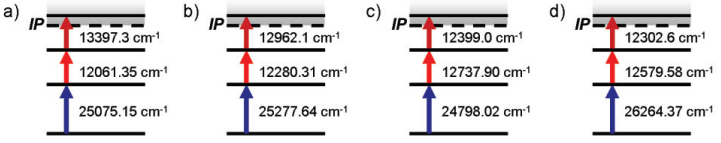

Fig. 2. Selection of excitation schemes for ^{237}Np.

In order to achieve a low limit of detection, a high ionization efficiency is required. Several excitation schemes have been tested for their efficiency. Due to the linewidth of 2-3 GHz of the Ti:sa lasers, a partial resolution of the hyperfine splitting (HFS) of ^{237}Np is possible. Since the resolution of the HFS will lead to a reduced ionization efficiency, energy levels with a small HFS should be preferred. With the excitation scheme shown in fig. 2b, an overall efficiency of $2 \cdot 10^{-6}$ was obtained. Fig. 3 shows a mass spectrum of 10^{10} atoms of ^{237}Np (4 pg) recorded with this excitation scheme.

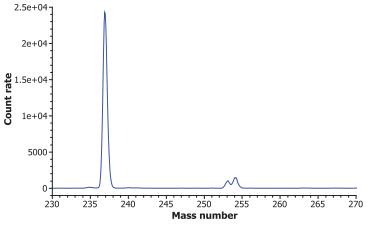

Fig. 2. Mass spectrum of 10^{10} atoms of ^{237}Np. No significant background is visible except of two peaks at masses 253 and 254. Probably, these peaks can be attributed to the nonresonant formation of NpO^+ and UO^+.

References

[1] A. Seibert, A. Mansel, C.M. Marquardt, H. Keller, J.V. Kratz, N. Trautmann, *Radiochim. Acta* **89**, 505-510 (2001)

[2] D. R. Fröhlich, S. Amayri, J. Drebert, T. Reich, *Radiochim. Acta* **99**, 71-77 (2011)

[3] S. Raeder, N. Stöbener, T. Gottwald, G. Passler, T. Reich, N. Trautmann, K. Wendt, *Spectrochim. Acta B*, accepted

[4] J. Blaise, J.-F. Wyart, Selected Constants, Energy Levels and Atomic Spectra Vol. 20, *Tables Internationales de Constantes*, Université P. et M. Curie, Paris, 1992

Uptake of Np(V) by Natural Clay – A Micro-scale Spectroscopic Study

Daniel R. Fröhlich[1], Samer Amayri[1], Jakob Drebert[1], Joachim Krause[2], Tobias Reich[1]

[1]*Institute of Nuclear Chemistry, Johannes Gutenberg-Universität Mainz, Fritz-Strassmann-Weg 2, 55128 Mainz, Germany , e-mail: froehlich@uni-mainz.de*
[2]*Max-Planck-Institute for Chemistry, Becherweg 27,55020 Mainz, Germany*

Until now the problem of high-level nuclear waste storage has not been solved. Besides rock salt and granite, argillaceous rocks are considered as a potential host rock formation fór nuclear waste repositories in several European countries. After a storage period of several thousand years, an escape of the radionuclides from their containers can not be excluded. Therefore, the interactions between long-lived transuranium elements (Np, Pu, Am and Cu) and the surrounding clay formation have to be examined in detail. Different mechanisms such as redox reactions, cation exchange, sorption and diffusion regulate the radionuclide uptake by clays and determine their transport into the environment. In this study, we investigated the sorption and diffusion of Np(V) using the natural reference mineral Opalinus Clay (OPA), which is present in Switzerland and southern Germany. While diffusion and batch experiments provide macroscopic data such as diffusion and distribution coefficients in dependence of different parameters, e.g. pH, partial pressure of CO_2 and radionuclide concentration [1,2], no molecular information about the Np speciation (oxidation state, bond distances and sorption mode) can be obtained.

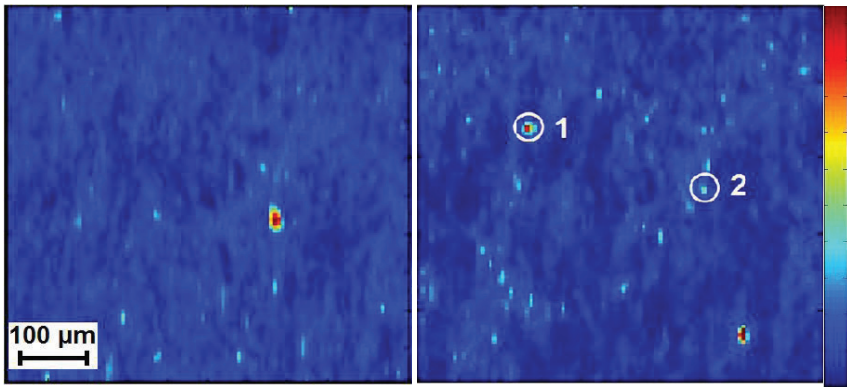

Fig. 1. µ-XRF mapping of an OPA thin section loaded with 2.5 Bq/cm^2 ^{237}Np(V): left: Fe distribution, right: Np distribution, the hot spot in the bottom right corner is caused by an interference of Sr (K_α)

We used X-ray absorption fine structure spectroscopy (XAFS) as a powerful tool to investigate the Np speciation in OPA samples on a microscopic level. Wet paste samples were measured by Np L_{III}-edge EXAFS at the ROBL beamline (ESRF, Grenoble) to determine the atomic surrounding of Np sorbed on OPA. These measurements showed that ternary Np(V) carbonate species are formed in dependence of partial pressure of CO_2. These EXAFS measurements provide an average molecular information over the whole sample, but there remain still important questions, which can not be answered by this method. In the case of a natural heterogeneous material such as OPA, which consists of different clay minerals, but also quartz, calcite and iron(II)-bearing minerals, it is useful to know whether neptunium has a particular tendency for sorption on one of those different mineral phases. Therefore, µ-XAFS

can be used to study the speciation with spatial resolution. We measured OPA thin sections loaded with Np(V) and a diffusion sample by μ-XRF and μ-XANES at the MicroXAS beamline of the Swiss Light Source (PSI, Villigen). We investigated the spatial distributions of Np, Fe and Ca by X-ray fluorescence (XRF) and studied Np hot spots by μ-XANES. Element maps of the lighter elements (especially Si and Al) were measured by electron microprobe.
From Fig. 1 it becomes obvious that Np is distributed very heterogeneously. Since the Np L_{III}-edge XANES structure is characteristic for the different oxidation states of Np [3], all spectra were compared to reference spectra of Np(IV) and Np(V) by an iterative transformation factor analysis (ITFA) [4] to determine the amounts of both oxidation states in the samples.

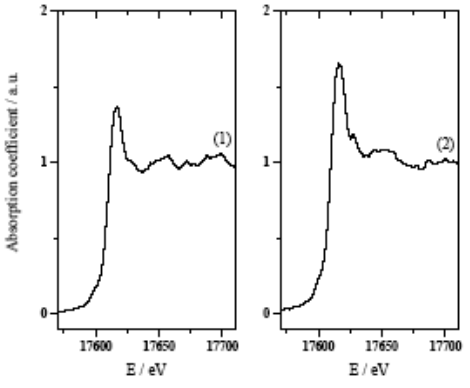

Fig. 2. Normalized Np L_{III}-edge μ-XANES spectra of spots 1 and 2 (Fig.1)

Fig. 2 shows the Np L_{III}-edge XANES spectra of two spots which are marked 1 and 2 in Fig.1. Spot 2, which is located near an iron rich region (see Fig.1), contains more than 80% Np(IV), while Np(V) dominates in spot 1 (>70%). In the case of the diffusion sample, all XANES spectra showed ≥80% Np(IV). These spectroscopic results indicate that Np(V) is reduced by iron(II) bearing minerals to Np(IV). The fact that spots enriched in Np(IV) seem to be related to iron rich regions leads to the conclusion that the reduction takes place at the mineral surface and not in the aqueous phase.

This work was financially supported by the Bundesministerium für Wirtschaft und technologie under contract No. 02E10166. Daniel Fröhlich has been supported by a fellowship of DFGGRK 826. Our local contacts of the ROBL and MicroXAS Beamlines as well as our colleagues of the MPI for Chemistry (Mainz) are acknowledged for their support during our studies.

References

[1] T. Wu et al., *Environ. Sci. Technol.* **43**, 6567 (2009).
[2] D.R. Fröhlich et al., *Radiochim. Acta* **99,** 71 (2011).
[3] T. Reich et al., *Radiochim. Acta* **88**, 633 (2000).
[4] A. Roßberg et al., *Anal. Bioanal. Chem.* **376**, 631 (2003).

Water Chemisorption on a Sputterdeposited Uranium Dioxide Film – Effect of Defects

S. Cohen[1,2], N. Shamir[1],S. Zalkind[1], A. Seibert[3], T. Gouder[3] and M. H. Mintz[1,2]

[1]Nuclear Research Center-Negev, POB 9001, Beer-Sheva 84190, Israel
[2]Dept. of Nuclear Eng, Ben-Gurion Univ. of the Negev, POB 653, Beer-Sheva 84104, Israel email: shaico@bgu.ac.il
[3] European Commission – Joint Research Centre, Institute For Transuranium Elements POB 2340, 76125 Karlsruhe, Germany

The characteristics of water vapor chemisorptions on a uranium dioxide film, obtained by reactive sputterdeposition, were studied over a temperature range of 300-500 K by combined measurements of Direct Recoil Spectrometry (DRS) and X-Ray Photoelectron Spectroscopy (XPS).
The effect of defects on the chemisorption behavior was evaluated by comparing sputtered and annealed surfaces. It seems that dissociative chemisorption takes place on both types of surfaces. However, clusters of tilted hydroxyls are formed on the annealed surface, whereas more isolated hydroxyls are predominant in the accumulation process on the sputtered surface. These differences lead to lower H/O intensity ratios in DRS measurements and lower desorption temperatures for the annealed sample.

Extraction Properties of Thiacalixarene Dendrimer Molecules

Špendlíková Irena,[1] John Jan[1,2], Lhoták Pavel[3]

[1] *Department of Nuclear Chemistry,* [2]*Centre for Radiochemistry and Radiation Chemistry, Faculty of Nuclear Sciences and Physical Engineering, Czech Technical University in Prague, Břehová 7, 115 19 Praha 1, Czech Republic, e-mail: spendlikovairena@gmail.com*
[3] *Department of Inorganic Chemistry, ICT Prague, Technická 5, 166 28 Praha 6, Czech Republic*

The reprocessing of spent nuclear fuel has recently become one of the issues mostly discussed within the scientific society. One of the reprocessing processes nowadays used in the industrial scale is called PUREX. After this step, the liquid raffinate still contains the actinoids, mainly americium and curium, together with a wide range of fission products, including the lanthanoids. The mutual separation of these groups is a key problem in the Partitioning processes. Among other tasks in their development, search for suitable extracting agents is critical. Thiacalixarenes belong among the recently tested extraction agent groups. This work focused on studying the extraction behaviour of the set of newly synthesized thiacalixarene dendrimer molecules and the respective thiacalixarenes used as the basic structural unit of tested dendrimers.

The solvent extraction experiments were carried out in order to determine the distribution ratios of ^{241}Am and ^{152}Eu, as the actinoid and lanthanoid representatives, respectively, and the values of separation factors of these radionuclides. The activities of aqueous and organic phases were measured via gamma spectrometry with HPGe detector. Showing low or even no extraction of americium and europium, the dendrimer and thiacalixarene molecules were successively studied in the synergistic mixture with COSAN molecules.

The extraction studies of synergistic mixtures (thiacalixarene/dendrimer + COSAN) were performed to find suitable conditions, mainly referring to the mutual ratio of extracting agent concentration. The ratio of 1 : 1 was used for the synergistic mixtures with thiacalixarenes and 1 : 4 (dendrimer : COSAN) in the case of dendrimer molecules. Several effects of the dendrimer molecule structure on the values of distribution ratios were identified and these results will be used in the synthesis of next generation of extracting agents prospective for the Partitioning process.

Separation of Curium from Americium

Kamila Šťastná

Department of Nuclear Chemistry, Faculty of Nuclear Sciences and Physical Engineering, Czech Technical University in Prague, Břehová 7, 115 19 Prague 1, Czech Republic,
e-mail: kamila.stastna@fjfi.cvut.cz

At present, there are two concepts of spent nuclear fuel treatment. The first one suggests its direct disposal into deep underground repository, but this approach leads to losses of nuclear material, posses considerable demands on the size of repository, and some radionuclides contained in spent fuel cause the time required to follow the safety of the repository to be in order of hundreds thousands years. The second concept is based on spent fuel reprocessing. The PUREX process recovers uranium and plutonium from spent fuel for preparation of fresh fuel, decreasing substantially the amount of material to be disposed of. Moreover, due to the separation of plutonium, the time necessary to follow the safety of the repository decreases by one order. Then, the long time radiotoxicity is caused namely by the presence of minor actinides (neptunium, americium, and curium), so attempts for their separation from spent fuel reprocessing solution are carried out. After their separation, the waste dedicated for underground reposition would contain only fission products, including lanthanides, reducing the time necessary for nuclear waste isolation from the biosphere to several hundreds years. Consequently, the separated actinides can be burned in fast reactors or accelerator driven systems. However, curium may pose problems in preparation of fuel or target because of its high heat output and neutron emission.

The minor actinides remaining in spent fuel reprocessing solution after the PUREX process, enabling also neptunium recovery, can be co-extracted with lanthanides using e.g. malonamide extractants (DIAMEX process) and then separated from them using e.g. bis-triazinyl-piridine extractants (SANEX process) [1]. The mutual separation of americium and curium is a very difficult task for their very similar chemical behaviour. The extraction and precipitation methods use the fact that americium can exist in aqueous solutions in oxidation states higher than III in contrast to curium. In this case, americium is electrochemically or chemically (by persulfate) oxidized to either Am(VI) and then extracted, e.g. by tributylphosphate in dodecane (SESAME process) [2] or bis(2,6-dimethyl-4-heptyl)phosphoric acid in n-heptane [3], or to Am(V) and precipitated as double carbonate $K_5AmO_2(CO_3)_3 \cdot nH_2O$ [4]. The main drawbacks of these methods are the instability of Am higher oxidation states and the large amounts of secondary wastes. The chromatographic methods attempt to separate Cm from Am in their most common oxidation states (III), e.g. cation exchange chromatography using metal-elution agent complex formation, e.g. with nitrilotriacetic acid, diethylenetriaminepentaacetic acid [5] or ammonium 2-hydroxyisobutyrate [6], anion exchange from nitric acid–methanol medium [7], and countercurrent chromatography using diamide extractants [8]. But the separation factors are low which requires a large number of process stages.

In CTU, the possibility of Am/Cm separation by extraction chromatography is being studied. The separation is carried out from nitric acid solution using bis-triazinyl-bipyridine (BTBP) extractants; proposed recently for the group separation of MAn from Ln, they also demonstrated to provide good separation factor for americium(III) over curium(III) [9]; impregnated or covalently bound to inert support (PAN or ST-DVB). Various complex forming agents are/will be tested for actinides elution from the chromatography column, e.g. 2-hydroxycarboxylic acids, water soluble BTBPs. The preliminary experiments carried out on

the column filled with Synachrom E5 impregnated by the solution of $CyMe_4$-BTBP in cyclohexanone and using 0.25M 2-hydroxyisobutyric acid as eluting solution showed that the elution curve of Cm was shifted forward relative to that of Am. The method is supposed not to require Am pre-oxidation and to significantly decrease secondary waste production. The data obtained will also contribute to the general knowledge of systems applicable to the mutual separation of ions with similar chemical and physico-chemical properties.

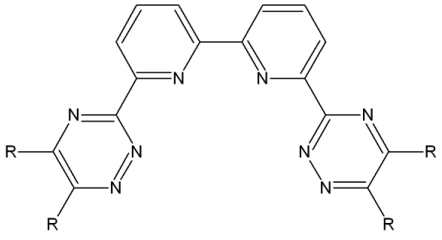

Fig.1: 6,6'-bis(5,6-dialkyl-[1,2,4-]triazin-3-yl)-[2,2']bipyridines (BTBPs)

References

[1] C. Madic, M. Lecomte, P. Baron, B. Boullis, *C. R. Physique* **3**, 797-811 (2002).
[2] L. Donnet, J.M. Adnet, N. Faure, P. Bros, Ph. Brossard, F. Josso, in: *Proc. 5th Int. Information Exchange Meeting on Actinide and Fission Product Partitioning and Transmutation*, Mol, Belgium, 161- 168 (1999).
[3] G.W. Mason, A.F. Bollmeier, D.F. Peppard, *J. Inor. Nucl. Chem.* **32**, 1011-1022 (1970).
[4] *Implications of Partitioning and Transmutation in Radioactive Waste Management,* Technical Report Series No. 435, IAEA, Vienna (2004).
[5] W.H. Hale, J.T. Lowe, *J. Inorg. Nucl. Chem.*, Letters Vol. **5**, 363-368 (1969).
[6] J.E. Bigelow, D.E. Benker, F.R. Chattin, L.J. King, J.B. Knauer, R.G. Ross, R.G. Stacy, J.T. Wiggins, in*: Proc. Int. Symp. on Actinide/Lanthanide Sep.*, Honolulu, Hawaii, USA, 194-211 (1985).
[7] A. Ikeda, T. Suzuki, M. Aida, K. Otake, Y. Fujii, K. Itoh, T. Mitsugashira, M. Hara, M. Ozawa, *J. Nucl. Sci. Technol.* **41**, 915-918 (2004).
[8] T.A. Maryutina, M.N. Litvina, D.A. Malikov, B.Ya. Spivakov, B.F. Myasoedov, M. Lecomte, C. Hill, C. Madic, *Radiochemistry* **46**, 549-554 (2004).
[9] M.G.B. Drew, M.R.S.J. Foreman, C. Hill, M.J. Hudson, C. Madic, *Inorg. Chem. Comm.* **8**, 239-241 (2005).

Extraction and Immobilization of Strontium in the Silicoantimonates

Yu. Kuryleva, A. Shumikhina Shumikhina, D. Zakharyevich

Chelyabinsk State University,Br.Kashirinykh str.129, 454001Chelyabinsk,Russia ,
e-mail: julieta-k@mail.ru

The existing nuclear fuel reprocessing facilities use a technique based on PUREX process. Huge volumes of liquid low- and intermediate-level wastes are generated during this process. If a material used for extraction of hazardous isotopes could be almost directly used also for immobilization, it would greatly improve the safety and reduce the cost of the process. Crystalline polyantimonic acid (PAA) is among the best inorganic ion-exchangers, and has wide application in extraction methods. Its ion-exchange capacity and selectivity could be easily tuned by chemical modification. On the other hand, PAA and some of its derivatives (antimonates) crystallize into structures types that possess unique radiation-resistance properties. In this report we describe and discuss the results of our pilot study of the suitability of antimonates doped with silicon for the extraction and immobilization of strontium.

PAA and some antimonates crystallize in the pyrochlore structure, the framework of which is built from corner-sharing octahedra SbO_6. Metal cations are placed in the cavities and channels formed by this framework. Antimony atoms are in a pentavalent state and strongly polarize oxygen atoms, which causes weakness of the bond of the cations in the voids of the structure with a framework and provides ion exchange properties of PAA. This view on the origin of ion-exchange properties is confirmed by the changes of ion-exchange properties when antimony atoms are substituted by other atoms in the framework. For example, mixed silicoantimonic acid (SAA), the framework of which contains silicon atoms in tetravalent state, together with antimony atoms, has a higher sorption capacity for divalent metals in comparison with the PAA, in accordance with the increase of negative charge of the framework. In particular, SAA has a high capacity to ions of strontium, including those in acidic solutions [1].

The immobilization of the waste components in the antimonates can be achieved either by blocking the diffusion paths for cations in the structure of antimonate or by strengthening the bonds between the framework and cations. The first way requires the introduction of atoms with a higher degree of oxidation in the structure, but under normal conditions such atoms with a high degree of oxidation would substitute antimony atoms in the framework and might lead to the disintegration of the material. The second path involves transformation of antimony atoms from the penta- to trivalent state.

When heating SAA containing extracted strontium decays into several phases. Full phase analysis of the products of thermolysis could not be performed because of the large quantity of overlapping peaks of low intensity. Nevertheless, it is established that perovskite phase is present in the product. Crystal-chemical analysis of the system shows that the resulting perovskite can be a mixed oxide of strontium, antimony and silicon. To test this hypothesis, we studied the phase composition of the products of solid-phase synthesis in the mixture of oxides of antimony and silicon and strontium carbonate at T = 1000 º C in air [2]. It is found that in this system mixed oxide of strontium, silicon, and antimony with the perovskite structure is formed. Gravimetric analysis of the synthesis process showed that antimony atoms are in the trivalent state. Structural analysis of these phases showed that they contain antisite defects in the cation sublattice, and they remain stable at relatively high concentrations of "stoichiometric" oxygen vacancies. The lattice stability at relatively high concentrations of

such defects are crucial in the radiation resistance of the structure of solids. Moreover, it suggests the possibility to immobilize alpha-emitters in the structure of these materials, which is of great importance in SNF management.

Thus, the thermolysis KSA containing strontium leads to the formation of strontium silicate-antimonate with perovskite structure, which is stable at least up to 1000 º C.

Study the behavior of silicate-antimonate strontium in different chemical environments showed high resistance in neutral and basic solutions. In highly acidic solutions silicate-antimonate decomposes into silica and insoluble strontium antimonate with pyrochlore structure.

In general, the results suggest that proposed approach is promising for the radioactive waste management. Mixed silicoantimonic acids have the high sorption capacity toward strontium in acidic solutions. The strontium silicoantimonates have the sufficient thermal and chemical stability and their structure can provide a high radiation resistance. Thus, the materials based on these compounds can be used in the proposed optimized process of radioactive waste management.

References

1. Möller T., et al. *J. Mater. Chem.* **11,** 1526 (2001)
2. Zakharyevich D.A., Rekunov A.V. *Vestnik ChelGU* **24**, 35 (2010)

Uranium(V) Species in Alkali Chloride Based Melts

Dmitry S. Maltsev,[1] Vladimir A. Volkovich[1], Denis E. Aleksandrov[1], Boris D. Vasin[1]

[1] *Department of Rare Metals and Nanomaterials, Ural Federal University, 19 Mira Street, Ekaterinburg, 620002, Russian Federation, e-mail: d.s.maltsev@gmail.com*

Molten alkali chlorides are considered as prospective reaction media for pyrochemical reprocessing spent nuclear fuels as well as for producing nuclear materials. Uranyl containing melts can be used for reprocessing oxide fuels, producing UO_2 or preparing MOX fuel. Understanding processes involved in reducing U(VI) species to UO_2, as well as behaviour and speciation of oxygen-containing uranium chloro-species is important for designing a feasible process. Intermediate uranyl(V) species are formed in uranyl(VI) containing melts but often overlooked. Fission product elements, as well as container materials in contact with the melt, can affect the speciation and behaviour of uranium.

In the present work a variety of reactions resulting in the reduction of uranyl(VI) species in alkali chloride melts were investigated. The processes studied included electrochemical and chemical reduction and thermal decomposition of uranyl(VI) ions. Elemental tellurium, palladium, silver, molybdenum, zirconium, niobium and hydrogen, and niobium(III) chloro-species were tested as reducing agents. The experiments were performed in LiCl, 3LiCl-2KCl, NaCl-KCl, NaCl-2CsCl melts between 450 and 850 ^{o}C employing high temperature spectroscopy and electrochemistry techniques.

Reduction of uranyl(VI) species results in the formation of UO_2^{+} ions and crystalline UO_2 and the relative amounts of $UO_2Cl_4^{2-}$, $UO_2Cl_4^{3-}$ and UO_2 present in the system depend on temperature, the melt composition and electrochemical properties of the reductant. The degree of the reduction increases from tellurium to zirconium. In certain instances additional reactions, leading to the formation of soluble U(IV) or even U(III) chloro-species, also take place. This is the case when, for example, niobium or zirconium ions are present or formed in the melt.

Some of the reactions studied can be applied for removing fission product elements from a melt by adding there a molybdenum rod of suitable size. Molybdenum reacts with the uranyl ions:

$$3\ UO_2Cl_4^{2-} + Mo + 6\ Cl^- \rightarrow 3\ UO_2Cl_4^{3-} + MoCl_6^{3-} \quad (1)$$

$$3\ UO_2Cl_4^{2-} + 2\ Mo \rightarrow 3\ UO_2 + 2\ MoCl_6^{3-} \quad (2)$$

At the same time noble fission products like ruthenium, rhodium and palladium will be reduced to the metallic state, *e.g.*,

$$3\ PdCl_6^{4-} + 2\ Mo \rightarrow 3\ Pd + 2\ MoCl_6^{3-} + 6\ Cl^- \quad (3)$$

and deposited on molybdenum. Zirconium and niobium will be deposited on uranium dioxide formed by the reaction (2):

$$ZrCl_6^{2-} + UO_2 \rightarrow ZrO_2 + UCl_6^{2-} \quad (4)$$

$$NbCl_6^{2-} + UO_2 \rightarrow NbO_2 + UCl_6^{2-} \quad (5)$$

$$NbCl_6^{-} + UO_2 + Cl^- \rightarrow NbO_2 + UCl_6^{2-} + \tfrac{1}{2}\ Cl_2 \quad (6)$$

A series of experiments was performed to study the distribution of the elements imitating fission products during the reaction of uranyl containing melt with metallic molybdenum. The progress of the reaction was followed by *in situ* electronic spectroscopy measurements and an example of the spectra recorded in given in Fig. 1. Depending on the initial uranium and the "fission products" content the concentration of Pd, Zr and Nb in the melt decreased, in some experiments to undetectable amounts.

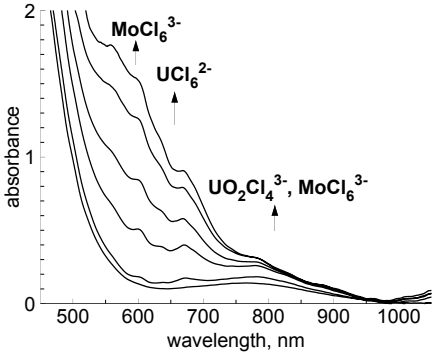

Fig. 1. Electronic absorption spectra recorded during reaction of NaCl-CsCl-UO_2Cl_2-$PdCl_2$-$NbCl_5$-$ZrCl_4$ melt with Mo metal (550 ^oC). Time after addition of molybdenum (min., bottom to top): 0, 4, 11, 16, 21, and 31.

Molybdenum(III) chloride formed in the melt was successfully removed by sparging the melt with chlorine and converting it to volatile $MoCl_5$ even at temperatures as low as 550 ^oC. During this operation soluble uranyl(V) species were oxidized back to uranyl(VI) and the resulting melt contained only $UO_2Cl_4^{2-}$ and UCl_6^{2-} ions. The latter can be converted to uranyl species by sparging the melt with a Cl_2-O_2 mixture:

$$UCl_6^{2-} + O_2 \rightarrow UO_2Cl_4^{2-} + Cl_2 \quad (7)$$

Thus a uranyl containing melt can be purified from a number of elements representing fission products by simple addition of molybdenum metal and without applying any current. Interestingly that the elements both more electropositive (like Pd) and more electronegative (like Zr and Nb) than molybdenum can be removed in one operation. Since some of uranium is lost due to reaction (2) such approach can be applied only to reprocessing fast neutron reactors spent mixed oxide fuel containing natural or depleted uranium of low economical value.

Hydrogen also reduces uranyl(VI) ions to uranyl(V) and ultimately to solid UO_2. This can be seen in the absorption spectra of the melt and also on the voltammograms (Fig. 2). Usual two-step reduction pathway $UO_2Cl_4^{2-} \rightarrow UO_2Cl_4^{3-} \rightarrow UO_2$ under inert atmosphere changes to a single $UO_2Cl_4^{3-} \rightarrow UO_2$ in the presence of hydrogen due to reduction of $UO_2Cl_4^{2-}$ ions.

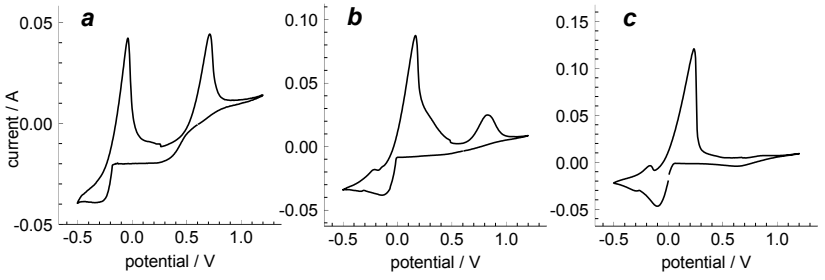

Fig. 2. Cyclic voltammograms of NaCl-KCl-UO_2Cl_2 melt, 750 ^oC: under argon (a), under hydrogen (b), with hydrogen bubbled through the melt (c). Starting [U] 0.787 wt. %. Scan rate 100 mV/sec. Reference electrode Ag/AgCl (1 mol. % in NaCl-2CsCl).

Sorption of Neptunium(V) on Mackinawite (FeS)

M. Lübke, J. Drebert, T. Reich

Institute of Nuclear Chemistry, Johannes Gutenberg-Universität Mainz, 55099 Mainz, Germany,
e-mail: marialue@students.uni-mainz.de

The radioactive isotope ^{237}Np, which is produced in nuclear reactors, is of particular interest for the long-term safety analysis of nuclear waste repositories due to its long half-life ($2.14 \cdot 10^6$ a) and high radiotoxicity [1]. Under aerobic conditions, the dominant species in aquifers is the stabile and mobile NpO_2^+ moiety, while the sparingly soluble $Np(OH)_4$ dominates the speciation under anaerobic conditions [2].
The Fe(II)/Fe(III) system is expected to play an important role in controlling the redox conditions and reactions in natural groundwater [3]. In near-surface environments isolated from the atmosphere, microbial activity may lead to reducing conditions. Under sulfate reducing conditions, mackinawite, tetragonal FeS, precipitates in the presence of Fe(II) and HS^-. Mackinawite is of interest because of its reactive surface and large specific surface area. Furthermore, mackinawite is a key intermediate in the low-temperature Fe-S system [4].
To investigate the sorption behaviour of Np(V) on mackinawite, batch experiments have been preformed in 0.1 M $NaClO_4$ under anaerobic conditions as function of mackinawite and neptunium concentrations, pH, and reaction time.
Nanocrystalline mackinawite used in this study was synthesized according to a modified method of Livens et al. [1] and characterized using XRD, XPS, and TEM. TEM measurements showed the formation of nanocrystalline FeS with a particles size of ≥ 5 nm and an estimated surface area of approximately 230 m^2/g. All experiments were carried out in a glove box under Ar atmosphere to prevent oxidation of mackinawite.
Kinetic studies showed that the sorption equilibrium is reached after about one hour (Fig. 1). A high uptake of Np of > 90% was observed in all batch experiments, independent of solid-to-

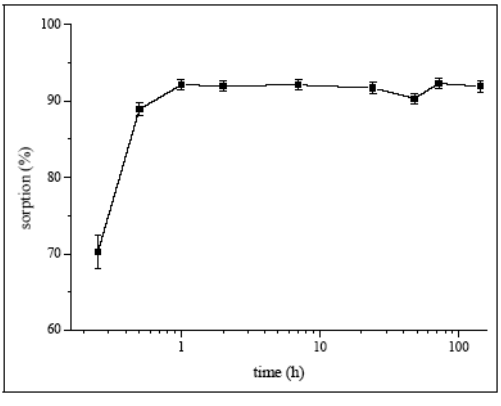

Fig. 1. Sorption of Np(V) on FeS as a function of time; [Np] = 8 µM, pH = 7, [FeS] = 3 g/L.

liquid ratio (1-20 g/L), Np concentration ($5 \cdot 10^{-12}$ -$5 \cdot 10^{-4}$ mol/L), and pH (5-10). The strong interaction between Np and mackinawite may be rationalized by the high surface area of the sorbent and the reduction of Np(V) to Np(IV) by Fe(II). To verify the formation of Np(IV) at the machinawite surface, several sorption samples were studied by X-ray photoelectron spectroscopy (XPS). Figure 2 shows the Np 4f spectrum of 36340 ppm Np sorbed on mackinawite at pH 6. The separation in energy between the Np 4f main lines and the corresponding shake-up satellites is indicative for Np(IV) [5]. Therefore, Np(V) is completely reduced to Np(IV) during the interaction with the mackinawite surface.

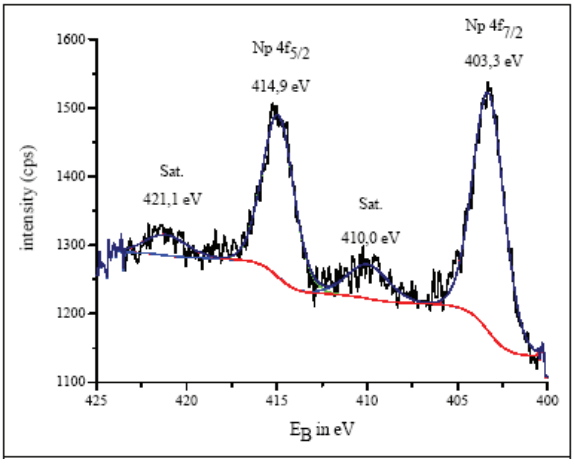

Fig. 2. Np 4f XPS spectrum of Np sorbed on mackinawite; [Np] = 0.5 mM, pH = 6, [FeS] = 3 g/L, energy calibration (S $2p_{3/2}$, 162.0 eV).

In conclusion, mackinawite is able to remove more than 90% of Np from the aqueous phase over a wide range of pH and Np concentration. The main mechanism responsible for this sorption behaviour is the formation of tetravalent Np at the surface of nanocrystalline mackinawite.

References:

[1] L. N. Moyes, et al., Environ. Sci. Technol., **36**, 179-183 (2002)
[2] K. H. Lieser, Radiochim. Acta, **43**, 27-35 (1988)
[3] K. Nakata, et al., Radiochim. Acta, **92**, 145-149 (2004)
[4] M. Mullet, et al., Geochim. Cosmochim. Acta, **66**, 829-836 (2002)
[5] Yu. A. Teterin, et al, Russ. Chem. Rev., **73**, 541-580 (2004)

Uranyl Interaction with Short Chain Carboxylic Acids in Aqueous Solutions Studied by Time-resolved Laser-induced Fluorescence Spectroscopy (TRLFS)

Vladimir Sladkov, Nicole Barre

CNRS, Institut de Physique Nucléaire (IPN), UMR 8608, Orsay, F-91406, France
e-mail: sladkov@ipno.in2p3.fr

The interaction of U(VI) with organic species is of great interest for environmental purposes: migration of species and their distribution in the geosphere. The short chain carboxylic acids present a special interest [1] as they may be released in the environment through the decay of plant matter, animal residue and microbial tissues. They can also be used as simple models of more complicated natural organic matter. In this work we study the uranyl interaction with short chain organic acids (formic, acetic, propionic).
Aqueous perchloric acid solutions containing 1×10^{-4} M of U(VI) and organic acid at different concentrations (from 0 up to 0.5 M) are studied by time-resolved laser-induced fluorescence spectroscopy (TRLFS) at pH 1.5 and 2.5.
The quenching of U(VI) fluorescence is observed in for all acids studied. In figure 1 the spectra of U(VI) are presented in the presence of formic acid at different concentrations. The graphs giving the U(VI) fluorescence intensity, measured at pH 1.5 and 2.5, as a function of total acid concentration, their anionic and acid forms are constructed to determine the quenching species [2]. In fig 2 these graphs are given for formic acid. We can state unambiguously the similarity of the curves in the case of acid anion for all studied pH values (fig 2, right). The differences observed in the intensities of uranyl fluorescence are due to the different pH values [2]. We can conclude that only the anionic acid species affect the U(VI) intensity. Thus, acid anion is demonstrated to be responsible for the fluorescence quenching.

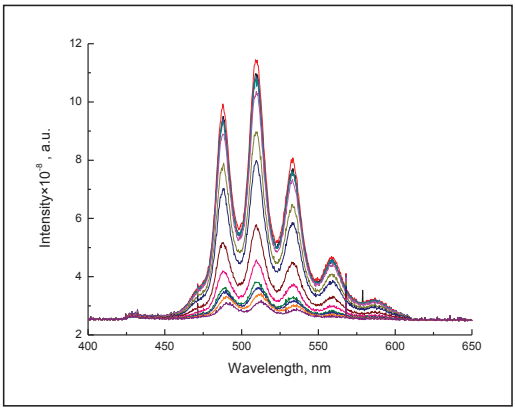

Fig. 1. TRLFS spectra of 1×10^{-4} M of U(VI) in presence of different formic acid concentrations from 0 to 0.3 M (from top to bottom); pH=2.5, μ=0.05 M ($NaClO_4$). 2000 accumulations. Initial delay: 0.15 μs; width: 20 μs.

Quenching experiments are evaluated according to Stern-Volmer analysis. The dynamic quenching rate constant values are obtained. Their values are in the rage from 10^8 to 10^9 $M^{-1}s^{-1}$. With an increase of acid anion concentration (more than 1×10^{-4} M of acid anion), static

quenching occurs in addition to the dynamic quenching due to the formation of a non fluorescent ground state complex between uranyl and acid anion. The stability constant values are calculated for complex species uranyl-acid anion (ratio 1:1). Obtained values are compared with literature data.
The formation of second complex species (uranyl with two acid anions) is also observed with an increase of acid anion concentration (from 5×10^{-4} M). The maxima of intensity spectrum bands are shifted and the second lifetime appears (Fig. 1).

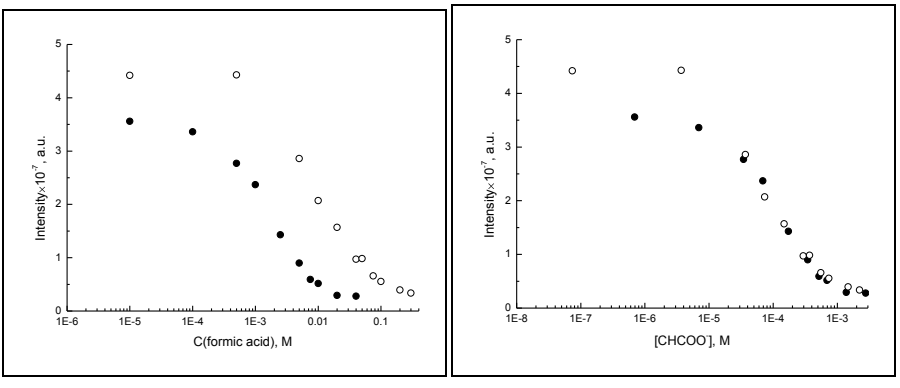

Fig. 2. Intensities of TRLFS spectra for 1×10^{-4} M of U(VI), measured at pH 1.5 () and 2.5 () as a function of total concentration of formic acid (left) and anionic form (right). pH=2.5, μ=0.05 M ($NaClO_4$). 2000 accumulations. Initial delay: 0.15 μs; width: 20 μs.

References

[1] V. Sladkov, Y. Zhao, F. Mercier-Bion, *Talanta* **83**, 1595 (2011) and references therein.
[2] V. Sladkov, B. Fourest, F. Mercier, *Dalton Trans.,* 7734 (2009).

5P1

Inorganic and organometallic chemistry

Thorium and Uranium Carbide Cluster Cations in the Gas Phase

António P. Gonçalves[1], Ana F. Lucena[1], Cláudia C. L. Pereira[1], Joaquim Marçalo[1], John K. Gibson[2], Lester Andrews[3]

[1] *Unidade de Ciências Químicas e Radiofarmacêuticas, Instituto Tecnológico e Nuclear, Estrada Nacional 10, 2686-953 Sacavém, Portugal, e-mail: apg@itn.pt*
[2] *Chemical Sciences Division, Lawrence Berkeley National Laboratory, One Cyclotron Road, Berkeley, California 94720, USA*
[3] *Department of Chemistry, University of Virginia, McCormick Road, Charlottesville, Virginia 22904-4319, USA*

Laser desorption/ionization (LDI) or laser ablation (LA) coupled with mass spectrometry (MS) is a technique that has produced numerous examples of novel molecular species [1]. Here we report that LDI/LA of AnC_4 alloys (An = Th, U) readily yields in the gas phase molecular thorium and uranium carbide cluster cations of compositions $[An_mC_n]^+$, with m = 1, n = 2-14, and m = 2, n = 2-18. In the case of thorium, $[Th_mC_n]^+$ cluster ions with m = 3-6 and n = 5-22 were also produced.

A standard arc-furnace melting method was employed for reacting thorium pellets or uranium turnings with graphite pieces, in An/C mole ratios of 1/4, to form the AnC_4 alloy targets. The same type of U/C samples were recently used to produce and spectroscopically characterize the UC and CUC molecules in a solid argon matrix [2].

A Nd:YAG laser (1064 nm) with an average focused power density of ca. 200 MW cm^{-2} was used in the LDI/LA experiments. The ions were detected by Fourier transform ion cyclotron resonance mass spectrometry (FTICR/MS) in a 3-T spectrometer with an "internal" source design in which the sample sits close to the ICR cell. Similar results were obtained with operating pressures of (2-5)x10^{-8} Torr of background gases (water and air) or ca. 10^{-6} Torr of argon. This LDI/LA-MS setup was recently employed in the synthesis of anionic and cationic uranium oxide clusters from UO_3 samples [3]. A seminal study of Ta carbide cluster ions using a similar LDI/LA-MS setup was reported ca. 20 years ago [4].

Fig. 1 displays a representative mass spectrum obtained from the ThC_4 sample. Abundant Th^+ and ThO^+ ions were ejected from the ICR cell prior to detection to enhance the signal of the less abundant thorium carbide cluster ions. Fig. 2 shows the $[ThC_n]^+$ and the $[Th_2C_n]^+$ regions of the spectrum of Fig. 1.

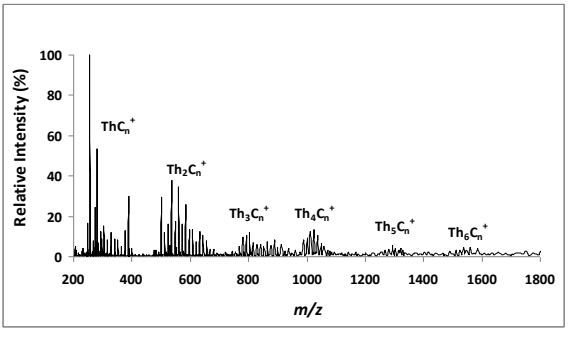

Figure 1. LA(+) mass spectrum of a ThC_4 sample.

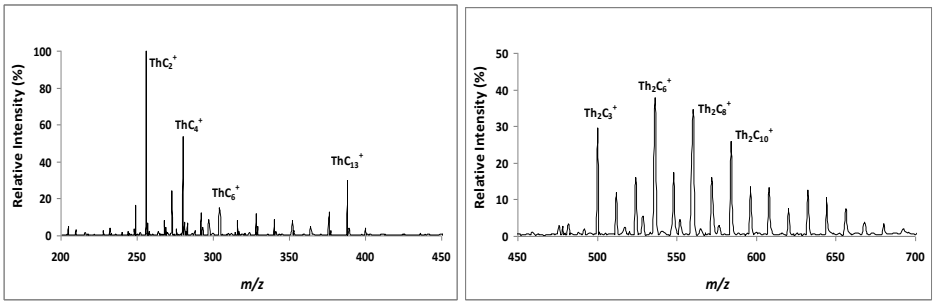

Figure 2. $[ThC_n]^+$ and $[Th_2C_n]^+$ regions of the LA(+) mass spectrum of Fig. 1.

For both Th and U, the $[AnC_n]^+$ cluster family showed higher abundances for the $[AnC_2]^+$, $[AnC_4]^+$ and $[AnC_6]^+$ ions, and a positive anomaly for the $[AnC_{13}]^+$ ions, which were clearly more abundant than the neighbouring ions (see Fig. 2 for the case of Th).

In the $[An_2C_n]^+$ cluster family, a significant difference was observed between Th and U as $[Th_2C_3]^+$ was one of the more abundant ions (see Fig. 2) while the enhanced abundance was observed for $[U_2C_4]^+$ instead. The $[An_2C_6]^+$ and $[An_2C_8]^+$ cluster ions were similarly abundant for both Th and U.

Previous studies of thorium and uranium carbides involved high-temperature Knudsen effusion mass spectrometric studies of metal/graphite powder mixtures [5,6]. In those experiments, the observed carbides were limited to AnC_n with n = 1-6 for both Th and U. The LDI/LA technique has the apparent advantage of yielding species with more carbon atoms, as well as polymetallic species. The mechanism of formation of the cluster cations by LDI/LA probably involves reactions in the laser-generated plasma.

The observed high abundances of the $[AnC_2]^+$ and $[AnC_4]^+$ ions (see Fig. 2 for the case of Th) are consistent with an enhanced stability of MC_2 and MC_4 species that has been attributed to strong metal-dicarbide (M-C_2 and C_2-M-C_2) bonds [4-6]. A recent theoretical study has corroborated this analysis, indicating an asymmetric L-type structure for ThC_2 and a planar fan-type structure for ThC_4 [7]. The structures of the larger species are uncertain.

Further gas-phase experiments to probe the properties of these Th and U cluster ions, as well as theoretical studies of selected species, are under way.

Acknowledgments

This work was supported by Fundação para a Ciência e a Tecnologia (SFRH/BD/70475/2010 and "Ciência 2007") and by the Director, Office of Science, Office of Basic Energy Sciences, Division of Chemical Sciences, Geosciences and Biosciences of the U.S. Department of Energy (LBNL and UVa).

References

[1] M.A. Almoster Ferreira, M.C. Oliveira, in *The Encyclopedia of Mass Spectrometry, Vol. 4*; N. Nibbering, Ed.; Elsevier: New York, 2005; p 621.

[2] X. Wang, L. Andrews, P.-A. Malmqvist, B.O. Roos, A.P. Gonçalves, C.C.L. Pereira, J. Marçalo, C. Godart, B. Villeroy, J. Am. Chem. Soc. **132**, 8484 (2010).

[3] J. Marçalo, M. Santos, A. Pires de Matos, J.K. Gibson, *Inorg. Chem.* **48**, 5055 (2009).

[4] S.W. McElvany, C.J. Cassady, *J. Phys. Chem.* **94**, 2057 (1990).

[5] S. Gupta, K.A. Gingerich, *J. Chem. Phys.* **71**, 3072 (1979).

[6] S. Gupta, K.A. Gingerich, *J. Chem. Phys.* **72**, 2795 (1980).

[7] A. Kovács, R.J.M. Konings, *J. Nucl. Mat.* **372**, 391 (2008).

Anna Maria	*Adamska*	anna@mag.mff.cuni.cz
Marek	*Antoňak*	antonak@saske.sk
Bingyun	*Ao*	aobingyun24@yahoo.com.cn
Zhaohui	*Bao*	Zhaohui.Bao@eu.europa.eu
Ivan	*Baťko*	batko@saske.sk
Marianna	*Baťková*	batkova@saske.sk
Ofer	*Beeri*	ofer.beeri@gmail.com
Shai	*Cohen*	shaico@bgu.ac.il
Colineau	*Eric*	eric.colineau@ec.europa.eu
Daniel	*Fröhlich*	froehlich@uni-mainz.de
Piotr	*Gaczyński*	piotr.gaczynski@ec.europa.eu
David	*Geeson*	david.geeson@awe.co.uk
Mauro	*Giovannini*	giovam@chimica.unige.it
Thomas	*Gouder*	thomas.gouder@ec.europa.eu
Roman	*Gumeniuk*	gumeniuk@cpfs.mpg.de
Itzhak	*Halevy*	halevyi@caltech.edu
Nicholas	*Harker*	N.J.Harker@bristol.ac.uk
Ladislav	*Havela*	havela@mag.mff.cuni.cz
Amir	*Hen*	amir.hen@mail.huji.ac.il
Margarida	*Henriques*	mish@itn.pt
Piheng	*Chen*	chenph@live.cn
Sergej	*Iľkovič*	ilkovic@unipo.sk
Igor	*Izosimov*	izig@mail.ru
Jean-Christophe	*Griveau*	jean-christophe.griveau@ec.europa.eu
Tomasz	*Klimczuk*	Tomasz.Klimczuk@ec.europa.eu
Yulia	*Kuryleva*	julieta-k@mail.ru
Michael	*Ling*	michael.ling@awe.co.uk
Maria	*Lübke*	marialue@students.uni-mainz.de
Dmitry	*Maltsev*	d.s.maltsev@gmail.com
Silvie	*Maskova*	maskova@mag.mff.cuni.cz
Štefánia	*Máťošová*	matosova@saske.sk
Marián	*Mihalik*	mihalik@saske.sk
Kim-Ngan	*Nhu-Tarnawska H*	tarnawsk@mag.mff.cuni.cz
Mathieu	*Pasturel*	mathieu.pasturel@univ-rennes1.fr
Antonio	*Pereira Goncalves*	apg@itn.pt
Jiří	*Prchal*	prchal@karlov.mff.cuni.cz
Eloirdi	*Rachel*	rachel.eloirdi@ec.europa.eu
Mark S D	*Read*	mark.read@awe.co.uk
Marian	*Reiffers*	reiffers@saske.sk
Jan	*Rusz*	jan.rusz@fysik.uu.se
Leonid	*Salamakha*	salamakhaleonid1@rambler.ru
Malgorzata	*Samsel-Czekala*	m.samsel@int.pan.wroc.pl
Thomas	*Scott*	t.b.scott@bristol.ac.uk
Noah	*Shamir*	noah.shamir@gmail.com
Alexander	*Shick*	shick@fzu.cz
Vladimir	*Sladkov*	sladkov@ipno.in2p3.fr
Aljoz	*Slaninka*	alojz.slaninka@vuje.sk
Nils	*Stöbener*	stoebenn@uni-mainz.de
Wojciech	*Suski*	w.suski@int.pan.wroc.pl
Irena	*Špendlíková*	SpendlikovaIrena@gmail.com

Kamila	*Šťastná*	kamila.stastna@fjfi.cvut.cz
Iveta	*Takáčová*	ivtakacova@saske.sk
James	*Tobin*	Tobin1@LLNL.Gov
Robert	*Troc*	r.troc@int.pan.wroc.pl
Sorin Octavian	*Vălu*	sorin.valu@ec.europa.eu
Martin	*Vavra*	vavra@saske.sk
David	*Wheeler*	david.wheeler@awe.co.uk
Harald	*Zänker*	h.zaenker@hzdr.de
Mária	*Zentková*	zentkova@saske.sk
Gertrud	*Zwicknagl*	g.zwicknagl@tu-bs.de

41èmes Journèes des Actinides

was supported by:

Expert Vacuum s.r.o., Varian
Eötvősova ul. 3195/21
945 01 Komárno
tel: 0910-109-650
fax: 0233-204-579
e-mail: info@expertvacuum.eu
www.expertvacuum.sk

Jánošíkova 1827/65
927 01 Šaľa
tel.: +421 31 770 7994,5
fax: +421 31 771 2155
e-mail: chromspec@chromspec.sk
www.chromspec.sk

Nové technológie a služby, s.r.o.
Cesta pod Hradovou 13/A
040 01 Košice

Tel: 055/63 23 019
Fax: 055/63 24 164
http://www.nts.sk/www/ntsw.nsf

ISBN 978-80-970625-1-4